PhD degree in Molecular Medicine (curriculum in Molecular Oncology)

European School of Molecular Medicine (SEMM)

University of Milan and University of Naples “Federico II”

Different extracellular vesicles subpopulations characterize metastatic progression: qualitative and quantitative analysis of isogenic melanoma cell lines and their secreted factors

Clara Bernardelli

Fondazione IFOM, Milan

Matricola n. R10759

Supervisor: *Dr. Angela Bachi*

Fondazine IFOM, Milan

Anno accademico 2016-2017

TABLE OF CONTENTS

LIST OF ABBREVIATIONS 7
FIGURES INDEX 9
TABLES INDEX 11
ABSTRACT 12
INTRODUCTION 13
1. The pre-metastatic niche 13
1.1 Pre-Metastatic Niche explains metastases formation 13
1.2 Pre-metastatic niches formation is a stepwise process 14
1.3 Tumor secreted factors are key players of the pre-metastatic niche establishment 15
1.4 Targeting PMN will improve cancer therapy 18
2. Extracellular Vesicles (EVs) 19
2.1 Extracellular Vesicles mediate intercellular communication 19
2.2 Classification, enrichment and characterization of Extracellular Vesicles are matter of debate 21
2.3 Biogenesis of Extracellular Vesicles 23
2.3.1 Exosomes originate from Multivesicular Bodies 25
2.3.2 Microvesicles originate from the plasma membrane 26
2.4 Extracellular Vesicles contain biological molecules 26
2.4.1 Extracellular Vesicles influence gene expression in target cells through mRNA delivery 26
2.4.2 Non-coding RNAs in Extracellular Vesicles can be used as biomarkers 27
2.4.3 Lipids on Extracellular Vesicles membrane have both structural and biological functions 28
2.4.4 Proteins in Extracellular Vesicles are characteristics of vesicles subtypes and donor cells 28
2.5 Tumor derived Extracellular Vesicles are key players in Pre-Metastatic Niche formation. 29
2.6 Extracellular Vesicles in clinics: promising biomarkers and therapeutic targets to block PMN establishment 31
3. Melanoma 32
3.1 Cutaneous melanoma is among the most aggressive and treatment-resistant human cancers 32
3.2 Extracellular Vesicles in melanoma 36
AIM OF THE PROJECT 38
MATERIALS AND METHODS 39
1. DNA procedures 39

1.1 Agarose gel electrophoresis 39
1.2 Transformation of competent cells 39
1.3 Plasmid isolation from individual bacterial colonies 39
1.4 Large scale plasmid preparation 39
2. Cell Culture 40
2.1 Cell lines and culture conditions 40
2.2 MTT assay. 40
2.3 Growth curve 41
2.4 *RAB27A* Knock Down of metastatic melanoma cells 41
2.4.1 ShRNA cloning into pLKO3.1 plasmid 41
2.4.2 Lentivirus production in HEK293T cells 41
2.4.3 WM266.4 and IGR37 cells lentiviral infection 42
2.5 Colony formation assay 42
2.5.1 Colony formation assay with conditioned media 42
3. Extracellular Vesicles enrichment from conditioned media 44
3.1 EVs harvesting by serial centrifugation 44
3.2 EVs fractionation on iodixanol gradient. 46
3.2.1 Discontinuos gradient fractionation 46
3.2.2 Calculation of the density of each fraction 46
4. Protein Procedures 48
4.1 Cells and EVs lysis 48
4.2 Western Blot 48
4.3 Antibodies 49
5. Immunofluorescence 49
6. Proteomics analysis 49
6.1 Sample preparation 49
6.2 Deep quantitative proteomics on isogenic melanoma cell lines and EVs 50
6.3 Secretome analysis 52
7. Atomic Force Microscopy analysis 52
8. Wound-Healing assay 53
9. Gelatin Degradation Assay 54
10. Proteostat® aggresome detection assay 55
RESULTS 56
1.Primary tumor and metastasis derived melanoma cells release qualitative and quantitative different Extracellular Vesicles 56
1.1 Metastasis and primary tumor derived cell lines have the same shape and proliferation rate 56

1.2 Ultracentrifugation of conditioned media results in enrichment of Extracellular Vesicles 57
1.3 Primary tumor cells release more and bigger EVs respect to metastatic cells 60
1.4 Deep quantitative proteomics on melanoma EVs 61
1.4.1 The majority of the identified proteins belong to primary tumor derived EVs 61
1.4.2 EVs protein content is different between primary tumor and metastatic cells 62
1.4.3 Isogenic primary tumor and metastatic melanoma cells have different secretomes, suggesting an invasive vs a proliferative behavior 63
2. Fibronectin and WNT5A are EVs-associated proteins, while APOE is mainly secreted as soluble factor 66
2.1 Fibronectin is the major component of metastasis derived EVs 66
2.2 WNT5A is enriched in primary tumor secreted EVs 68
2.3 APOE is mainly secreted as soluble factor in metastatic melanoma cells 69
3. Deep quantitative proteomics on isogenic melanoma cell lines 71
3.1 Method development 71
3.1.1 Peptide fractionation increases protein quantitation accuracy 71
3.1.2 Deep quantitative proteomics method is reproducible and can be used to compare different samples 72
3.2 Primary and metastatic isogenic melanoma cells show differences in their proteome 74
3.3 EVs proteome reflect the cells proteome but the secretion of the proteins in EVs is specifically regulated 75
3.4 RAB27A is up-regulated in metastasis vs primary tumor 76
4. *RAB27A* Knock Down affects metastatic melanoma cells clonogenic ability and motility and impairs EVs release 78
4.1 RAB27A KD affects IGR37 cells pigmentation and conformation 79
4.2 RAB27A-KD metastatic melanoma cells have increased clonogenic ability 80
4.2.1 RAB27A KD increases the number of colonies formed by metastatic melanoma cells 80
4.2.2 EVs secreted by wild type metastatic melanoma cells impair the clonogenic ability of RAB27A-KD cells 81
4.3 RAB27A KD reduces both EVs number and EVs size 82
4.4 Proteomics analysis of RAB27A-KD cells secreted vesicles 83
4.4.1 RAB27A KD affects the levels of specific EVs enriched proteins 83
4.4.2 RAB27A KD impairs the secretion of proteins related to ECM organization 85
4.4.3 WNT5A secretion in EVs is increased after RAB27A KD, while APOE does not change 85
4.5 RAB27A KD increases the motility of metastatic melanoma cells 87
DISCUSSION 89
Future Plans 99
1. Evaluation of ECM proteins association to EVs 99

2. Characterization of the biological function of EVs-associated APOE 100
3. Characterization of the biological function of the EVs-associated WNT5A..... 100
4. Investigation of the role of RAB27A-dependent EVs sub population..... 101
REFERENCES..... 103

ACN	Acetonitrile
AFM	Atomic Force Microscopy
APOE	Apolipoprotein E
BMDCs	Bone Marrow Derived Cells
BRAF	B-Raf Proto-Oncogene, Serine/Threonine Kinase
CAM	Chloroacetamide
CDKN2A	Cyclin-Dependent Kinase Inhibitor 2A
CTCs	Circulating Tumor Cells
ECM	Extracellular Matrix
ESCRT	Endosomal Sorting Complex Responsible for Transport
EVs	Extracellular Vesicles
FBS	Fetal Bovine Serum
FN	Fibronectin
HSP	Heat Shock Protein
IF	Immunofluorescence
ILVs	Intraluminal Vesicles
ISEV	International Society of Extracellular Vesicles
KD	Knock Down
LB	Luria-Bertani
MAGE	Melanoma-Associated Antigens
MAPK	Mitogen-Activated Protein Kinase
MHC	Major Histocompatibility Complex
miRNAs	Micro RNAs
MITF	Microphthalmia-Associated Transcription Factor
MMPs	Matrix Metalloproteinases
MTT	Methyl-Thiazol-Tetrazolium
MVBs	Multivesicular Bodies
NRAS	Neuroblastoma RAS Viral Oncogene Homolog

PBS	Phosphate Buffered Saline
PMEL	Premelanosome Protein
PMN	Pre Metastatic Niche
PTEN	Phospatase and Tensin Homologue
RAB27A	Ras-Related protein Rab-27A
RAB27B	Ras-Related protein Rab-27B
Scr	Scramble
SCX	Strong Cationic Exchange
SILAC	Stable Isotope Labeling with Amino acids in Cell culture
TCA	Tricarboxylic Acid
TCEP	Tris(2-carboxyethyl)Phosphine
TCL	Total Cell Lysate
TE	Tris-EDTA
TFA	Trifluoroacetic Acid
UA	8M Urea, 100mM Tris HCl Buffer
WB	Western Blot
WH	Wound-Healing
WNT5A	Wingless-related integration site, Family member 5A
WT	Wild Type

FIGURES INDEX

Figure 1	Model of the pre-metastatic niche formation	Pag. 14
Figure 2	The number of studies on EVs is increased in the last years	Pag. 20
Figure 3	Schematic representation of Microvesicles and Exosomes origin	Pag. 24
Figure 4	FN-coated EVs determine directional cells movement through tissues	Pag. 30
Figure 5	Model of melanoma progression	Pag. 34
Figure 6	Schematic workflow of the colony formation assay with conditioned media	Pag. 43
Figure 7	Workflow of EVs enrichment from cells'conditioned media	Pag. 45
Figure 8	Reproducibility of the density gradient distribution of each fraction in different samples	Pag. 47
Figure 9	Schematic workflow of the deep quantitative proteomics analysis of isogenic melanoma cell lines	Pag. 51
Figure 10	Metastasis and Primary Tumor isogenic melanoma cell lines show the same aspect and proliferation rate	Pag. 57
Figure 11	Viability of isogenic melanoma cells is maintained in EVs-depleted DMEM	Pag. 58
Figure 12	The ultracentrifuged pellet is enriched in EVs and is not contaminated by organelles coming from other cellular compartments	Pag. 58
Figure 13	EVs size in the ultracentrifuged pellet is consistent with exosomes size	Pag. 59
Figure 14	Ultracentrifuged pellet are enriched in melanoma exosomes	Pag. 60
Figure 15	EVs from primary tumor cells are more and bigger than EVs released by metastatic cells	Pag. 61
Figure 16	The majority of identified proteins belongs to primary tumor EVs	Pag. 62
Figure 17	Primary tumor cells have an invasive behavior	Pag. 65

Figure 18	Summary of the proteomics results on EVs proteome, isogenic melanoma cells secretome and proteome	Pag. 66
Figure 19	Fibronectin is enriched in metastatic cells secreted EVs	Pag. 67
Figure 20	Fibronectin is enriched at higher densities in WM266.4 respect WM115 samples	Pag. 67
Figure 21	WNT5A is enriched in primary tumor EVs	Pag. 68
Figure 22	APOE is secreted as soluble factor by metastatic melanoma cells	Pag. 69
Figure 23	Proteostat reagent accumulates in dots inside and outside metastatic melanoma cells	Pag. 70
Figure 24	Peptides fractionation increases protein quantitation accuracy	Pag. 72
Figure 25	Deep quantitative proteomics method is reproducible	Pag. 73
Figure 26	Deep quantitative proteomics can be used to compare different samples	Pag. 74
Figure 27	Primary tumor and metastatic melanoma cells from different origin up-regulate similar pathways	Pag. 75
Figure 28	The secretion of proteins in EVs is regulated	Pag. 76
Figure 29	RAB27A is overexpressed in metastatic melanoma cells	Pag. 78
Figure 30	*RAB27A* KD affects IGR37 cells pigmentation and conformation	Pag. 79
Figure 31	*RAB27A* KD affects the clonogenic ability of metastatic melanoma cells	Pag. 80
Figure 32	EVs secreted by WT cells impair *RAB27A*-KD cells clonogenic ability	Pag. 81
Figure 33	*RAB27A* KD reduces both EVs number and EVs size	Pag. 83
Figure 34	Not all the EVs enriched proteins decrease after *RAB27A* KD	Pag. 84
Figure 35	WNT5A secretion in EVs is increased after *RAB27A* KD	Pag. 87
Figure 36	*RAB27A* KD increases the motility of metastatic melanoma cells	Pag. 88

TABLES INDEX

Table 1	Known secreted molecules that determine organotropic metastasis	Pag. 16
Table 2	Expected presence of proteins in EVs samples	Pag. 23
Table 3	Principal characteristics that distinguish exosomes from microvesicles	Pag. 24
Table 4	Calculated density of each iodixanol solution	Pag. 47
Table 5	Proteins significantly regulated in metastasis-derived or primary tumor-derived EVs	Pag. 63
Table 6	List of known melanoma progression markers used as quality control for proteomics analysis	Pag. 72
Table 7	List of RAB27A and its known effectors significantly enriched in metastatic melanoma cells proteome	Pag. 76
Table 8	Proteins related to ECM organization decrease in EVs after *RAB27A* KD	Pag. 84

ABSTRACT

The survival and proliferation of metastases is a consequence of the pre-metastatic niche (PMN) evolution, an abnormal, tumor growth-favoring microenvironment devoid of cancer cells. Among tumor derived secreted factors, extracellular vesicles (EVs) are key players in PMN establishment and facilitate organotropic metastasis. Compared to normal melanocytes, melanoma cells produce a large quantity of EVs, that can be detected in the plasma of melanoma patients. For this reason, a full characterization of secreted vesicles subpopulations and of their cargo is necessary to understand how EVs affect PMN formation.

In this study, we demonstrated for the first time that EVs secreted by isogenic primary tumor and metastatic melanoma cell lines are quantitatively and qualitatively different, suggesting that diverse EVs subpopulations characterize metastatic progression. We also set a deep quantitative proteomics protocol to analyze the proteome of these cells and of their EVs and soluble secreted factors. WNT5A was found as an important component of primary tumor secreted EVs; on the contrary, we observed a specific APOE and Fibronectin sorting to EVs in in metastasis versus primary tumor cell. Finally, we observed that increased levels of RAB27A protein in metastatic cells do not correlate with an increased EVs secretion. Our preliminary results demonstrate that EVs secreted by *RAB27A*-KD cells maintain cancer cells clonogenic ability and that low levels of RAB27A expression correlate with higher cells motility. These findings suggest a paracrine activity of a RAB27A -independent EVs subpopulation in tumor-PMN communication to promote cancer progression.

1. The pre-metastatic niche

1.1 Pre-Metastatic Niche explains metastases formation

Metastases are characterized by a unique microenvironment, composed of neoplastic cells, tumor-associated cells, endothelial cells, inflammatory cells, extracellular matrix and soluble factors.

The secondary organs involved in this process do not passively accept cancer cells, but are selectively modified by the primary tumor through the Pre-Metastatic Niche (PMN) establishment {Peinado H., et al., 2017}. Indeed, the primary tumor, co-evolving with its microenvironment, secrete factors that reach the bone marrow to educate and mobilize Bone Marrow Derived Cells (BMDCs). The same factors are also delivered to the secondary organs, where they induce vascular leakiness, alterations of resident cells (such as fibroblasts) and recruit the mobilized BMDCs promoting processes including Extracellular Matrix (ECM) remodeling, immunosuppression, inflammation, and vascular hyper permeability {Sceneay J., et al., 2013}. By preparing the microenvironment of secondary organs in advance, the PMN formation allow the colonization and the outgrowth of Circulating Tumor Cells (CTCs), without needing for the primary tumor cells to acquire extra mutations before starting the colonization of the metastatic site {Psaila B. and Lyden D., 2009} (Figure 1).

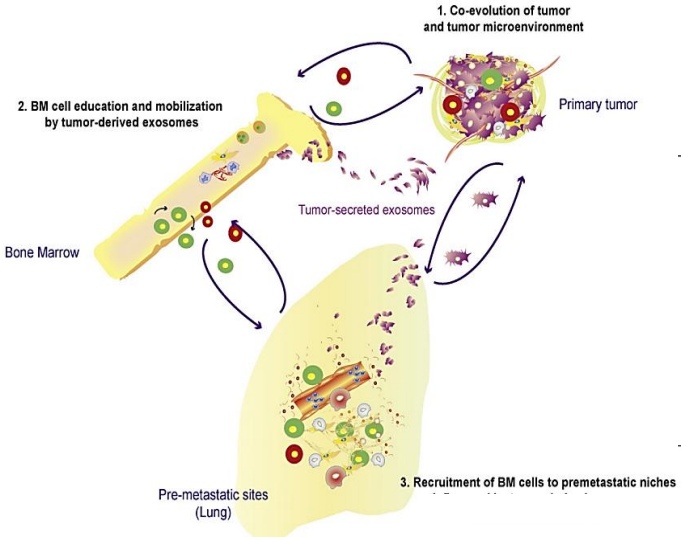

Figure 1: Model of the pre-metastatic niche formation.

During primary tumor development, secreted factors attract BMDCs and stromal cells to tumor microenvironment (1). At the same time, they are delivered both to the bone marrow, promoting BMDCs education and mobilization (2), and to the secondary organ, to recruit BMDCs and CTCs to pre-metastatic sites (3). *(Adapted from Peinado H., et al., 2011)*

So far, the interaction between CTCs and the microenvironment in secondary organs has been only hypothesized {Paget S., 1889; Fidler I.J. and Nicolson G.L., 1976}. The PMN discovery demonstrated for the first time that the primary tumor preconditions specific organ sites for future metastases before CTCs arrival, representing an abnormal, tumor growth-favoring microenvironment devoid of cancer cells.

The existence of PMNs in tissue samples was observed in patients with colorectal, prostate, breast, thyroid, bladder, gastric and renal cell carcinomas {Sleeman J.P., 2015}, and there are evidences of PMN establishment also in preclinical models of melanoma {Peinado H., et al., 2012} and acute myeloid leukemia {Kumar B., et al., 2017}.

1.2 Pre-metastatic niches formation is a stepwise process

The initial steps of PMN development are clot formation and vascular disruption. Clots are a source of inflammatory signals able to reduce both shear stress and interstitial flow, providing docking sites for CTCs {Gay L.J. and Feldi-Habermann B., 2011}. On the other hand, the loss of vascular integrity is achieved by a combination of focal adhesion kinase activation, to disrupt endothelial cell–cell contacts, and of enhanced microvessels permeabilization through tumor-secreted factors such as

vascular endothelial growth factor A and angiopoietin-like 4 {Hiratsuka S., et al., 2011}. Additionally, BMDCs are recruited by local increase in cytokines and their adhesion is promoted by the deposition of ECM, in particular by the accumulation of Fibronectin (FN) and by the crosslinking of Collagen I via lysyl oxidase. ECM remodeling is also promoted by distant and local secretion of Matrix Metalloproteinases (MMPs), which also contributes to the early vascular disruption step {Erler J.T., et al., 2009}. The future infiltration of metastasis-initiating cells is also sustained by the WNT signaling via transforming growth factor-ß dependent production of proteins such as periostin {Kudo A., 2011}. Inflammatory responses within PMNs is mediated by the S100 family of proteins, that are crucial in intercellular crosstalk between tumor cells and stromal cells during PMN formation. These proteins have both autocrine and paracrine effects on proliferation, differentiation, apoptosis, Ca^{2+} homeostasis, migration and invasion because they activate cell surface receptors, G-protein-coupled receptors, scavenger receptors, heparan sulfate proteoglycans and *N*-glycans {Lukanidin E. and Sleeman J.P., 2012}. The metastatic niche is therefore the combined result of BMDC recruitment, ECM remodelling and inflammation, and the survival and proliferation of cancer cells is a consequence of PMN evolution.

1.3 Tumor secreted factors are key players of the pre-metastatic niche establishment

Tumor derived factors are molecules directly secreted from the cell in the extracellular space or Extracellular Vesicles (EVs) (better described in section 2).
Those factors exert crucial effects on PMN establishment and facilitate organotropic metastasis; indeed, Kaplan and colleagues demonstrated that in mice pretreated with melanoma cells-conditioned medium it is possible to detect metastases of Lewis lung carcinoma cells in the spleen, the kidney, the oviduct and the intestine, even if those cells are expected to colonize only the lung {Kaplan R.N., et al., 2005}. Subsequently, other studies have demonstrated that a pre-conditioned microenvironment is a key determinant of organ-specific metastasis, showing that tumor cell-intrinsic metastatic

properties are not enough for metastatic colonization. To date, the understanding of which characteristics distinguish PMNs in each organ is still a matter of debate.

The majority of the studies on PMNs have been performed on orthotopic and transgenic mouse models of lung metastases, that are one of the most frequent sites of metastasis both in humans and mice {Francia G., et al., 2011}. Furthermore, PMNs were identified in sentinel lymph nodes, where it was demonstrated that tumor cells encounter immune cells and interact with them to modulate immune response {Jung T., et al., 2009} and in bones with osteolytic lesions {Cox T.R., et al., 2015}. Moreover, exosomes (a specific class of extracellular vesicles; better described in section 2) were demonstrated to be biomarkers and functional contributors to liver PMNs {Costa-Silva B., et al., 2015}. Finally, the presence of PMNs in the brain is still under investigation {Peinado H., et al., 2017}.

Table 1 summarizes the known molecules that determine organotropic metastasis.

Molecule	**Target**	**Tumor type**
Integrin α_6	Laminin-expressing epithelial cells and fibroblasts in **lung**	Lung-metastatic breast cancer, osteosarcoma and rhabdomyosarcoma
Integrin α_v	Fibronectin-expressing Kupffer cells in **liver**	Colorectal cancer, pancreatic cancer, gastric cancer and uveal melanoma
Integrin β_3	Endothelial cell in **brain**	Brain-metastatic breast cancer and brain-metastatic melanoma
Integrin β_4	Laminin-expressing epithelial cells and fibroblasts in **lung**	Lung-metastatic breast cancer, osteosarcoma and rhabdomyosarcoma
Integrin β_5	Fibronectin-expressing Kupffer cells in **liver**	Colorectal cancer, pancreatic cancer, gastric cancer and uveal melanoma
Integrin β_1	Endothelial cell and collagen I– and VCAM1-expressing cells in **bone marrow**	Prostate cancer
IL-1β and TNF	Endothelial cell in **liver**	Colorectal and hepatic cancer

Integrin α_2	Endothelial cell and collagen I-expressing cells in **bone marrow**	Prostate cancer
Integrin α_3	Laminin-expressing cells in **lung**	Breast cancer
Integrin α_4	Endothelial cell and VCAM1-expressing cells in **bone marrow**	Myeloma
MIF	Kupffer cells in **liver**	Pancreatic cancer
miR-105	Endothelial cell in **brain**	Breast cancer
FUT3	**Liver**	Colorectal cancer
SELPLG	Endothelial cells in **bone marrow**	Prostate cancer
Integrin β_3	Endothelial cell and OPN-, FN- and VN-expressing cells in **bone marrow**	Breast and prostate cancer
Integrin $\alpha_v\beta_3$	**Lung**	Osteosarcoma
CDH11	Osteoblast in **bone**	Ewing sarcoma
CXCR4	SDF1-expressing cells in **lymphnodes, bone marrow, lung** and **liver**	Breast cancer
FN	DPP4-expressing endothelial cells in **lung**	Breast cancer
FUT4	Endothelial cells in **brain**	Non-small-cell lung cancer
GLG1	Endothelial cells in **bone marrow**	Prostate cancer
SPARC, MMP1 and IL13Rα2	**Lung**	Breast cancer
CTGF, FGF5, IL-11, MMP1 and ADAMTS1	Osteoblasts, osteoclasts and endothelial cells in **bone**	Breast cancer

Table 1: Known secreted molecules that determine organotropic metastasis.

Abbreviations: ADAMTS1, a disintegrin and metalloproteinase with thrombospondin motifs 1; CDH11, cadherin 11; CTGF, connective tissue growth factor; CXCR4, C-X-C motif chemokine receptor 4; DPP4, dipeptidyl peptidase 4; FGF5, fibroblast growth factor 5; FN, fibronectin; FUT, fucosyltransferase; GLG1, Golgi apparatus protein 1; IL, interleukin; IL13Rα2, interleukin-13 receptor-α2; MIF, macrophage migration inhibitory factor; miR, microRNA; MMP1, matrix metalloproteinase 1; OPN, osteopontin; SDF1, stromal cell-derived factor 1; SELPLG, P-selectin glycoprotein ligand 1; SPARC, secreted acidic and rich in cysteine; TNF, tumor necrosis factor; VCAM1, vascular cell adhesion molecule 1; VN, vitronectin. *(Adapted from Peinado H., et al., 2017)*

1.4 Targeting PMN will improve cancer therapy

The discovery of the PMN allowed a better understanding of metastatic progression and, at the same time, indicated new challenges in finding a cure for cancer. Indeed, the majority of current treatments for metastatic diseases only help to prolong patient survival, while a complete eradication of the tumor is still to be achieved. The cause of therapy ineffectiveness could be the failure of drugs to reach the PMN. Indeed, since it is clear that the PMN maturation requires a continuous incoming of primary tumor-derived factors {Deng J., et al., 2012}, the complete removal of the primary tumor at early stage by surgery is currently the first and the most effective treatment to prevent metastasis formation. However, cancer cells that have reached the PMNs before the intervention could continue secreting PMN-promoting factors even if the primary tumor has been removed, supporting the formation of further metastases. For this reason, targeting pre-metastatic niches to reduce or prevent metastatic disease is highly desirable in cancer therapy {Sceneay J., et al., 2013}.

One of the major challenge in PMNs targeting is the fact that it is difficult to predict if and how a novel therapy could impact PMN formation: for example, it has been shown that the removal of hematopoietic stem cells from their niches alter the bone marrow microenvironment, allowing cancer cells to engraft {Scadden D.T., et al., 2014}. It was also hypothesized that both specific targeting of PMN components and the use of angiogenesis inhibitors to stabilize PMN vasculature could reduce metastasis, but the efficacy of this approach has yet to be determined due to the lack of clinical trials to test any drug in pre-metastatic patients. Moreover, both in patients and in preclinical models there are technical limitations in detecting PMNs with current technologies. Indeed, the detection of hyper permeable regions, hypoxic and inflammatory areas, ECM alterations or BMDC recruitment at pre-metastatic stages needs to be improved with more sensitive approaches, such as the labeling of specific factors that are up-regulated in PMNs, as it was done detecting melanoma exosomes in lymph nodes {Hu L., et al., 2014}.

Finally, biomarkers discovery and 3D modeling of organ-specific niches to enable a systematic dissection of its cellular and extracellular components could help to determine when PMN will originate metastatic disease, improving early diagnosis.

2. Extracellular Vesicles (EVs)

2.1 Extracellular Vesicles mediate intercellular communication

Intercellular communication requires cell-to-cell contacts through highly-organized cell-cell structures such as gap junctions, intercellular bridges or synapses (short-distance communication) and/or involves the secretion of specific factors for long-distance communication. Cells derived secreted factors can be molecules directly secreted in the extracellular space (the so called secretome) or Extracellular Vesicles, a heterogeneous population of vesicles whose size varies between a range of 30 to 1000 nm constituted by a lipid bilayer and containing all the known families of biomolecules {Mittelbrunn M. and Sánchez-Madrid F., 2013}.

EVs-mediated communication is conserved through evolution, being reported not only in mammals but also in bacteria, *archea*, fungi, parasites {Deatherage B.L., et al., 2012} and plants {Regente M., et al., 2012}. In humans, the first study on EVs in the plasma was published in 1946 {Chargaff E. and West R., 1946} but only in 1983, after the demonstration of the role of EVs in the transferrin receptor turnover during reticulocytes to erythrocytes maturation, the modern idea of EVs was established in the scientific community {Pan B.T. and Johnstone R.M, 1983}.

The study of EVs has undergone a great expansion in the last years (Figure 2), and nowadays the presence of these vesicles has been demonstrated in almost all biologic fluids (plasma, urines, saliva, synovial and cerebrospinal fluid, breast milk) {Raposo G. and Stoorvogel W , 2013}.

Of note, EVs are also secreted by tumor cells. In the last year, the physiological role of EVs in cancer has been intensively investigated; in particular, it was established that tumor exosomes can inhibit antitumor immune response and promote angiogenesis

and metastasis, leading to the conclusion that these vesicles have pro-tumoral effect. At the same time, other studies demonstrated that tumor exosomes can present tumor antigens to dendritic cells, inducing antitumor immune response. For this reason, further studies on EVs in cancer are needed, taking into consideration that not all vesicles could exert the same function in all cancer types {Bobrie A. and Théry C., 2013}.

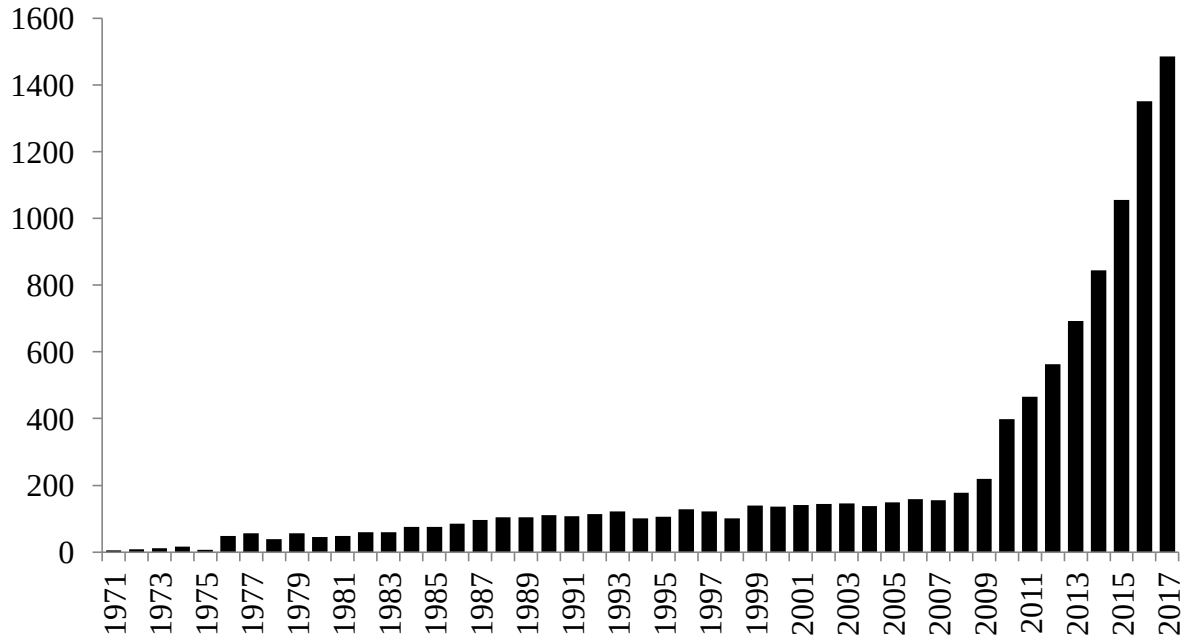

Figure 2: The number of studies on EVs is increased in the last years.

The graph represents the number of papers per year that have Extracellular Vesicles as topic (source: PubMed; last update: December 2017)

The growing interest on EVs is also proved by the foundation of the International Society for Extracellular Vesicles (ISEV) in 2011, to facilitate the communication and the exchange of information between groups who deal with this issue. On the same line, international databases such as EVpedia {Kim D.K., et al., 2015}, ExoCarta {Mathivanan S., et al., 2012} and Vesiclepedia {Karla H., et al., 2012} were implemented to collect information about EVs proteomic, lipidomic and transcriptomic content.

2.2 Classification, enrichment and characterization of Extracellular Vesicles are matter of debate

EVs can be divided in three main populations: apoptotic bodies, released by dying cells during apoptosis, exosomes and microvesicles, actively secreted by viable cells {Raposo G. and Stoorvogel W, 2013}.

Excluding apoptotic bodies, whose characteristics are known, there is still a big confusion on the other EVs nomenclature. Indeed, these vesicles were not only identified with more than 20 different names according to their biogenesis, function, donor cells or biological properties but, according to different authors, the term "exosomes" was used to describe both vesicles coming from Multivesicular Bodies (MVBs), vesicles isolated after ultracentrifugation between 70000 and 100000g and all the extracellular vesicles with a biological function. Also the term "microvesicles" was used to identify both budding vesicles from plasma membrane, vesicles enriched after 10000g centrifugation and all the EVs {Gould S.J. and Raposo G., 2013}. Since there is still no universally accepted nomenclature, the ISEV suggests the use of the term "Extracellular Vesicles" to define all the secreted vesicles, regardless of their biogenesis, characteristics and donor cells phenotype {Simpson R.J., 2012}.

Moreover, due to limitations in enrichment and characterization assays, EVs samples often contain heterogeneous population of vesicles, that are different in composition, properties and functions, depending on the assay used to enrich them from biological samples {Taylor D.D. and Shah S., 2015}. Nowadays, differential centrifugation is the method of choice to collect EVs, and it is indeed used in the majority of the studies often in combination with centrifugation on a density gradient, in order to differentiate between the desired vesicles subpopulation (that is expected to have a specific density) and other soluble secreted factors. Other approaches, including filtration, precipitation, size-exclusion chromatography and affinity binding on magnetic beads are used as well {Gardiner C., et al., 2016}. To overcome the problem of heterogeneity in isolation methodologies and to increase the transparency of

reporting data in EVs studies, in 2017 the EV-TRACK consortium created an open-source knowledgebase in which a EV-METRIC measures for each specific work how much the reporting of generic and method-specific information is complete and allows the possibility to interpret and reproduce the experiments {Van Deun J., et al., 2017}.

The heterogeneity in EVs studies is also complicated by the fact that, to date, the assays used to characterize the vesicles in a biological sample are western blot analysis, single particle tracking analysis, atomic force microscopy and electron microscopy, that are not only different in sensitivity, but are also able to better highlight different EVs characteristics. Furthermore, there are no specific markers that let scientists to univocally differentiate between microvesicles and exosomes. For this reason, the ISEV published some guidelines to standardize the definition of EVs {Lötvall J., et al., 2014}, as reported in Table 2.

Category	1	2	3	4
Class	Transmembrane or lipid-bound extracellular proteins	Cytosolic proteins with membrane- or receptor-binding capacity	Intracellular proteins not associated with plasma membrane or endosomes	Extracellular proteins binding to membranes
Examples	Tetraspanins Phosphatidylserine binding proteins Integrins and cell adhesion molecules Growth factor receptors G proteins	Endosomal proteins Membrane binding proteins Signal transduction or scaffolding proteins	Mitochondrial proteins Proteins of endoplasmic reticulum Proteins of Golgi Apparatus Nuclear proteins	Acetylcholinesterase Extracellular Matrix proteins Soluble secreted proteins Serum albumin

Table 2: Expected presence of proteins in EVs samples.

As indicated by ISEV, at least one protein of each category 1 and 2 should be quantified in the EV preparations, proteins of category 3 should be absent in EVs sample and EVs association of proteins of category 4 should be demonstrated by other means *(Adapted from Lötvall J., et al., 2014)*

2.3 Biogenesis of Extracellular Vesicles

Despite all of the above-mentioned problems to standardize EVs enrichment and characterization, in the majority of the studies, the term "exosomes" is referred to small-size vesicles (30-100 nm) originating in the endosomal compartment, while the term "microvesicles" indicates all the vesicles that originate by the budding from the plasma membrane and whose size is comprised between 100 and 1000 nm (Figure 3).

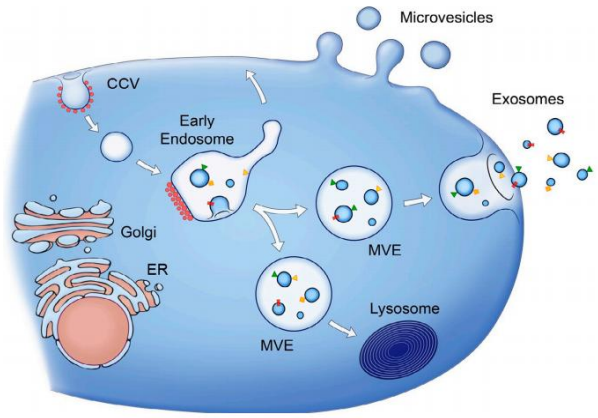

Figure 3: Schematic representation of Microvesicles and Exosomes origin.

Exosomes have a size between 30 and 100 nm and originate from the endosomal compartment, while microvesicles are bigger (100 to 1000 nm) and originate by budding from the plasma membrane *(Adapted by Raposo G. and Stoorvogel W., 2013)*

Table 3 summarizes the characteristics usually associated to the two vesicles populations according to their origin {Mathivanan S., et al., 2010}.

	Exosomes	**Microvesicles**
Size (diameter)	30–100 nm	100–1000 nm
Flotation density	1.10–1.21 g/mL	NA
Morphology	Cup-shaped	Various shape
Lipid composition	LBPA, low phosphatidylserine exposure, cholesterol, ceramide, contains lipid rafts, sphingomyelin	High phosphatidylserine exposure, cholesterol
Protein markers	Alix, TSG101, CD63, CD81, CD9	Selectins, integrins, CD40, metalloproteinases
Site of origin	Multivesicular Bodies	Plasma membrane
Release	Constitutive and regulated	Regulated
Mechanism of discharge	Exocytosis of MVBs	Budding from plasma membrane
Cargo	Proteins, miRNA, mRNA, lipids, mitochondria	Proteins, miRNA, mRNA, lipids

Table 3: Principal characteristics that distinguish exosomes from microvesicles.

Abbreviations: HSP70, heat shock protein family A member 8; LBPA, lyosbisphosphatidic acid; MV, microvesicles; MVBs, multivesicular bodies; NA, not assessed; TSG101, tumor susceptibility gene 101. *(Adapted from Mathivanan S., et al., 2010)*

2.3.1 Exosomes originate from Multivesicular Bodies

After the formation of the Intraluminal Vesicles (ILVs), early Endosomes mature into MVBs through the activation of the 4 multiprotein complex called the Endosomal Sorting Complex Responsible for Transport (ESCRT)-0, -I, -II, -III. In particular, ILVs formation seems to be promoted by the presence of tetraspanins- and Phosphatidylinositol 3-Phosphate- rich domains. These molecules are able to sequentially recruit the proteins of the ESCRT complex to bind ubiquitinated proteins and to induce the inward budding of endosomal membrane that forms the vesicles, involving also ancillary proteins such as ALIX {Kalra H., et al., 2016}. For this reason, the commonly used markers for exosomes are TSG101 (a member of the ESCRT-I complex), CD63, CD81, CD9 (members of the tetraspanins family), and ALIX. Finally, mature MVBs can either fuse with lysosomes to promote the degradation of their cargo, or with the plasma membrane to release ILVs and their content in the extracellular space. This process is mediated by cytoskeleton –associated or –non associated proteins (kinesines, myosins, small GTPases and SNAREs proteins) that deliver the MVBs to the plasma membrane and promote their fusion {Cocucci E. and Meldolesi J., 2015}. Among small GTPases, almost 70 proteins of the RAB and RAB-like family were identified in humans to control budding, motility, docking and fusion of vesicles to acceptor membranes {Zerial M. and McBride H., 2001}. By a short-hairpin RNAs-based screening, Ostrowski and colleagues demonstrated that the Ras-Related proteins RAB27A and RAB27B have a non-redundant role in the exosomes secretion pathway, as they promote the vesicles docking to the plasma membrane in HeLa cells {Ostrowski M., et al., 2010}. Moreover, it was demonstrated that the knock-down of *RAB27A* in mouse mammary carcinoma cells prevent metastasis formation {Bobrie A., et al., 2012} and that human melanoma cells that have high metastatic capability correlate with high levels of RAB27A mRNA {Peinado H., et al., 2012}, suggesting a pro-tumoral and pro-metastatic function of this protein in cancer progression.

2.3.2 Microvesicles originate from the plasma membrane

Microvesicles release is usually a very rapid and calcium-depending mechanism. The increase of intracellular calcium induces the activation of calcium-depending enzymes, such as translocases, that mediate the formation of cholesterol-, sphingomyelin-, phosphatidylserine- and ceramide- rich domains on the plasma membrane. As a consequence, proteins with phospholipidic anchors, cytoskeletal proteins and heat-shock proteins accumulate in those lipid rafts. Due to the particular lipids and proteins composition, the plasma membrane bends outward in a process promoted by enzymes such as calpains that induce cytoskeleton disassembly in that specific region. Vesicles budding is mediated by a signaling cascade that starts from ADP-ribosylation factor 6 and ends with the phosphorylation of the myosin light chain to induce actomyosin contraction {Cocucci E. and Meldolesi J., 2015}.

2.4 Extracellular Vesicles contain biological molecules

It is now well established that EVs can deliver all the known biological molecules (proteins, lipids, metabolites and nucleic acids), but it is very difficult to define components that are univocally conveyed by exosomes or microvesicles because EVs content is distinctive of the donor cell and of its functional and metabolic conditions at the moment of the release {Tetta C., et al., 2013}.

2.4.1 Extracellular Vesicles influence gene expression in target cells through mRNA delivery

The horizontal transfer of genetic material through EVs was discovered in 2007 {Valadi H., et al., 2007}. Of note, in 2008 Skog and colleagues demonstrated that mRNAs are not only delivered by EVs but are also translated by target cells, since they measured a positive luciferase signal in endothelial cells after the uptake of EVs released by glioblastoma donor cells transfected with the luciferase gene {Skog., et al., 2008}. In this study, it was also demonstrated that the EVs transcriptome is not an exact mirror of the donor cells transcriptome, but is enriched in specific RNAs,

indicating a high level of cargo selection during EVs biogenesis and suggesting the possibility to use those RNAs as biomarkers. Indeed, vesicles enriched from primary glioblastoma cells contain almost 2000 RNAs involved in migration, proliferation, histone modification and immune response modulation pathways that are 380 times more enriched respect to the donor cells. On the other hand, 1200 RNAs were found 90 times less enriched. In particular, ribosomal RNAs are always down-represented in EVs, so the absence 18S e 28S in EVs sample is widely used as quality control {Lässer C., et al., 2012}. Moreover, since it was reported that RNAse-treated EVs lose their ability to induce a phenotype in target cells, {Deregibus M.C., et al., 2007}, it was hypothesized that donor cells convey nucleic acids to EVs and transfer them in a way that prevents their degradation {Colombo M., et al., 2014}.

2.4.2 Non-coding RNAs in Extracellular Vesicles can be used as biomarkers

The increasing interest in the study of EVs-delivered micro RNAs (miRNAs) is also due to the fact that these molecules can be used as biomarkers for tumors: indeed, EVs miRNAs profiling in biological fluids could become a non-invasive analysis for cancer diagnosis, as was reported for the staging of ovarian cancer {Taylor D.D. and Gercel-Taylor C., 2008} and for the possibility to early detect a relapse after acute myeloid leukemia {Hornick N.I., et al., 2015}. The use of EVs miRNAs as biomarkers can be extended also to other diseases, as it was demonstrated that neuronal cells infected by prions release EVs that contain a characteristic miRNAs profile, allowing an early diagnosis for a disease that, so far, can be diagnosed *post-mortem* {Bellingham S.A. et al., 2012}.

Moreover, not only miRNAs but also others non-coding RNAs (tRNAs, SRP-RNAs, Y-RNAs and *vault*-RNAs) are selectively conveyed to vesicles and are able to induce a long-term alteration in target cells of their genetic expression {Huang X., et al., 2013}.

2.4.3 Lipids on Extracellular Vesicles membrane have both structural and biological functions

Lipids are essential components of EVs, as they represent almost 2/3 of exosomes' volume {Kreimer S., et al., 2015}. EVs membrane is composed by phospholipids (sphingomyelin and phosphatidylserine above all), ceramide, cholesterol and ganglioside GM3 {Choi D.S., et al., 2013}. The distribution of these molecules mainly depends on the vesicles origin: indeed, the lipidic composition of vesicles released from the plasma membrane is very similar to the one of the donor cells' membrane, while exosomes usually have higher cholesterol levels {Osteikoetxea X., et al., 2015}.

In addition to structural functions, the lipids carried by EVs can exploit biological functions on target cells, for example as it was demonstrated for cancer-derived EVs, in which sphingomyelin on the vesicles membrane has a pro-angiogenic function, promoting endothelial cells migration to form new vessels {Kim C.W, et al., 2002}. On the other side, lipid rafts enriched in cholesterol, sphingomyelin and ceramide and present in EVs can induce apoptosis in cancer cells by activating the NOTCH pathway {Beloribi S., et al., 2012}.

2.4.4 Proteins in Extracellular Vesicles are characteristics of vesicles subtypes and donor cells

EVs proteome has been studied both by semi-quantitative methods such as western blot and immune electron microscopy and by high-throughput methods such as mass spectrometry, liquid chromatography and flow cytometry.

Searching in ExoCarta and Vesiclepedia databases it is possible to understand that basically all the known families of proteins have been detected in EVs isolated both from cell culture media and biological fluids. In particular, as discussed above, these vesicles seem to be enriched in proteins involved in MVBs formation (ALIX, TSG101) and docking (Annexins, Flotillin-1, RAB GTPases), in tetraspanins (CD9, CD63, CD81) and in Heat Shock Proteins (HSP60, HSP70, HSP90), that are often considered as exosomes markers. There are also evidences of a conserved presence of metabolic

enzymes, ribosomal proteins, ubiquitinated proteins, ATPases, adhesion molecules and proteins of the cytoskeleton {Mathivanan S., et al., 2010}, as well as metalloproteinases, glycoproteins and integrins {Kalra H., et al., 2016}.

Several studies tried to identify specific markers to distinguish exosomes from microvesicles, but, up to now, there are not conclusive data. Kowal and co-workers analyzed EVs released by dendritic cells after their fractionation by differential centrifugation at 2000, 10000 and 100000g, demonstrating that tetraspanins, TSG101 and Syntenin-1 are effectively enriched in the population resulting after 100000g ultracentrifugation, while Flotillin-1, Actin, HSP70 and Major Histocompatibility Complex (MHC) -I and –II were identically represented in all of the vesicles populations {Kowal J., et al., 2016}. Finally, it is important to consider the presence of specific proteins in donor cells: for example, neutrophils-derived EVs contain proteolytic enzymes {Gasser O., et al., 2003}, epatocytes-derived EVs contain enzymes involved in detoxification processes {Conde-Vancells J., et al., 2008} and cancer cells-derived EVs contain proteases and growth factors involved in tumor progression {Minciacchi V.R., et al., 2015}.

2.5 Tumor derived Extracellular Vesicles are key players in Pre-Metastatic Niche formation

It has been shown that tumor cells release a larger amount of EVs in comparison with normal cells {Al-Nedawi K., et al., 2009} and that some stimuli, such as hypoxia that normally occurs in a fast-growing tumor mass, promote the production of EVs and modify their composition {Park J.E., et al., 2010}. Taken together, these evidences lead to the conclusion that EVs secretion, composition and function are altered during tumor progression and that EVs play an important role in tumor-host crosstalk, facilitating tumor growth and spreading (that is, PMN formation) {Zhang H.G., et al., 2014}.

Tumor cells-derived EVs have been shown to contribute to PMN formation by transferring their cargo (genetic material, metabolites and proteins) to stromal cells

which populate PMNs {Ratajczak J., et al., 2006}, that are thus reprogrammed towards a pro-metastatic and a pro-inflammatory phenotype in a cancer type and pre-metastatic organ depending manner. For example, Peinado and co-workers demonstrated that B16-F10 murine melanoma cells -derived exosomes are able to horizontally transfer the hepatocyte growth factor receptor Met to bone marrow progenitors cells, that would acquire pro-angiogenic and pro-migratory properties. This resulted in BMDCs exit from the bone marrow to contribute to the formation of PMNs in lungs. The same vesicles also promoted vascular leakiness in lung PMNs, inducing a pro-inflammatory response by increasing the expression of cytokines and chemokines which, in turn, recruit BMDCs to the lung {Peinado H., et al., 2012}. Moreover, it was demonstrated that integrins expressed on breast and pancreatic cancer cells-secreted exosomes determine metastasis organotropism: indeed, the integrin $\alpha_6\beta_4$ heterodimer on the surface of tumor- derived exosomes promotes their homing to lung PMNs, whereas $\alpha_v\beta_5$ targets them to liver PMNs {Hoshino A., et al., 2015}. Furthermore, Sung and colleagues hypothesized a role of EVs in regulating directional cell movement through tissues, in a process that is dependent on integrins/ FN interaction. Indeed, they showed that fibrosarcoma cells secrete FN-coated exosomes at the leading edge that bind collagen fibrils and then interact with cellular integrin receptors, facilitating integrin clustering and strong adhesion formation and leading to accelerated migration (Figure 4) {Sung B.H., et al., 2015}.

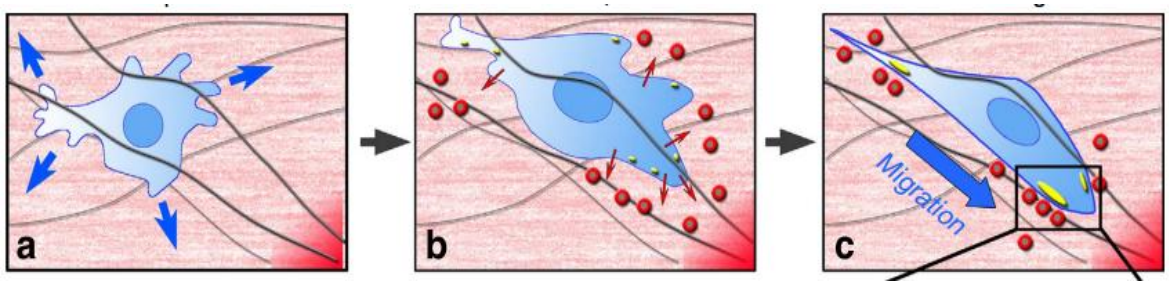

Figure 4: FN-coated EVs determine directional cells movement through tissues.

The unstable protrusions make the cells unable to migrate effectively (a). The secretion of FN-coated exosomes allows cells to reinforce nascent adhesions and stabilize protrusions (b). FN-coated exosomes promote effective and directional motility (c). *(Adapted from Sung B.H., et al., 2015)*

Finally, not only the convey of proteins in EVs is highly regulated and can determine organotropic metastasis, but also the genomic content (in particular miRNAs) is packaged selectively within EVs and is involved in PMN formation, as it was reported for brain metastasis, in which tumor-derived microvesicles suppress glucose uptake by stromal cells through the transfer of miR-122 and the inhibition of pyruvate kinase, increasing glucose availability in PMNs to attract tumor cells {Fong M.Y., et al., 2015}.

2.6 Extracellular Vesicles in clinics: promising biomarkers and therapeutic targets to block PMN establishment

Given their role in PMN formation, their persistence and considered their stability, abundance and easy accessibility in body fluids, EVs are the most promising biomarkers for assessing the risk of tumor progression and metastasis. Indeed, a retrospective study on a cohort of patients with stage III melanoma demonstrated that exosomal levels of the melanoma-specific protein Tyrosinase-Related Protein 2 correlate with metastatic progression {Peinado H., et al., 2012}, while the detection of exosomal miR-105 in the serum of breast cancer patients has been shown to occur at an early stage {Zhou W., et al., 2014}. These evidences lead to the hypothesis that addressing composition of EVs in body fluids of cancer patients can predict both metastatic potential and organotropism before their clinical detection. On the other hand, these vesicles could be therapeutic targets to block PMN formation and metastatic colonization.

Furthermore, since exosomes are able to induce a reprogramming of systemic energy metabolism thus facilitating disease progression, a similar exosome-based strategy could be applied to hinder PMN formation: for example, engineered exosomes might facilitate the delivery of molecules that inhibit the repression of glucose uptake by stromal cells in brain PMNs {Peinado H., et al., 2017}.

Regarding the use of EVs for diagnostic purpose, proof-of-principle studies have demonstrated that exosomes loaded with superparamagnetic iron oxide nanoparticles

or iodine isotopes enables sensitive magnetic resonance or radiographic tracking, demonstrating that approaches of non-invasive imaging of PMN formation *in vivo* are possible {Zhu L., et al., 2014}.

Technical limitations in PMNs analysis (*i.e.* the requirement for *in vivo* microscopy) have hindered the analysis of EV dynamics within PMNs; for this reason, it is important to better define the EVs cargo in order to identify tumor-specific biomarkers that can be then validated in patients {Gold B., et al., 2015}.

Finally, a full characterization of secreted vesicles sub-populations and of their associated cargo is necessary to understand how EVs affect PMN formation, defining, for example, how EVs form, adhere, fuse and educate recipient cells within PMNs, how long does EV-mediated education of recipient cells lasts, and if EVs-mediated education could be reverted to impair metastasis formation and spreading.

3. Melanoma

3.1 Cutaneous melanoma is among the most aggressive and treatment-resistant human cancers

Melanoma represents the 4% of all dermatologic cancers but it is responsible for approximately 80% of skin cancer mortalities and its survival rate dramatically decreases once the tumor has metastasized: indeed, only 14% of patients with metastatic melanoma survive for five years after the diagnosis {Miller A.J. and Mihm M.C. Jr, 2006}.

This cancer originates from melanocytes, that are neural-crest derived cells located not only in the *stratum basale* of the epidermis and in hair follicles, but also in the ear's cochlea and the eye's uvea, as well as in the brain {Yamaguchi Y. and Hearing V.J., 2014}. These cells produce the pigment melanin, which is stored in specific organelles termed melanosomes, that are present within the cells in different maturation steps. In particular, immature melanosomes (stages I and II) lack pigment and are located in the central cytoplasm, while mature melanosomes

(stages III and IV) are heavily pigmented and are placed at distal dendrites of the cells, being ready to be secreted {Raposo G. and Marks M.S., 2007}. Melanosomes secretion occurs in physiological conditions to transfer the melanin from melanocytes to keratinocytes in response of ultraviolet radiation. It was also hypothesized that drug resistance in melanoma is partially due to melanosomes trafficking, that export the chemotherapeutic agents out of the tumor cells {Chen K.G., et al., 2006}, but a direct role of those organelles in promoting melanoma tumorigenesis has yet to be defined.

Melanoma growth is a stepwise process in which melanocytes proliferate from the basal epidermis toward the upper epidermis during the primary stages (melanoma *in situ*). Later, melanoma cells invade the dermis, engaging contacts with blood vessels to start metastatization. The Clark's model describes the histological changes associated with the progression from melanocyte to malignant melanoma {Clark W.H. Jr, et al., 1984}. It was demonstrated that in each stage specific gene mutations affect molecular pathways, driving the process of nevi formation and the subsequent development of dysplasia, hyperplasia, invasion and metastasis {Miller A.J. and Mihm M.C. Jr, 2006}. In particular, mutations in the Neuroblastoma RAS Viral Oncogene Homolog (*NRAS)* and in the B-Raf Proto-Oncogene, Serine/Threonine Kinase (*BRAF)*, that are upstream the Mitogen-Activated Protein Kinase (MAPK) pathway, induce higher melanocytes proliferation, with the formation of benign nevi. These lesions could remain in this stage or become pre-malignant lesions (dysplastic nevi) characterized by the loss of function mutations in *CDKN2A* (Cyclin-Dependent Kinase Inhibitor 2A) and *PTEN* (Phosphatase and Tensin homologue), that control the PI3Kinase/AKT pathway. The combination of *NRAS* and *BRAF* mutations with the loss of *CDKN2A* and *PTEN* drives the melanoma radial growth phase. Vertical growth phase is the following step, in which melanoma cells loose cell-cell adhesion and penetrate through the basement membrane as a consequence of the loss of E-cadherin and gain of *N*-cadherin expression. Finally, the loss of E-cadherin leads to

the dissociation of ß-catenin from the cell adhesion complex. Then, ß-catenin translocates to the nucleus and positively regulates expression of CyclinD1 and of Microphthalmia-Associated Transcription Factor (MITF), which are associated to melanoma cell proliferation, survival and invasion {Prasad C.P., et al., 2015} (Figure 5).

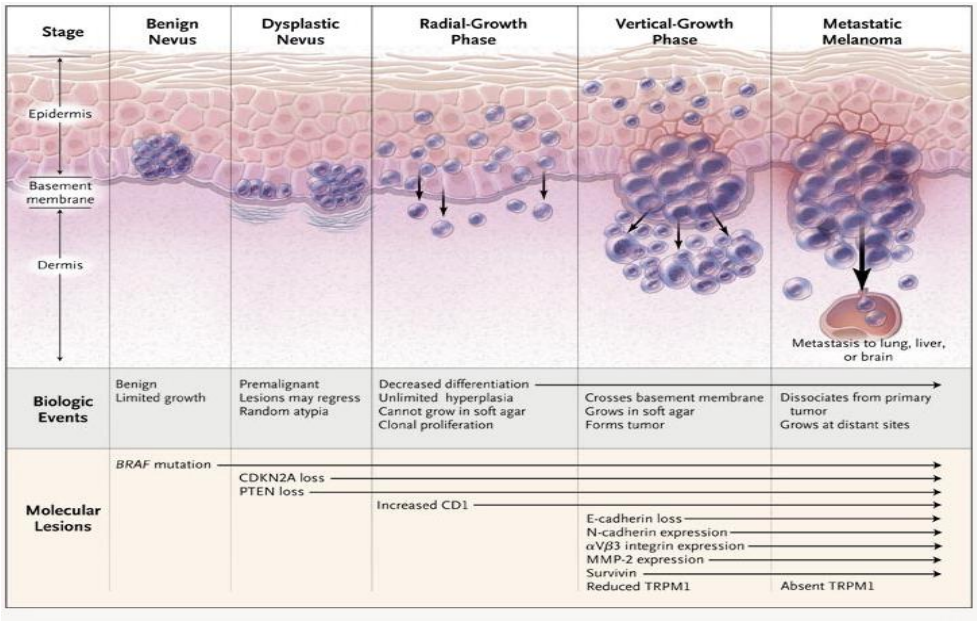

Figure 5: Model of melanoma progression.

The biological events and the molecular lesions that characterize melanoma progression are related to the tumor staging according to the Clark's model. *BRAF* mutation and activation of the MAPK pathway lead to the limited growth of benign lesions within the epidermis (Benign Nevus). Then, mutations of *CDKN2A* and *PTEN* cause the formation of pre-malignant lesions that weak the basement membrane (Dysplastic Nevus). The decreased expression of melanoma markers regulated by MITF leads to a decrease in cells differentiation and to dermis invasion (Radial Growth Phase). Subsequently, the control of cell adhesion is strikingly de-regulated and the tumor mass grow inside the dermis (Vertical Growth Phase). Finally, the loss of E-cadherin and the increased expression of N-cadherin, αVβ3 integrin, and matrix metalloproteinase 2 (MMP-2), as well as the loss of the melanocyte-specific gene melastatin 1 (TRPM1) cause the dissociation of melanoma cells from primary tumor and the growth at metastatic sites (Metastatic Melanoma). *(Adapted from Miller A.J. and Mihm M.C. Jr, 2006)*

It was shown that mutations in *BRAF* gene at codon 600 ($BRAF^{V600}$) occur at early stage in 50% of all melanomas. The most common *BRAF* mutations are $BRAF^{V600E}$ (almost 74% of *BRAF* mutations) and $BRAF^{V600K}$ (almost 20% of *BRAF* mutations), that result in the constitutive up-regulation of the MAPK pathway, thereby promoting cell proliferation and metastasis {Prasad C.P., et al., 2015}. Several studies have been performed to inhibit V600 mutated *BRAF*, leading to the approval

of Vemurafenib and Dabrafenib to target *BRAF*^{V600E} and *BRAF*^{V600K}, that, alone or in combination with other MAPK inhibitors, are able to induce rapid regression of metastatic melanoma. Unfortunately, after the immediate antitumor effect, in patients treated with *BRAF* inhibitors resistance often occurs {Monsma D.J., et al., 2015}. The combination of *BRAF* targeted therapy with immunotherapy has even less positive effects {Luke et al., 2017}. For these reasons, recent studies have highlighted a mechanism that might be responsible for resistance to *BRAF* inhibitors, in order to find new approaches for future combinatorial therapy for malignant melanoma. For instance, it was shown that the signaling of Wingless-related integration site, Family member 5A (WNT5A) is involved in melanoma resistance to *BRAF* inhibitors in addition to MAPK and PI3K/AKT signaling. Indeed, it was demonstrated that different melanoma cell lines have variable WNT5A protein levels, that are very high in *BRAF* inhibitors-resistant cells, and this phenotype was confirmed in clinical specimens, since patients who relapsed after *BRAF* inhibitors therapy showed increased positivity for WNT5A expression {Anastas J.N., et al., 2014}. WNT5A signaling in melanoma cells can trigger the PI3K-AKT pathway, whose up-regulation occur during melanoma progression, as well as it can activate EGFR signaling by MITF inhibition {Prasad C.P., et al., 2015}. Moreover, targeting WNT5A is a promising therapeutic option for melanoma because WNT5A promotes migration and invasion in both normal and *BRAF* inhibitors-resistant melanoma cells {Weeraratna A.T., et al., 2002}.

BRAF inhibitors-resistant melanoma cells can also educate neighboring cells to acquire resistance trough the secretion of EVs: indeed, it was recently published that *BRAF*^{V600E} inhibitor–sensitive metastatic melanoma cells become resistant after the uptake of EVs secreted by neighboring drug-resistant melanoma cells carrying PDGFRß, that is a resistance-driver {Vella L.J., et al., 2017}. Furthermore, the miRNA cargo in the EVs of *BRAF*^{V600E} malignant melanoma cells is altered after the treatment with *BRAF* inhibitors, suggesting that molecules present in EVs may

promote disease progression in patients that receive *BRAF*-targeted treatment {Lunavat T.R., et al., 2017}. Since the majority of *BRAF* inhibitors target only $BRAF^{V600E}$ mutations, it will be important to perform further studies on melanoma cells bearing different *BRAF* mutations to better understand which molecules carried by EVs drive the acquisition of resistance after *BRAF* inhibitors treatment.

3.2 Extracellular Vesicles in melanoma

Several studies reported the secretion of EVs in melanoma, even if it is difficult to clearly identify which EVs subpopulations are secreted by melanoma cells and if one is predominant above the others to sustain cancer progression (see section 2.1). Indeed, it was reported that malignant melanocytes maintain their capability to produce melanin and to transfer it to adjacent keratinocytes trough melanosomes secretion {García-Silva S. and Peinado H., 2016}. At the same time, it is well established that metastatic melanomas secrete high amounts of exosomes, even if NanoSight analysis demonstrated that the size distribution and number of those organelles in the plasma of melanoma patients did not differ based on melanoma clinical stage. Exosome protein concentrations in subjects with Stage IV disease affected the survival rate. Indeed, the prognosis for patients with protein-rich exosomes (>50 $\mu g/mL^{-1}$) has been demonstrated to be worse than the one for patients with protein-poor exosomes (<50 $\mu g/mL^{-1}$) {Peinado H., et al., 2012}. The predominant role played by those organelles in metastatic melanoma was also demonstrated by their capability to promote mobilization of bone marrow progenitors to PMN in distal sites, by increasing vascular permeability in metastatic tissues and by contributing to the organotropism of metastatic cells {Hoshino A., et al., 2015}. Despite these findings, those studies did not evaluate the relevance of melanosomes, since it is not clear if ultracentrifugation and the subsequent fractionation of EVs pellet on sucrose cushion is enough to separate melanosomes from exosomes {García-Silva S. and Peinado H., 2016}.

Moreover, the role of EVs in primary melanoma is still not clearly understood {García-Silva S. and Peinado H., 2016}. Dror and colleagues showed that primary melanoma cells secrete mainly melanosomes, that could be separated from exosomes by centrifugation of the cell culture medium at 20000g {D'Souza-Schorey C. and Clancy J.W., 2012 }. Pigmented melanosomes are transferred to dermal fibroblasts surrounding melanoma *in situ* and promote a cancer-associated phenotype up-regulating genes associated with proliferation, motility and inflammation. In this experiment, the authors postulated that primary melanoma cells hijack melanosome secretory pathways to establish a protective niche, allowing tumor cells to grow and to invade the dermis {Dror S. et al., 2016}.

Considering what mentioned above about the role of exosomes in promoting metastatic progression {Peinado H., et al., 2012} and the role of melanosomes in the early stages of melanoma tumorigenesis {Dror S. et al., 2016}, it is tempting to hypothesize that the secretion of different EVs subpopulations could be an adaptive mechanism employed by melanoma cells to corrupt the surrounding microenvironment favoring tumor progression, and further studies are needed to demonstrate which are the characteristics of those vesicles in order to identify new therapeutic strategies.

Depending on the aggressive state of tumor cells, the extracellular environment is expected to have qualitative and quantitative differences in its composition. A comparative proteomic characterization of the exosomes secreted by isogenic melanoma cell lines to address different contribution to the pre-metastatic niche establishment in metastatic versus primary tumor cells has never been performed.

In this study, we optimized a deep quantitative proteomics protocol to analyze exosomes and secretome composition, as well as the proteome, of primary tumor and metastasis-derived isogenic melanoma cell lines, and we set assays to investigate how the qualitative and quantitative differences we observed in primary tumor versus metastatic microenvironment can affect the behavior of cancer cells.

1. DNA procedures

1.1 Agarose gel electrophoresis

DNA samples were loaded on 1% agarose gels made in TAE buffer containing Gel Red (1:10000; Biotium, Fremont, CA, USA), and then samples were run at 90 V until desired separation was achieved. DNA bands were visualized under a UV lamp.

1.2 Transformation of competent cells

Plasmid DNA was added on a vial containing Stbl3 E.Coli competent cells (Invitrogen, Carlsbad, CA, USA) and incubated on ice for 30 minutes. After 30 seconds of heat-shock at 42°C to promote the entrance of DNA, Stbl3 cells were left on ice for 5 minutes and allowed to grow in Luria-Bertani (LB) medium at 37°C for 60 minutes. Bacteria were harvested by gentle centrifugation (4000rpm for 5 minutes) and resuspended in 50µL of LB before plating them onto LB-Agar plates containing the appropriate antibiotic for the positive selection of bacterial colonies. Plates were incubated overnight at 37°C.

1.3 Plasmid isolation from individual bacterial colonies

Clones picked from individual colonies were allowed to grow at 37°C in 5 mL of LB containing the appropriate antibiotic and then harvested by centrifugation at 16000g for 5 minutes. The Wizard Plus SV Minipreps Kit (Promega, Fitchburg, WI, USA) was used to isolate intact plasmid DNA in TE buffer according to manufacturer's instructions.

1.4 Large scale plasmid preparation

Stbl3 E.Coli competent cells containing plasmid DNA were grown overnight at 37°C into 500mL of LB containing the appropriate antibody. Plasmid DNA was isolated from these cells using the NucleoBond®Xtra Maxi Kit (Macherey-Nagel, Duren, Germany) according to manufacturer's instructions.

2. Cell Culture

2.1 Cell lines and culture conditions

Isogenic melanoma cell lines isolated from the primary tumor and the metastasis of the same patient were used to study melanoma metastasis progression. Providing that, coming from the same patient, these cells share the same karyotype, this model allowed us to be focused on differences in the proteomic content of cells and their secreted vesicles.

In particular, we used WM115 and IGR39 as primary tumor cells, both established from a primary (achromic) cutaneous malignant melanoma, and WM266.4 and IGR37 as metastatic melanoma cells, established from skin and lymph node metastatic sites respectively. All of these cells were available in our cell culture facility and are described as tumorigenic in mice. Moreover, WM115 and WM266.4 cell lines were isolated from a female patient and have V600D mutated *BRAF*, while IGR39 and IGR37 cells were established from a male patient and have the V600E *BRAF* mutation, most common in melanoma (source: Cancel Cell Line Encyclopedia).

Isogenic cell lines were cultured in DMEM medium (Lonza, Basel, Switzerland) supplemented with 10% Fetal Bovine Serum (FBS), 1% penicillin-streptomycin (Microtech, Naples, Italy) and 4mM L-Glutammine (Life Technologies, Carlsbad, CA, USA) at 37°C in a 20%O_2 and 5% CO_2 humidified incubator. All cells were regularly tested for the absence of mycoplasma.

2.2 MTT assay.

Methyl-thiazol-tetrazolium (MTT) assay was performed as previously described {Riss T.L. et al., 2013}. For each cell line tested, 10^4 cells per well were plated in a 96-wells plate and cultured in ultracentrifuged medium for 48 hours or in serum-free medium for 20 hours. MTT (0.5 mg/mL) was added to each plate and incubated for 4 hours to allow formazan crystals formation. After medium removal, DMSO was added to each well and plates were leaved in agitation for 5 minutes at room temperature to allow

formazan crystals resuspension. For each well, the absorbance at 570 nm was read at the Victor multilabel plate reader machine (Perkin Elmer, Waltham, MA, USA). For each cell line, three biological replicates were done and measured in triplicates.

2.3 Growth curve

Primary tumor and metastatic melanoma cells were plated at 10^5 cells/mL in a six well plate. Growth curve was built by counting cells everyday by using a Coulter Counter instrument (Beckman Coulter, Brea, CA, USA). The experiment was conducted as biological replicates and technical triplicates. Statistical analysis and graphic presentations were done using GraphPad Prism Software version 4.01 (GraphPad Software, La Jolla, CA).

2.4 RAB27A Knock Down of metastatic melanoma cells

Mission® Oligos shRNAs 5'-CCAGTGTACTTTACCAATATA-3' (Oligo1) and 5'-CGGATCAGTTAAGTGAAGAAA-3' (Oligo2) were purchased from Sigma-Aldrich. These sequences were chosen in exone-junction region of the *RAB27A* gene to improve Knock Down (KD) efficiency and cloned in a lentiviral shRNA expression system pLKO3.1 (gift of Prof. Giovanni Tonon from Università San Raffaele, Milan, Italy) to stably KD *RAB27A* in WM266.4 and IGR37 cell lines.

2.4.1 ShRNA cloning into pLKO3.1 plasmid

ShRNA oligos were annealed at room temperature and cloned into pLKO.1 puro plasmid upon digestion of the vector with AgeI and EcoRI restriction enzymes (New England Biolabs, Ipswich, MA, USA), followed by ligation reaction using Quickligase (New England Biolabs). Stbl3 E.Coli cells were transformed and positively selected clones were screened for cloning efficiency by sequencing of the pLKO-1 puro plasmid.

2.4.2 Lentivirus production in HEK293T cells

HEK293T cells were plated on 10 cm dishes in order to obtain for the day after cells at 70% of confluence. Cells were transfected with 1mL of a Oligo mix composed by 500µL of the mix containing 10µg of pLKO3.1 plasmid carrying Oligo1, Oligo2 or a Scramble

(Scr) sequence, the third generation lentiviral packaging vectors (pMD2.g_Env, pMDL-RRE_Gag&Pol, pRSV_Rev), 2M $CaCl_2$ and 0.1% Tris-EDTA pH8 (TE), added dropwise to 500µL of HBS solution (50 mM HEPES, 280 mM NaCl, 1.5 mM Na2HPO4, pH to 7.0). The reaction was left for 5 minutes at RT to allow the formation of complexes and then was added to 9 mL of complete cells medium and left over-night at 37°C. The day after, viral particles were concentrated by replacing HEK293T cells supernatant with 5 mL of fresh medium.

2.4.3 WM266.4 and IGR37 cells lentiviral infection

5 mL of HEK293T medium containing concentrated viral particles were filtered with a 0.45µm filter and used to infect $5x10^5$ WM266.4 cells in a 6 wells plate or $5x10^5$ IGR37 cells in a 10cm dish. To increase infection efficiency, polybrene (8µg/mL) was added to the viral supernatant.

RAB27A-KD cells were positively selected for puromycin resistance (final concentration: 1µg/mL) starting from 48h after the infection.

2.5 Colony formation assay

A colony formation assay was used to test the clonogenic ability of both primary tumor and metastatic melanoma cells as previously described {Franken N.A., et al., 2006}. Briefly, $1.5x10^3$ WM115 or WM266.4 cells and $2x10^3$ IGR39 or IGR37 cells were carefully resuspended in 5mL of complete DMEM and seeded in 6 wells to allow the formation of the colonies. After 15 days, colonies were stained with Crystal Violet and counted using FIJI/ImageJ Software {Schindelin J., et al., 2012} in collaboration with Stefano Freddi at MolMed.

2.5.1 Colony formation assay with conditioned media

To investigate if *RAB27A* KD have an impact on a vesicles population that could influence the clonogenic ability of metastatic melanoma cells, EVs were isolated from a 15cm dish of *RAB27A*-wild-type (Scr) or -KD donor cells with the ultracentrifugation protocol and carefully resuspended in the same volume of EVs-depleted DMEM to

maintain the physiological EVs concentration. The supernatant of the 100000g ultracentrifugation contained the soluble factors released by the cells together with the EVs, so it was filtered with a 0.22µm filter and used in parallel with resuspended EVs sample to stimulate *RAB27A*-Scr or -KD cells. Stimulation of recipient cells was done for 6 hours in order to allow them to uptake EVs or soluble factors, then cells were seeded in 6 wells as previously described and colonies stained after 15 days (Figure 6).

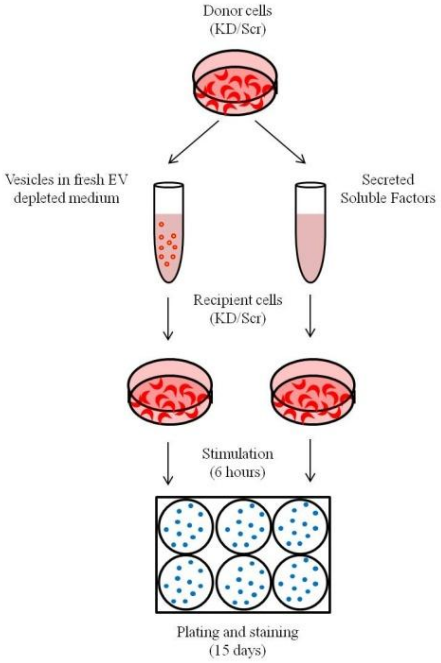

Figure 6: Schematic workflow of the colony formation assay with conditioned media

The supernatant of either *RAB27A*-KD and -WT cells (Scramble) cells was ultracentrifuged to separate EVs from soluble secreted factors. The vesicle pellet was resuspended in the same volume of EVs depleted medium to maintain the physiological vesicles concentration and used in parallel with the secreted soluble factors containing sample to stimulate *RAB27A*-KD and –WT cells for 6 hours before plating. Colonies were stained after 15 days.

The assay was repeated in at least 3 biological replicates in order to have a statistical significance of the results. Statistical analysis was performed with Prism GraphPad Software.

3. Extracellular Vesicles enrichment from conditioned media

3.1 EVs harvesting by serial centrifugation

DMEM medium were supplemented with 20% FBS and ultracentrifuged twice for 16h at 100000g to remove EVs coming from the serum, then diluted 1:2 with serum-free DMEM and supplemented with 1% penicillin-streptomycin and 4mM L-Glutammine, to generate EVs-depleted DMEM.

Melanoma cells were plated at 50% of confluence. The day after, the medium was replaced with EVs-depleted DMEM and cells were grown for 48h to allow the release of EVs in the supernatant. The 48h time point was considered the best moment to collect EVs because cells were at 90% of confluency and over 95% of viability, that allowed us to have a good EVs concentration in the supernatant without possible contamination coming from apoptotic bodies. Cells viability was checked both by Erythrosine incorporation, MUSE®Count&Viability assay (MerkMillipore, Darmstadt, Germany) and MTT assay.

Vesicles were enriched by serial centrifugation as previously described {Thery C. et al., 2006}. Conditioned media were clarified from cells and debris by centrifugation at low speed (5 minutes at 300g). Then, bigger vesicles were removed after centrifugation at 10000g for 30 minutes. The supernatant was filtered in a Stericup Vacuum Driven Sterile Filter (PVDF membrane, very low protein binding, pore size 0.22 µm; MerkMillipore, Darmstadt, Germany), to eliminate protein aggregates and particles bigger than 0.22µm. The EVs pellet was obtained by ultracentrifugation of the filtered supernatant at 100000g for 90 minutes in a Beckman Coulter Optima L-90K ultracentrifuge with a 50.2 Ti rotor (Beckman Coulter). Finally, EVs were washed twice with Phosphate Buffered Saline (PBS) by ultracentrifugation at 100000g for 60 minutes (Figure 7).

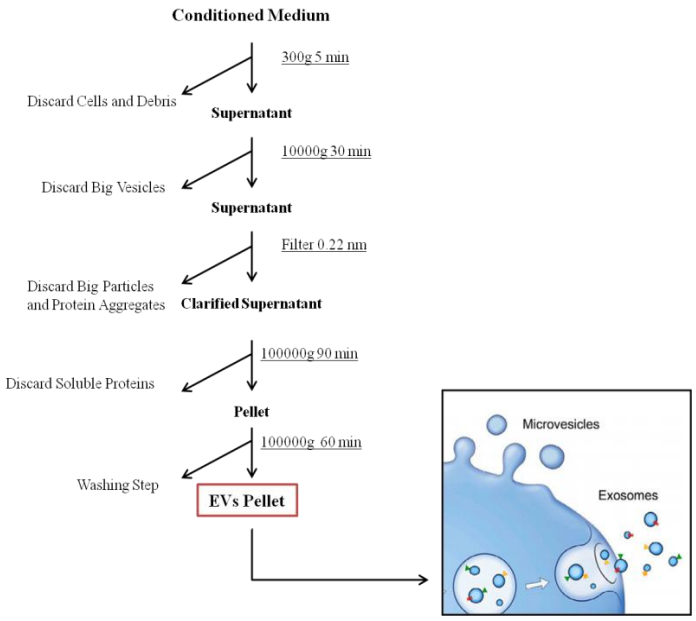

Figure 7: Workflow of EVs enrichment from cells'conditioned media.

The supernatant of donor cells (Conditioned medium) was centrifuged at low speed to discard cells and debris. Big vesicles were eliminated trough 10000g centrifugation and the supernatant was filtered to discard big particles and protein aggregates. The pellet obtained after the ultracentrifugation of the clarified supernatant at 100000g was washed in PBS. It contained a heterogeneous population of EVs, composed of both microvesicles and exosomes. *(Adapted from Théry et al., 2006)*

The number of donor cells was $50x10^6$ for Atomic Force Microscopy analysis and $100x10^6$ for Mass Spectrometry analysis, while for Western Blot analysis we used a number of donor cells that was sufficient to obtain 30 µg of protein lysate.

For all the assays, EVs were not subjected to freeze/thaw cycles. According to the assay, the fresh EVs pellet was resuspended in an appropriate volume of PBS or EVs depleted medium or lysed in RIPA buffer (50mM TrisHCl pH8, 1% NP40, 0.5% Sodium Deoxycholate, 0.1% Sodium Dodecyl Sulfate, 150mM NaCl, 20mM Sodium Pyrophosphate, 2mM PhenylMethylSulfonyl Fluoride, 10mM Sodium Orthovanadate, 50mM NaF) for Western Blot analysis or in Lysis Buffer (8M Urea, 100 mM Tris-HCl, 10mM TCEP, 40mM CAM) for MS analysis.

3.2 EVs fractionation on iodixanol gradient.

3.2.1 Discontinuos gradient fractionation

To further investigate if EVs sample was not contaminated by other organelles, a fractionation of the ultracentrifuged EVs pellet on a discontinuous iodixanol gradient was performed as previously described {Sung B.H. et al., 2015}.

EVs pellet was resuspended in 500µL of Buffer A, composed by 0.25M Sucrose (Carlo Erba Reagents, Milan, Italy), 10mM Tris-HCl, 1mM EDTA pH 7.4. Then, 40% (w/v), 20% (w/v), 10% (w/v) and 5% (w/v) iodixanol solution were prepared by diluting OptiPrep™ (60% (w/v) iodixanol solution; Axis-Shield PoC, Dundee, UK) with Buffer A. The discontinuos gradient was created manually stratifying 20% (3mL), 10% (3mL) and 5% (2.5mL) iodixanol solutions in decreasing densities from the bottom to the top in a 14x89 polyallomer tube (Beckman Coulter) and adding EVs pellet in Buffer A on top of the gradient.

Samples were ultracentrifuged at 100000g for 18h in a SW41Ti rotor (Beckman Coulter). A long ultracentrifugation time was chosen in order to eliminate protein aggregates that could have the same density of EVs, as usual for top-loaded gradients. Eleven fractions were collected from the top to the bottom of the tube. Each fraction was washed twice in 5mL of PBS by 100000g ultracentrifugation for 1 hour to remove iodixanol.

3.2.2 Calculation of the density of each fraction

The density of each fraction was measured plotting the absorbance read at the NanoVue (GE Healthcare, Little Chalfont, UK) on a calibration curve built on 40% (w/v) 20% (w/v) 10% (w/v) and 5% (w/v) iodixanol solutions. In particular, to build the calibration curve it was considered that the density of any gradient solution can be calculated using the equation $\rho = (Vd+V_1d_1)/(V+V_1)$, where ρ is the density of the solution, V and d are the volume and the density of the stock (60% iodixanol solution) respectively and V_1 and d_1 are the volume and the density of the diluent (Buffer A)

respectively. Knowing the amount of iodixanol and Buffer A in each solution and knowing that d=1.320g/mL and d_1=1.030g/mL, the density (ρ) of each solution was calculated as reported in Table 4.

% Iodixanol	ρ g/mL
5%	1.054
10%	1.079
20%	1.127
40%	1.223

Table 4: Calculated density of each iodixanol solution

Calibration curve linearity and reproducibility was tested in order to be sure that experiments done in different days with fresh made or overnight stored at 4°C iodixanol solutions can be compared.

To read the absorbance of the fractions and of iodixanol solutions, 20µL of each sample were diluted 1:10 twice (final dilution: 1:100), then 3 dilution of the same sample were read 3 times at the NanoVue and the average of the measurements was plotted on the calibration curve to calculate the density of each fraction. This protocol allows good gradient reproducibility in different samples (Figure 8).

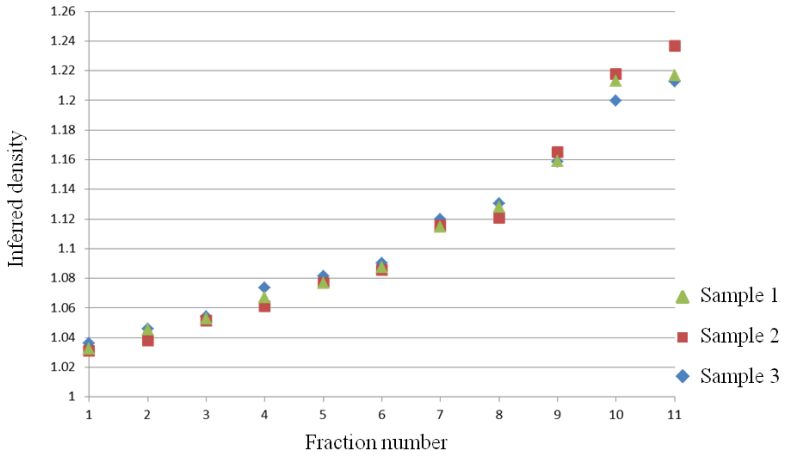

Figure 8: Reproducibility of the density gradient distribution of each fraction in different samples
After the fractionation on discontinuos iodixanol gradient,the density of each fraction was calculated plotting the absorbance read at Nano Vue on the calibration curve built with the standard solution used to prepare the gradient. The graph summarizes the inferred densities calculated for 3 independent samples in 3 different days .

4. Protein Procedures

4.1 Cells and EVs lysis

For western blot analysis, cells were washed in PBS to remove serum proteins and then lysed on ice in RIPA buffer supplemented with Protease Inhibitor Cocktail (Sigma) directly in the cell culture plates using a cell-scraper. EVs lysis was performed in RIPA buffer on the ultracentrifuged pellet.

For proteomics analysis, both cells and EVs pellet were lysed at room temperature in UA Buffer containing 8M Urea (MerkMillipore, Darmstadt, Germany) and 100mM Tris HCl.

Cells membranes and nucleic acids were fragmented by 3 cycles of 30 seconds of sonication at 4°C using a Bioruptor® (Diagenode, Seraing, Belgium) and removed from the samples by centrifugation at 16000g for 20 min at 4°C.

Protein concentration of clarified supernatants was measured by the Bradford assay (Bio-Rad, Hercules, CA, USA) according to manufacturer's instructions.

4.2 Western Blot

The desired amounts of proteins were loaded onto 1 mm thick Criterion™ gels for electrophoresis (Bio-Rad). Proteins were transferred to a nitrocellulose membrane (Bio-Rad) in a Trans-Blot®Turbo™ Transfer System (Bio-Rad). Ponceau staining was used to determine the efficiency protein transfer onto the filters. Filters were blocked for 1 hour (or overnight) in 5% milk in TBS supplemented with 0.1% Tween (TBS-T). After blocking, filters were incubated with the primary antibody, diluted in TBS-T 5% milk, for 1 hour at room temperature, followed by three washes of five minutes each in TBS-T. Filters were then incubated with the appropriate horseradish peroxidase-conjugated secondary antibody diluted in TBS-T for 30 min. After the incubation with the secondary antibody, the filter was washed 3 times in TBS-T (5 minutes each) and the bound secondary antibody was revealed using the ECL method (Amersham) with

a ChemiDoc MP System (Bio-Rad). Densitometric analysis on RAB27a protein levels was performed with Image Lab 5.2 Software (Bio-Rad).

4.3 Antibodies

Antibodies used for western blot analysis were: mouse anti-human Fibronectin (ab26245 Abcam), rabbit anti-human RAB27A (HPA001333, Sigma), mouse anti-human ALIX (2171, Cell Signaling), rabbit anti-human CD81 (HPA007234, Sigma), goat anti-human TSG101 (M-19, Santa Cruz), rat anti-human WNT5A (MAB645, R&D Systems), mouse anti-human Apolipoprotein E (Ab1906, Abcam)

5. Immunofluorescence

WT and *RAB27A*-KD WM266.4 cells were cultured for 24 hours in complete DMEM on gelatine-coated coverslips, then cells medium and soluble debris were removed with 3 washing in PBS. Cells were fixed with 4% paraformaldehyde for 10 minutes and permeabilised at room temperature with 0.25% TritonX-100 in PBS on ice. Cells were incubated with primary antibodies for 1 hour followed by secondary antibodies (Cy3, LifeTechnologies) for 30 minutes, at room temperature. Nuclei were stained by 5 minutes incubation with DAPI (1:5000 in PBS). Coverslips were mounted in glycerol solution (20% glycerol, 50 mM Tris pH=8.4) to avoid mechanical deformation of the sample. Images were captured using a Leica inverted SP2 microscope with a laser scanning confocal system.

6. Proteomics analysis

6.1 Sample preparation

To increase protein recovery, both cells and EVs lysis was performed in strong denaturing conditions in UA Buffer supplemented with 10mM Tris(2-carboxyethyl)Phosphine (TCEP; ThermoFisher Scientific, Waltham, MA, USA) and 40mM Chloroacetamide (CAM), to reduce and alkylate the sample simultaneously. This lysis condition was demonstrated to prevent the loss of sample that typically

occurs in the canonical in-solution digestion, in which centrifugation steps on FASP filters are needed to change the buffer between lysis, reduction and alkylation {Kulak N.A. et al., 2014}.

6.2 Deep quantitative proteomics on isogenic melanoma cell lines and EVs

We optimized a deep quantitative proteomics assay to analyze isogenic melanoma cells proteome and vesicles protein content, coupling the SILAC-based approach with Strong Cationic Exchange (SCX) peptide fractionation, in order to increase both proteome coverage and proteins quantitation accuracy, as represented in Figure 9.

Cells were cultured in complete DMEM supplemented with 10% of dialyzed FBS and the required amounts of isotopically labeled Arginine ($^{13}C_6$ $^{15}N_4$, heavy and $^{13}C_6$, medium) and Lysine ($^{13}C_6$ $^{15}N_2$, heavy and $^{4,4,5,5}D_4$, medium) (CIL laboratories, Tewksbury, MA, USA). We chose heavy and medium labeling instead of the classical heavy and light labeling to avoid any possible contamination of serum proteins for EVs and secretome proteomics analysis, as they would be light labeled. For all SILAC analyses on EVs and soluble secreted factors, samples were mixed 1:1 normalizing on donor cells number.

For deep quantitative analysis of cell proteome, 250µg of protein lysates (medium+heavy) were diluted from 8M Urea to 6M Urea with 100mM Tris HCl and digested 3 hours with Lys-C (WAKO Chemicals, Neuss, Germany). Then, samples were diluted to 2M Urea with 100mM Tris HCl and digested over night with Trypsin (Sigma-Aldrich, Saint Louis, MO, USA). For both the digestions, a 1:50 ratio ($\mu g_{enzyme}/\mu g_{protein}$) was used.

Digested peptides were acidified with 1% Trifluoroacetic Acid (TFA). Urea was removed from the sample by precipitation on ice for 10 minutes and centrifugation at 3000g for 10 minutes. The supernatant was loaded on a Sep-Pak C18 Cartridge (Waters, Milford, MA, USA), that was previously equilibrated with 100% Acetonitrile (ACN) and washed 3 times with 1, 3 and 6 mL of 0.1% TFA. After washing the sample with 1, 5 and 6 mL of 0.1% TFA, peptides were eluted 2 times with 2 mL and once

with 1 mL in 0.1% TFA and 50% ACN, then the eluate was frozen and lyophilized over night.

Lyophilized samples were resuspended in 1% TFA before fractionation on SCX resin beads (ThermoFisher Scientific, Waltham, MA, USA) equilibrated in 0.2% TFA. Peptides were eluted in 4 fractions with increasing concentration of Ammonium Acetate (75-125-200-300 mM Ammonium Acetate in 20% ACN, 0.5% Formic Acid, FA), while the 5th fraction was eluted in 20 mM Ammonium Hydroxide and 80% ACN. Solvents were removed from the sample with centrifugation in a SpeedVac™ Vacuum System and peptides were resuspended in 0.1% FA. 5µg of each eluted fraction was analyzed by combining UPLC with the Q-Exactive HF mass spectrometer (ThermoFisher Scientific, Waltham, MA, USA) on a 180 minutes gradient (Figure 9).

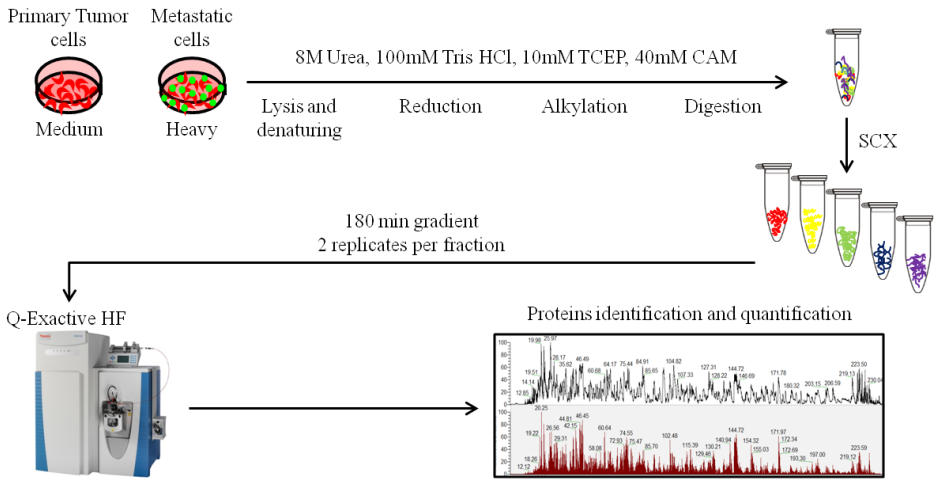

Figure 9: Schematic workflow of the deep quantitative proteomics analysis of isogenic melanoma cell lines.
Primary tumor and metastatic melanoma cells were cultured in DMEM supplemented with either heavy or medium -labeled aminoacids, mixed 1:1 according to their number and lysed in strong denaturing, reducing and alkylating conditions. After digestion, peptides were fractionated in 5 samples through SCX and run on the Q-Exactive HF instrument in technical duplicates on a 180 minutes gradient to identify and quantify differentially expressed proteins.

For deep quantitative proteomics on melanoma EVs, only tryptic digestion and desalting on C18 StageTip were performed as previously reported {Rappsilber J., et al., 2003}. All the peptides were eluted in one single fraction using a 80% ACN 0.1% FA solution and a 75 minutes gradient was used for MS analysis.

For each assay, reverse-labeling experiments were performed to obtain statistical significance.

MaxQuant Software {Cox J. and Mann M., 2008} was used for protein identification and Perseus {Cox J. and Mann M., 2012} was used for quantification and statistical analysis.

Statistically regulated proteins were clustered using EnrichR enrichment analysis {Kuleshov M.V., et al., 2016}.

6.3 Secretome analysis

For the analysis of all the secreted elements in cell culture medium (the so-called secretome, composed by both EVs and soluble proteins), heavy and medium-labeled melanoma cells were plated at 80% of confluence in 15cm dishes and washed three times with PBS and twice with serum-free DMEM to remove serum proteins. Then, cells were cultured in serum-free DMEM for 20h in order to allow the release of a good amount of secreted protein maintaining cells viability over 95% (tested with MUSE® Count&Viability assay).

Secretome analysis was performed in collaboration with Vittoria Matafora in the group. Briefly, conditioned media were centrifuged on VivaSpin 20 PES, 10000 MWCO (Sartorius Stedim Biotech, Aubagne, France) that allowed both to concentrate soluble elements and to change DMEM with UA Buffer in order to perform MS analysis. Since soluble proteins are highly glycosylated, samples were treated with the endoglycosidase PNGaseF (New England Biolabs) to remove N-glycosidic groups before reduction and alkylation and a double digestion (Lys C/Trypsin) was performed to improve secretome coverage.

7. Atomic Force Microscopy analysis

Since EVs size is under the limit of detection of the optical microscopy, Atomic Force Microscopy (AFM), that have resolution at nanometric level, was used to obtain topographic images to have information about vesicles size maintaining vesicles integrity, as previously described {Sharma S., et al., 2011}.

Fresh EVs obtained by ultracentrifugation were resuspended in PBS, previously filtered with a 0.22μm filter in order to eliminate salt aggregates and other particles that could interfere with the analysis, and diluted in de-ionized water (from 1:10 to 1:30 according to vesicles concentration from different donor cells).

Samples were adsorbed to freshly cleaved mica sheets and then dried under a stream of nitrogen. EVs were then analyzed with a Nanowizard 3 AFM instrument (JPK Instruments, Berlin, Germany) under tapping mode and using silicon probes (ACTG probes; AppNano, Mountain View, CA, USA). Topographic height, amplitude, error and phase images were recorded simultaneously at 512x512 pixels (scan area: 25μm^2) at a scan-rate of 0.8Hz.

The measurements of EVs size was done analyzing the topographic height of the acquired images using a macro in FIJI/ImageJ Software in collaboration with Stefano Freddi at MolMed (IEO Milan).

The measurement of EVs size was repeated in at least 3 biological replicates per sample in order to have a statistical significance of the results. Statistical analysis was performed with Prism GraphPad Software.

8. Wound-Healing assay

A Wound-Healing (WH) assay was performed to analyze the collective motility of primary and metastatic melanoma cells.

$3x10^4$ WM115 or WM266.4 cells were carefully resuspended in 70μL of DMEM and plated into each chamber of a Culture-Insert 2 Well (Ibidi GmbH, Planegg, Germany), that allows the formation of a defined 500μm cell free gap in different biological replicates and different cell lines. The inserts were removed after 48 hours, when a uniform cells monolayer was formed, and wound closure was followed for 24 hours in live-imaging using an ORCA-AG camera (6.45μm pixel size; Hamamatsu, Sunayamacho, Japan) on an Olympus IX81 automatic microscope (Olympus, Tokyo, Japan) equipped with an environmental microscope incubator that maintained a

constant temperature of 37°C and a constant perfusion of 5% CO_2 during the whole experiment. Cells pictures were acquired every 5 minutes by differential interference contrast imaging using a 10X objective (binning 2). For IGR39 and IGR37 cell lines, wounds were done manually by scratching the cells monolayer in a 6 well plate with a p200 tip because these cells do not move when seeded in Culture-Insert chambers.

Data analysis was performed in collaboration with Emanuele Martini of the Imaging Technological Development Unit in the Institute using a custom MatLab and FIJI/Image J Software as previously described {Malinverno C., et al., 2017}. Wound closure values correspond to average slopes of linear equations derived from the analyses of the area (μm^2) covered by the cells during the time.

The WH assay was repeated in at least 3 biological replicates in order to have a statistical significance of the results.

9. Gelatin Degradation Assay

Fluorescent-labeled gelatin was prepared with Alexa Fluor®594 Protein Labeling Kit (Thermo Fisher Scientific) according to manufacturer instruction.

The assay was carried out as previously described {Artym V.V., et al., 2009} with the following modifications. Autoclaved glass coverslips were washed once in 70% Ethanol, three times in sterile PBS and finally in sterile H_2O to remove salt aggregates from PBS. Then, air-dried coverslips were coated with fluorescent-labeled gelatin (final concentration: 2mg/mL) and fixed with 0.5% ice-cold glutaraldehyde in PBS at 4°C for 15 minutes. After three washes in PBS, coverslips were incubated for 3 minutes at room temperature with 5mg/mL Sodium Borohydride in PBS to reduce aldheydic groups, washed and sterilized again with 70% Ethanol and finally quenched in complete DMEM for 1h at 37°C.

10^5 WM115 or WM266.4 cells were seeded on fluorescent gelatin coated coverslips transferred in 6wells and fixed with 4% parafolmaldheyde 9 or 12 hours after their adhesion; these time points were chosen as the best condition to allow invadopodia

formation before cells start to move. After the permeabilization in 0.25% TritonX-100 in PBS on ice, actin structures and nuclei in the cells were stained by 1h incubation of FITC-Phalloydin (1:50 in PBS) and 5 minutes incubation with DAPI (1:5000 in PBS) respectively, then coverslips were mounted in mowiol solution and images were captured using a wide-field Olympus BX51 Upright microscope.

10. Proteostat® aggresome detection assay

In order to detect intracellular amyloids in primary and metastatic melanoma cells, Proteostat® Aggresome Detection Kit (Enzo Life Sciences, Farmingdale, NY, USA) was used according to manufacturer's instructions.

Briefly, $1.6x10^5$ WM115 or WM266.4 cells were plated in 6 wells and allowed to adhere on 0.5% gelatin-coated glass coverslips. After 24 hours, cells were fixed with 4% paraformaldehyde for 10 minutes, and permeabilized on ice with 0.25% Triton-X100 and then incubated with Proteostat® reagent (1:2000 dilution) for 1 hour followed by DAPI nuclear staining for 5 minutes, at room temperature. Coverslips were mounted in a 20% glycerol solution to avoid mechanical deformation of the sample and images were captured using a Leica inverted SP2 microscope with a laser scanning confocal system.

1.Primary tumor and metastasis derived melanoma cells release qualitative and quantitative different Extracellular Vesicles

1.1 Metastasis and primary tumor derived cell lines have the same shape and proliferation rate

Advanced melanoma is among the most aggressive human cancers whose survival rate dramatically decreases once the tumor has metastasized {Miller A.J. and Mihm M.C. Jr, 2006}. Melanoma cells produce a large quantity of exosomes in comparison to normal melanocytes {Dror S., et al., 2016} and several studies have shown that the plasma of melanoma patients contains increased amounts of exosomes compared to plasma of healthy individuals {Logozzi M., et al., 2009}. However, a comparative proteomic characterization of the exosomes secreted by isogenic melanoma cell lines to address different contribution to the pre-metastatic niche establishment in metastatic versus primary tumor melanoma cells has never been performed.

As model of primary tumor and metastatic melanoma, we choose the isogenic cell lines WM115 (primary tumor)/WM266.4 (skin metastasis), and IGR39 (primary tumor)/IGR37 (lymph node metastasis). Despite the fact that these cells pairs share the same karyotype, their aspect and their proliferation rate is very different. More in detail, both metastatic cells (WM266.4 and IGR37) have a spindle-like shape (Figure 10A) and grow faster than primary tumor cells (WM115 and IGR 39) (Figure 10B).

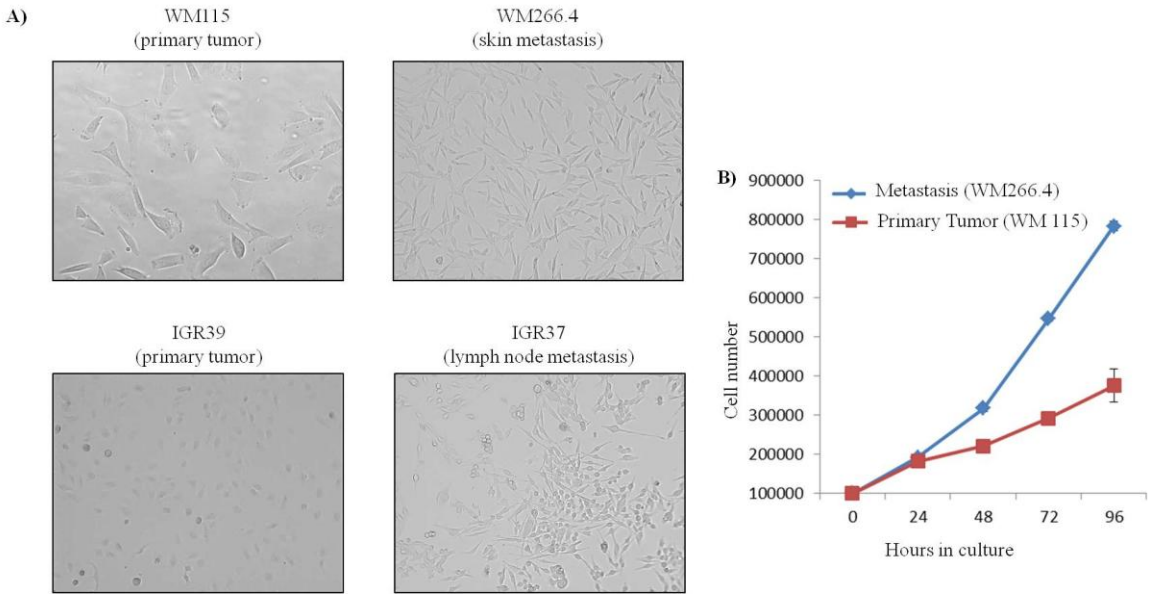

Figure 10: Metastasis and Primary Tumor isogenic melanoma cell lines show the same aspect and proliferation rate.

A) Metastasis derived cells WM266.4 and IGR37 are small and show a spindle-like shape while primary tumor derived WM115 and IGR39 cells are bigger and show epithelial-like shape.

B) Metastatic cells have higher proliferation rate when compared to primary tumor cells. The graph is referred to WM266.4/WM115 cells pairs as example

1.2 Ultracentrifugation of conditioned media results in enrichment of Extracellular Vesicles

So far, the term "exosomes" is often referred to an heterogeneous population of vesicles isolated through several techniques without any demonstration of their intracellular origin into multivesicular bodies (as discussed in the introduction, section 2.1) {Tkach M. and Théry C., 2016}. For this reason, we refer to Extracellular Vesicles (EVs) as the population of vesicles obtained following the canonical vesicles enrichment from conditioned media based on serial centrifugation {Théry C., et al., 2006}.

Isogenic melanoma cells were plated at 50% of confluence and, one day after plating, the medium was replaced with EVs-depleted DMEM. Conditioned media were then collected after 48 hours, when cells reached about 90% of confluency. No significant impairment in cell viability was observed by Methyl-Thiazol-Tetrazolium (MTT) assay when cells were cultured in EVs-depleted DMEM. Moreover, both erythrosine incorporation and MUSE®Count&Viability measurements resulted in >95% cells

viability, indicating that the presence of apoptotic bodies in the cells conditioned medium is irrelevant for the purpose of the EVs study (Figure 11).

A)

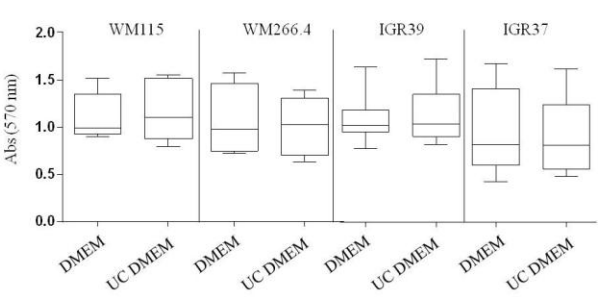

B)

	WM 266.4		WM 115		IGR-37		IGR-39	
Hours	n of cells	Viability (%)	n of cell	Viability (%)	n of cells	Viability (%)	n of cell	Viability (%)
0	100000		100000		100000		100000	
24	108000	98.8	94000	98.4	96700	94.2	163000	98.6
48	222000	99.6	221000	99.2	265000	99.4	334000	95.6

Figure 11: Viability of isogenic melanoma cells is maintained in EVs-depleted DMEM.

A) MTT assay demonstrates that no significant impairment in cells viability can be observed when comparing EVs-depleted DMEM (UC DMEM) and control medium (DMEM).

B) MUSE®Count&Viability Assay shows that isogenic melanoma cells are able to duplicate after 48 hours in EVs-depleted DMEM maintaining their viability above 95%.

The quality of vesicles enrichment was assessed by Western Blot (WB) analysis evaluating the enrichment of well-known EVs-associated proteins (TSG101, ALIX, CD9, CD63, and CD81) and the absence of other cellular compartment-markers, following the guidelines published by Lötvall et al.{Lötvall J., et al., 2014} (Figure 12).

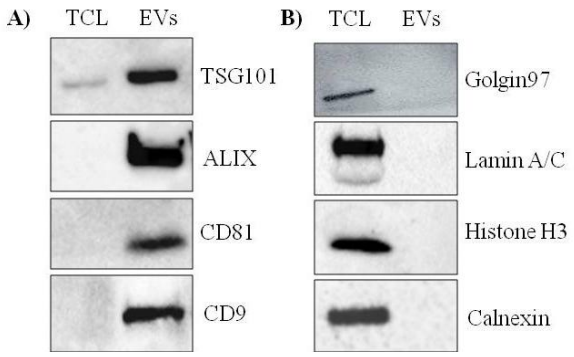

Figure 12: The ultracentrifuged pellet is enriched in EVs and is not contaminated by organelles coming from other cellular compartments.

A) EVs specific proteins TSG101, ALIX, CD81 and CD9 are enriched in the pellet (EVs) when compared to the Total Cell Lysate (TCL).

B) Markers of Golgi Apparatus (Golgin 97), Nucleus (Lamin A/C and Histone H3) and Endoplasmic Reticulum (Calnexin) are enriched in TCL respect to EVs.

The panel shows results obtained with WM266.4 cells and is indicative of all the four isogenic melanoma cell lines.

Considering that EVs size is under the limit of detection of optical imaging, we used nanometer-resolved Atomic Force Microscopy (AFM) to obtain topographic images maintaining vesicles integrity. The diameter of EVs was calculated with ImageJ Software as previously described {Sharma S., et al., 2011}. Our analysis showed that the mean size of enriched vesicles is 60nm in diameter, consistent with the presence of exosomes (Figure 13, A). These data confirmed previous measurement by Nanosight analysis, that revealed the presence of a distinct vesicles population with an average size of 75nm (Figure 13, B).

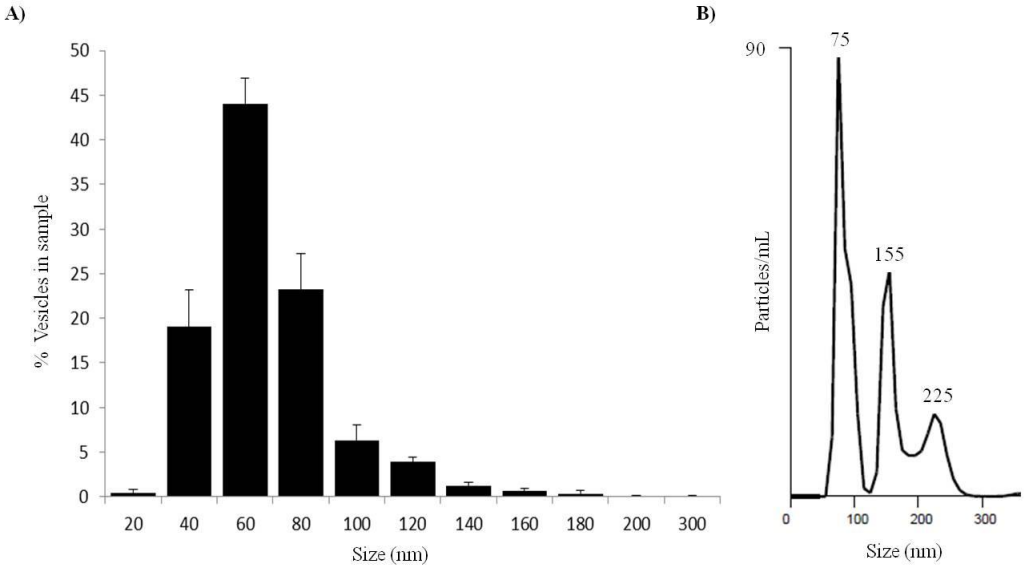

Figure 13: EVs size in the ultracentrifuged pellet is consistent with exosomes size.

A) AFM analysis on EVs demonstrated that the mean EVs diameter is 60 nm.

B) Nanosight analysis on EVs showed enrichment in a population with 75nm of diameter.

Finally, to better differentiate between vesicles and protein aggregates that could precipitate together during the ultracentrifugation step, we optimize a fractionation of the EVs pellet on a discontinuous iodixanol gradient. For both primary tumor and metastatic cell lines, we enriched EVs in a density between 1.08 and 1.11 g/mL of iodixanol, which is the one reported in literature for melanoma exosomes {Sung B.H., et al., 2015} (Figure 14).

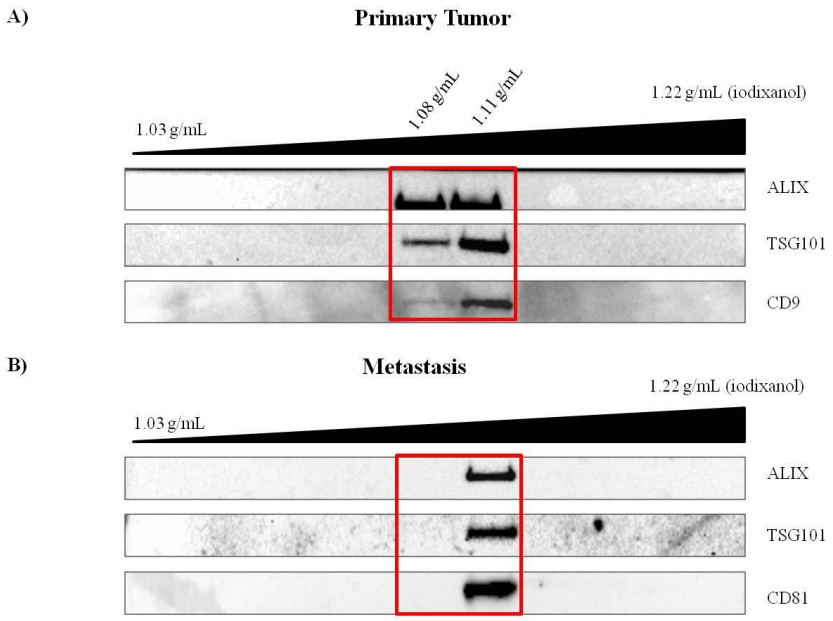

Figure 14: Ultracentrifuged pellet are enriched in melanoma exosomes.

WB analysis on isolated EVs fractions demonstrates an enrichment of EVs proteins ALIX, TSG101, CD9 and CD81 in a density range between 1.08 and 1.11 g/mL both in WM115 primary tumor cells (Panel A) and in WM266.4 metastatic cells (Panel B).

1.3 Primary tumor cells release more and bigger EVs respect to metastatic cells

Providing that the extracellular environment is expected to contain qualitative and quantitative differences depending on the tumor progression state {Muralindharan-Chari V., et al., 2010}, we used AFM imaging and FIJI/ImageJ Software to count the number of vesicles released by the same number of donor cells and to measure their size.

For both WM115/WM266.4 and IGR39/IGR37 couples, we found that primary tumor cells release a larger number of vesicles with respect to metastatic ones (Figure 15, A and B). Moreover, we observed that the area of EVs released by primary tumor cells was bigger when compared to the area of EVs released by metastatic cells (Figure 15, C), indicating that primary tumor and metastatic cells could secrete different population of EVs.

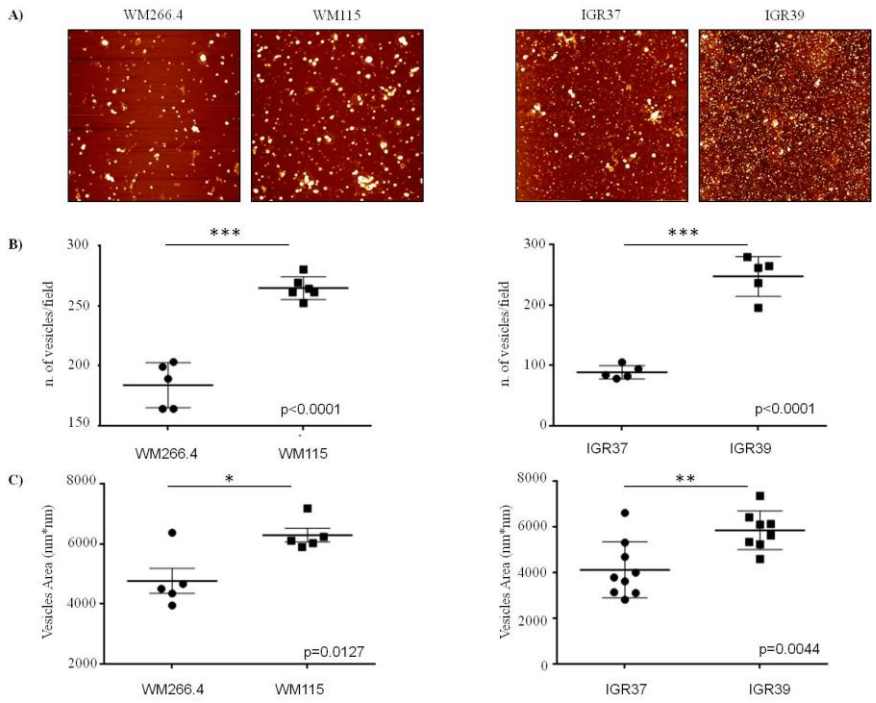

Figure 15: EVs from primary tumor cells are larger in number and size than EVs released by metastatic cells.

A) Images of topographic height of the EVs released by the four melanoma cell lines.

B) Statistical analysis of the number of EVs per field demonstrates that for both isogenic melanoma cells pairs primary tumor cells release more EVs than metastatic cells.

C) Statistical analysis of the EVs area (expressed in nm*nm) demonstrates that for both isogenic melanoma cells pairs primary tumor cells release bigger EVs than metastatic cells.

1.4 Deep quantitative proteomics on melanoma EVs

1.4.1 The majority of the identified proteins belong to primary tumor derived EVs

We performed a deep quantitative proteomics analysis on EVs enriched from the same number of isogenic melanoma cells. We took advantage of the SILAC approach, labeling cells with heavy- and medium aminoacids, to measure the relative quantitation of each protein and to discriminate contamination from FBS proteins. The latter ones, being naturally light-labeled, could be excluded from the analysis by selecting only the heavy and medium-labeled aminoacids.

As reported in the graph in figure 16A, we observed an increased amount of proteins coming from the primary tumor *vs* metastatic cells, and this observation was also validated by WB (Figure 16).

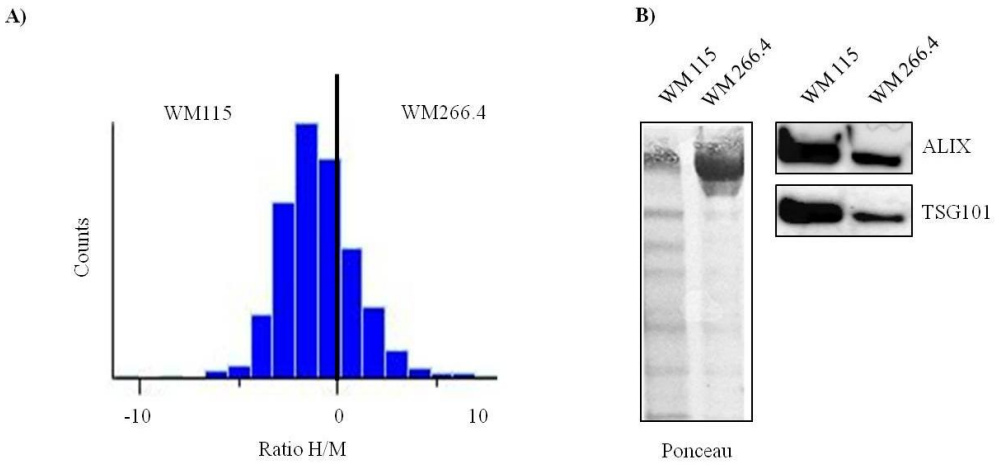

Figure 16: The majority of identified proteins belong to primary tumor EVs.

A) Ratio distribution of quantified proteins in primary tumor (WM115) vs metastatic (WM266.4) isogenic melanoma cells derived EVs shows that the majority of the proteins belongs to primary tumor derived EVs, that are medium-labeled.

B) WB analysis validates the proteomics analysis both at the global proteome level (Ponceau) and following EVs enriched proteins expression (ALIX, TSG101).

This result confirmed what we have previously observed by AFM analysis, where we noticed that primary tumor released EVs are bigger and more abundant with respect to metastatic EVs (Figure 15).

1.4.2 EVs protein content is different between primary tumor and metastatic cells

With deep quantitative proteomics, we were able to identify and quantify more than 700 proteins in EVs released from WM cells and close to 1000 proteins in EVs released by IGR cells. Since about 350 proteins were shared between the two isogenic melanoma cells pairs, we looked at the normalized ratio of those proteins in order to identify candidates that can be considered markers of primary tumor-derived or metastasis-derived EVs. In particular, we focused on proteins that were significantly regulated (p value <0.05) in both WM and IGR EVs. We noticed that the majority of the proteins significantly enriched in EVs released by metastatic cells belongs to metabolic pathways or have a function in the Extracellular Matrix (ECM) organization. This observation can explain the fact that the EVs pellet enriched from metastatic cells is sticky and hard to be re-dissolved in PBS, in accordance with the physical characteristics of the ECM components. On the contrary, primary tumor

derived EVs are enriched in proteins related to signaling pathways and cell migration (Table 5).

	Pathway	Molecular Function	Gene name	WM266.4/WM115 Log_2 Ratio	IGR37/IGR39 Log_2 Ratio
Up-regulated in EVs secreted by metastatic cells	Metabolism	Lipid digestion, mobilization, and transport	**APOE**	**7,04791**	**6,60733**
			APOB	2,0181	3,76589
			APOM	5,30906	3,31341
			BMP1	1,92522	1,48306
			HSPG2	4,85433	3,89731
			P4HB	1,18652	1,6505
		Metabolism of carbohydrates	EXT1	1,2041	1,13144
			MDH1	1,35003	2,19428
			PYGL	2,34499	0,951156
			OGN	2,22176	3,38071
			TKT	0,993063	0,846163
			PGD	3,17488	1,37028
			ADH5	1,1269	1,14871
			IDH1	1,69493	1,40314
			GSTP1	1,84902	3,42719
			GSTA2	4,87032	4,98763
	Extracellular matrix organization	Collagen fibers formation	MMP14	0,75441	2,89305
			COL4A1	5,37536	1,82411
			SERPINH1	1,08473	0,672313
			PLOD3	3,48424	2,25105
			PLEC	1,1141	1,32399
		Integrin/cell surface interaction	**FN1**	**5,73255**	**2,70512**
	Membrane trafficking	Vesicles mediated transport	HSPA8	0,55669	2,65829
			MYO1C	0,64434	1,14393
			TFRC	0,625442	5,64594
			RAB14	1,89022	1,24374
			GALNT2	1,06676	1,2678
			KIF5B	1,37851	0,579292
			HSP90B1	2,8196	2,3413
Up-regulated in Evs secreted by primary tumor cells	Axon guidance	Cell migration in response to chemotaxis	**WNT5a**	**-5,39163**	**-1,37093**
			SLIT2	-3,72072	-1,88185
	Organization of actin cytoskeleton	Actin fibrils and adhesion formation	EDIL3	-4,22779	-1,74521
			TMSB10	-1,10216	-1,77201
	MAPK activation		TLN1	-1,08309	-2,13463
	Pyrimidine metabolism		NT5a	-3,09909	-1,44848
	Synthesis of GPI-anchored proteins		PLAUR	-3,73837	-1,82518

Table 5: Proteins significantly regulated in metastasis-derived or primary tumor-derived EVs.

Proteins up-regulated in EVs secreted by metastatic cells belong to pathways highlighted in red, while proteins up-regulated in EVs secreted by primary tumor cells belong to pathways highlighted in green.

1.4.3 Isogenic primary tumor and metastatic melanoma cells have different secretomes, suggesting an invasive vs a proliferative behavior

Since the extracellular environment is expected to contain qualitative and quantitative differences between primary tumor and metastatic cells, we decided to use deep quantitative proteomics to analyze the isogenic melanoma cells secretome. We refer to secretome as the sample obtained after the concentration of the whole cell culture supernatant, containing both EVs and soluble secreted factors.

The study of the entire secretome together with the EVs proteome allowed us to have a complete overlook of the proteins differentially secreted by isogenic primary tumor and metastatic melanoma cells, providing better indications of the cells behavior. Moreover, since the secretome samples contains EVs, the results obtained with this

analysis validated what we observed by deep quantitative proteomics on EVs, indicating candidates that can be considered markers secreted by primary tumor or metastatic melanoma cells.

As we did for EVs deep quantitative proteomics, we used heavy- and medium-labelled aminoacids to achieve relative quantitation of each protein. We plated the cells in FBS-depleted media to eliminate FBS proteins, that could impair the identification of proteins coming from the cells. Moreover, as a large number of proteins in the secretory pathway are N-Glycosylated {Aebi M., 2013}, to improve secretome coverage we decided to use the endoglycosidase PNGaseF to remove N-glycosidic groups from the proteins before the reduction and alkylation steps, thus allowing the digestion of highly glycosylated proteins.

We identified and quantified more than 2000 proteins in the secretome of both isogenic melanoma cells pairs, and around 200 of them were differentially secreted (FDR <0.05) in primary tumor vs metastatic cells.

In particular, both WM115 and IGR39 cells secretome was enriched in Matrix Metalloproteinases (MMPs), that contribute to ECM remodeling and vascular disruption trough ventral actin-rich membrane protrusions called invadopodia. The ability of tumor cells to form invadopodia directly correlates with their capacity to invade the local stroma and its associated vascular components {Martin K.H., et al., 2012}. Therefore, we used gelatin degradation assay to visualize invadopodia-mediated ECM degradation of cells by fluorescence microscopy, demonstrating that primary tumor cells form a higher number of invadopodia than metastatic cells (Figure 17). This finding suggests that primary tumor cells have an invasive phenotype, having the ability to degrade ECM to pass through the basement membrane and the walls of the circulatory and lymphatic systems.

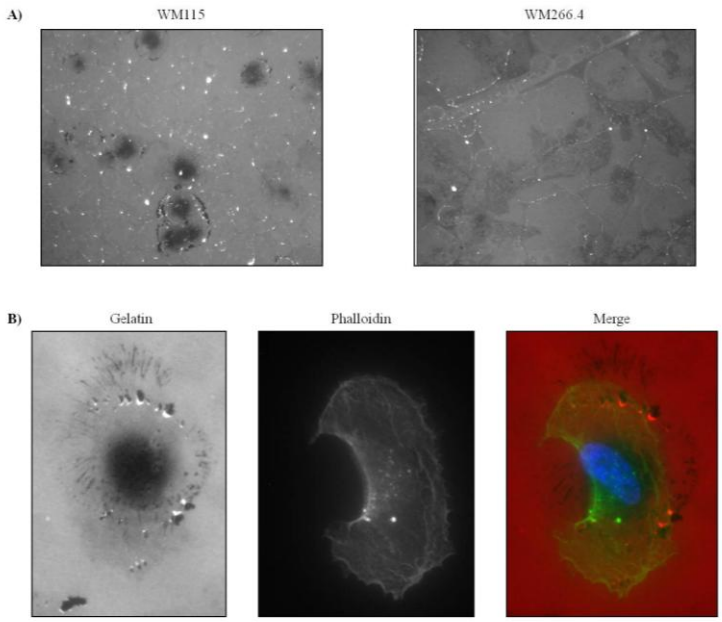

Figure 17: Primary tumor cells show invasive behavior.

A) 20X images of fluorescent-gelatin coated coverslips show that primary tumor cells are able to degrade fluorescent gelatin more than metastatic cells (time point: 9 hours).

B) 40X magnification on a WM115 cell showing gelatin degradation by invadopodia: the black dots inside the cell in the gelatin channel correspond to the brighter dots in the phalloidin channel, used to label actin.

On the contrary, WM266.4 and IGR37 cells secretome is enriched in proteins involved in ECM deposition, fibril deposition and cell adhesion molecules. Since the deposition, remodeling and signaling of ECM components influences the final outgrowth of macrometastases {Venning F.A., et al., 2015}, we hypothesize that metastatic cells have a proliferative behavior but further assays are necessary to validate this hypothesis. Moreover, lipid transporters such as Apolipoprotein E (APOE) and proteins belonging to the vesicles trafficking pathway, in particular melanosomal proteins, are significantly enriched in the secretome of metastatic cells (Figure 18).

By combining the deep quantitative proteomics results obtained on EVs proteome, total cell proteome (see paragraph 3) and secretome, we decided to focus our following studies on APOE, Fibronectin (FN) and Wingless-related integration site family member 5A (WNT5A), highlighted in the Table 5 and in Figure 18.

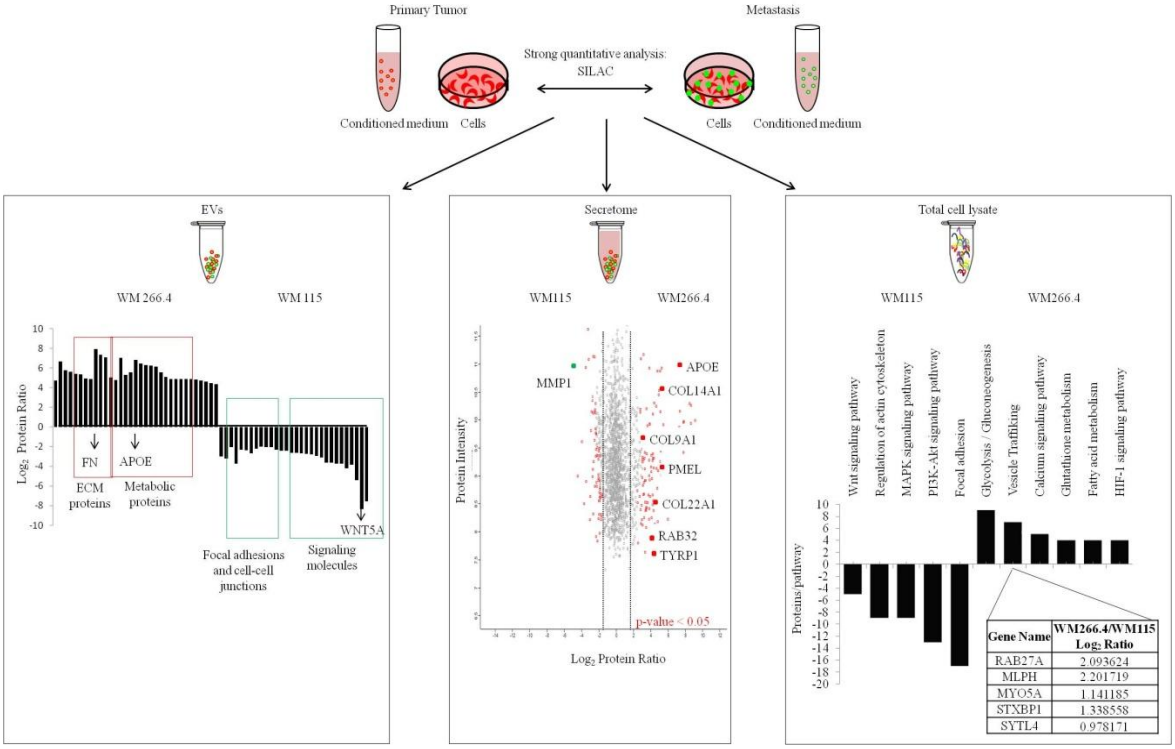

Figure 18: Summary of the proteomics results on EVs proteome, isogenic melanoma cells secretome and proteome.

Left: The majority of the proteins significantly enriched in metastatic melanoma cells derived EVs are involved in metabolic pathways and extracellular matrix deposition, while primary tumor cells derived EVs are enriched in proteins involved in cell adhesion and in signaling pathways. Fibronectin (FN) , Apolipoprotein E (APOE) and WNT5A are the most significantly regulated proteins in metastatic and primary tumor cells derived EVs, respectively (better described in Table 5).

Middle: Matrix Metalloproteinase 1 (MMP1) is significantly enriched in the secretome of primary tumor cells. On the contrary, the proteins significantly enriched in the secretome of metastatic melanoma cells belong to the collagens family (COL14A1, COL9A1, COL22A1) or are melanosomal proteins (RAB32, TYRP1). Of note, PMEL and APOE are significantly enriched in the secretome of metastatic melanoma cells.

Right: The graph represent the pathways significantly up-regulated in the proteome of isogenic primary tumor and metastatic melanoma cells (better described in in section 3). Among proteins of the vesicles trafficking pathway, RAB27A and its known effectors are highlighted in the table.

2. Fibronectin and WNT5A are EVs-associated proteins, while APOE is mainly secreted as soluble factor

2.1 Fibronectin is the major component of metastasis derived EVs

ECM proteins were significantly enriched in metastatic cells derived EVs (Table 5).

In particular, Fibronectin (FN) was found as the major component of WM266.4 EVs, and its specific EVs enrichment was sustained by the observation that this protein is not significantly enriched in metastatic cells proteome and secretome, suggesting that this protein could have an important role in metastatic cells derived EVs (Figure 19).

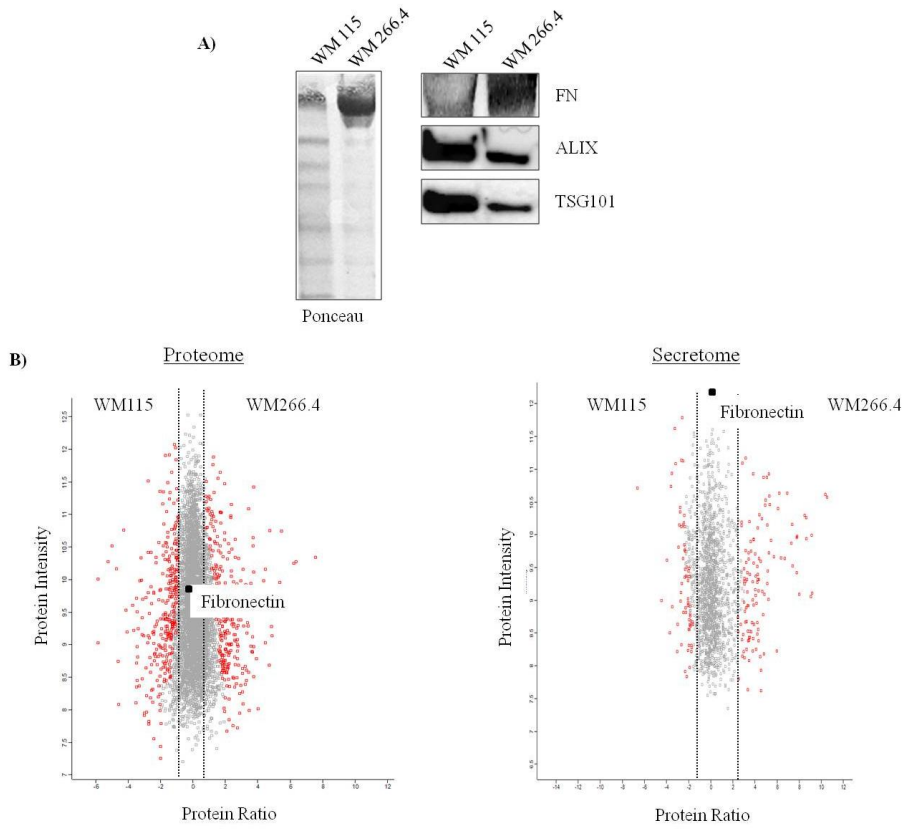

Figure 19: Fibronectin is enriched in metastatic cells secreted EVs.

A) WB analysis to validate that Fibronectin is the most abundant protein in WM 266.4 EVs.

B) Fibronectin enrichment is not significant in WM266.4 proteome and secretome.

Significantly enriched proteins (p value <0.05) are highlighted in red and are distributed outside of the dotted lines.

To investigate the role of EVs-associated FN, we optimized a discontinuous iodixanol gradient for EVs fractionation. When applied to metastatic cells derived EVs, this approach resulted in FN enrichment in two different fractions, suggesting that it may be present in two different form: one soluble and another EVs-associated (Figure 20).

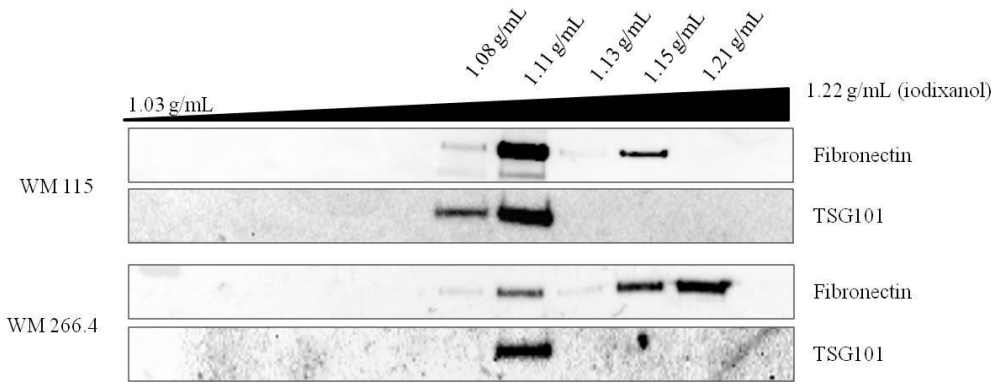

Figure 20: Fibronectin is enriched at higher densities in WM266.4 respect WM115 samples.

WB analysis demonstrates that, after the fractionation of EVs pellets on iodixanol gradient, fibronectin secreted by WM266.4 cells is enriched mainly at higher iodixanol densities. TSG101 is used as control for EVs banding densities.

The dual behavior of FN, that is both soluble and EVs-associated, is still under investigation. We reasoned that the EVs-associated FN could regulate the directional cell movement through tissues, as it was described by Sung and colleagues in fibrosarcoma-derived exosomes {Sung B.H., et al., 2015}.

2.2 WNT5A is enriched in primary tumor secreted EVs

The quantitative proteomics analysis revealed that WNT5A is one of the more significantly enriched proteins in primary tumor-released EVs (FDR <0.05). Since this protein is known to be secreted as soluble factor and its presence in melanoma exosomes has hardly been described, we validated its EVs-association by WB analysis after the fractionation on iodixanol gradient (Figure 21, A). Moreover, for both primary tumor and metastatic melanoma cell lines, we demonstrated that WNT5A is mainly enriched in EVs pellet rather than in the EVs-depleted-soluble factors-containing sample (named soluble factors) obtained by concentrating the supernatant of the 100000g ultracentrifugation step (Figure 21, B).

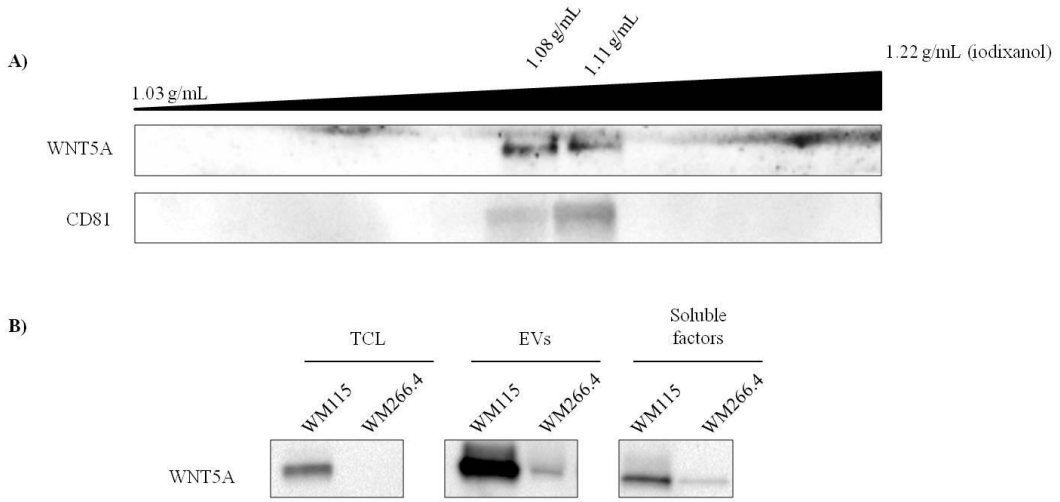

Figure 21: WNT5A is enriched in primary tumor EVs.

A) The fractionation of EVs pellet secreted by IGR39 cells demonstrates the presence of WNT5A protein in the same fraction of EVs (CD81 was used as control of EVs banding density).

B) The enrichment of WNT5A protein is higher in EVs than in the Total Cell Lysate and in the soluble factors containing sample. Images were cut to display only significant lanes (Loading: 30µg of each sample).

It was reported that *WNT5A* overexpression in melanoma cells leads to an increased motility and invasion {Weeraratna A.T., et al., 2002}; for this reason, we hypothesized

that the delivery of WNT5A inside EVs might determine its horizontal transfer to neighboring cells to allow melanoma progression.

2.3 APOE is mainly secreted as soluble factor in metastatic melanoma cells

By combining the proteomics results on EVs and secretome in WM115/WM266.4 and IGR39/IGR37 cells, we found APOE as abundant component of metastatic microenvironment, being significantly enriched (FDR <0.05) both in EVs and in the secretome (Figure 22, A). However, differently from WNT5A, we observed the majority of the secreted APOE in the soluble factors sample (Figure 22, B) even if the fractionation of EVs pellet on iodixanol gradient demonstrated that this protein is enriched also in metastatic melanoma EVs (Figure 22, C).

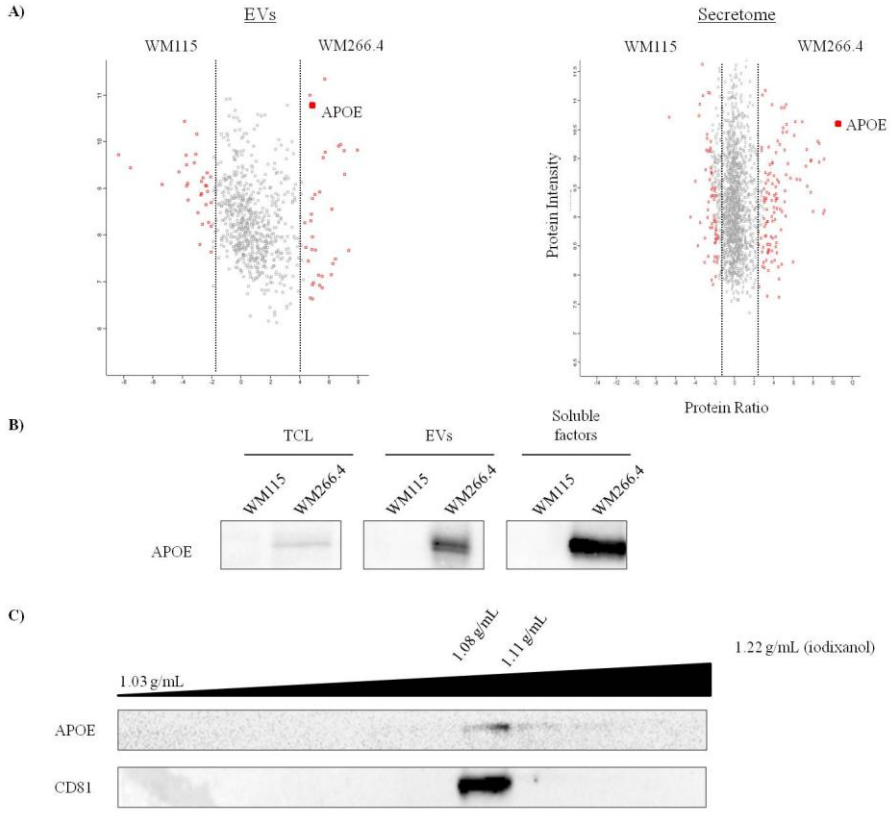

Figure 22: APOE is secreted as soluble factor by metastatic melanoma cells.

A) APOE is significantly enriched both in metastatic melanoma cells secreted EVs and in metastatic melanoma cells secretome. Significant proteins (FDR<0.05) are highlighted in red outside the dotted lines.

B) The enrichment of APOE protein is higher in the soluble factors containing sample than in the Total Cell Lysate and in the EVs. Images were cut to display only significant lanes (Loading: 30µg of each sample).

C) The fractionation of EVs pellet secreted by WM266.4 cells demonstrates the presence of APOE in the same fraction of EVs (CD81 was used as control of EVs banding density).

Membrane-bound APOE in exosomes has been shown to regulate Premelanosome Protein (PMEL) amyloid fibrils loading it into vesicles during melanogenesis in normal melanocytes {Bissig C., et al., 2016}. For this reason, we are still investigating whether specific APOE sorting to EVs in metastasis versus primary tumor cells can help metastatic progression. In particular, we tested if higher levels of APOE in metastatic melanoma cells correlate with higher PMEL fibril deposition and if this process is mediated by vesicles secretion. To this aim, we started preliminary assays using Proteostat® Aggresome Detection Kit to visualize protein aggregates inside the cells. Our results demonstrate that in metastatic cells there is an accumulation of the Proteostat reagent in dotted structures, suggesting the presence of protein aggregates not only inside but also outside metastatic melanoma cells. This result confirmed what we observed by AFM analysis on metastatic melanoma EVs (Figure 23).

Co-localization assays with PMEL, APOE and known vesicles enriched proteins and a screening of *APOE* isoforms are needed to demonstrate that these structures can be considered as amyloid plaques precursors.

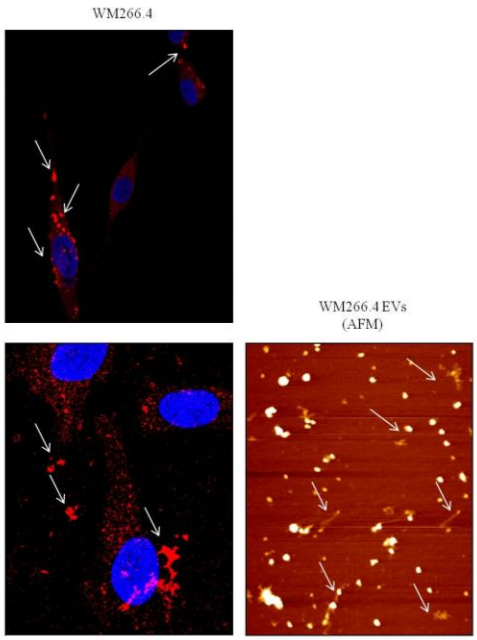

Figure 23: Proteostat reagent accumulates in dots inside and outside metastatic melanoma cells.

Confocal images of WM266.4 cells labeled with Proteostat aggresome detection reagent demonstrate that Proteostat accumulates in dot structures (white arrows) both inside (upper image) and outside (lower image) metastatic melanoma cells. The aggregates outside metastatic melanoma cells can be the same structures that surround metastatic cells secreted EVs visualized by AFM (right image, white arrows).

3. Deep quantitative proteomics on isogenic melanoma cell lines

3.1 Method development

3.1.1 Peptide fractionation increases protein quantitation accuracy

One of the purposes of our study was to dissect how the cells proteome can sustain metastatic progression. To better understand the differences in protein expression between primary tumor and metastatic cells, we used isogenic melanoma cells pairs, that share the same karyotype but show different phenotypes (Figure 10).

To dissect the pathways that can induce metastatic progression, we optimized the deep quantitative proteomics protocol published by Kulak et al. as described in Materials and Method section (Figure 9). In particular, to prevent sample loss, cells were lysed in strong denaturing conditions and proteins were alkylated, reduced and digested in the same lysis buffer. To achieve a robust quantitative result, we coupled the canonical SILAC-based approach with Strong Cationic Exchange (SCX) peptide fractionation. Indeed, SCX fractionation allowed us to obtain a considerable number of peptides that eluted only in one of the five fractions in which the digested sample was split (Figure 24). This approach not only allowed us to increase the number of identified proteins but also improves protein quantitation accuracy, having more peptides that can be used to quantify the same protein.

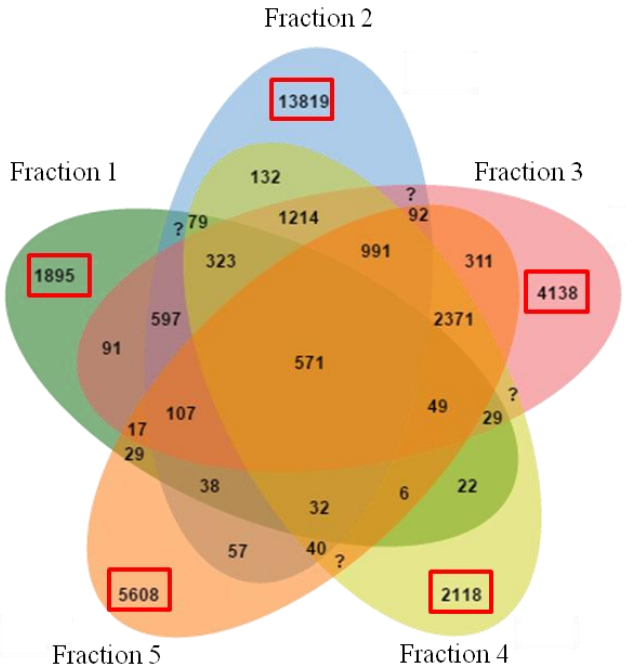

Figure 24: Peptides fractionation increases protein quantitation accuracy.

Distribution of peptides among the five SCX fractions. Red squares indicate the number of peptides eluted exclusively in one specific fraction, demonstrating the efficacy of the fractionation protocol.

3.1.2 Deep quantitative proteomics method is reproducible and can be used to compare different samples

As quality control for quantitative proteomics analysis, we followed the expression of reported melanoma progression antigen in metastatic versus primary tumor cells, according to the literature (Table 6). In particular, in metastatic cells we observed increased levels of MITF, Tyrosynase and Melanotrasferrin, which are critical master regulators of melanocytes development. Moreover, we found the overexpression of the oncofetal/cancer testis antigens of the melanoma-associated antigens (MAGE) family, which are normally expressed in testis or in placenta and increase their expression after cancer onset. Finally, Nestin levels were increased in metastatic versus primary tumor cells, as it is reported to significantly correlate with advanced stage of the disease{Hodi F.S., 2006}. On the contrary, Microtubule Associated Protein MAP2 was overexpressed in primary tumor cells, as it is frequently abundant in melanocytic nevi respect to metastatic cells {Maddodi N. and Setaluri V., 2010}. In these cells, we also observed the loss of Beta Catenin, associated with aggressive melanoma behavior {Bachmann I.M., et al., 2005}. Finally, primary tumor cells have higher levels of

CDK4, that leads to increased cells proliferation and resistance to BRAF inhibition in V600E mutated melanoma cells {Smalley K.S. et al., 2008}.

Protein name	Gene name	Metastasis/Primary tumor Log_2 Ratio
Microphthalmia-associated transcription factor	MITF	3,157577344
Tyrosinase	TYR	2,961771479
Melanotransferrin	MFI2	1,025524968
Nestin	NES	0,863304159
Melanoma-associated antigen C2	MAGEC2	3,211572959
Melanoma-associated antigen 6	MAGEA6	2,784964567
Melanoma-associated antigen 10	MAGEA10	1,876133814
Melanoma-associated antigen 3	MAGEA3	1,171399003
Cyclin-dependent kinase 4	CDK4	-0,207211267
Catenin beta-1	CTNNB1	-0,827051715
Microtubule-associated protein 2	MAP2	-1,433934999

Table 6: List of known melanoma progression markers used as quality control for proteomics analysis.

The correlation of Log_2 ratios between biological replicates demonstrates that our proteomics method is highly reproducible (Figure 25).

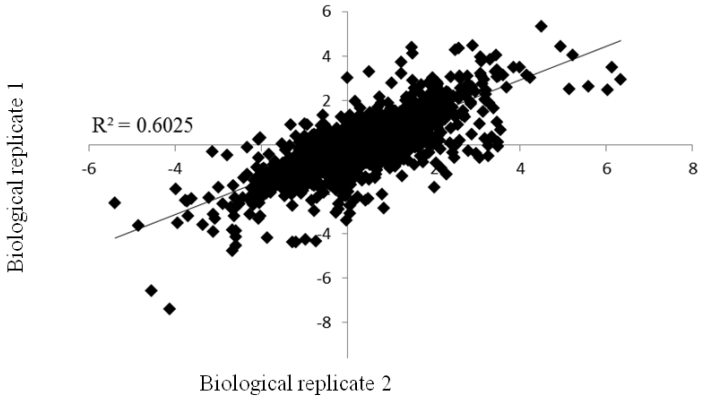

Figure 25: Deep quantitative proteomics method is reproducible.

Pearson correlation to demonstrate the reproducibility among two different biological replicates.

For both isogenic melanoma cells pairs used in this study, we identified and quantified more than 6000 proteins, and around 200 proteins were significantly regulated (FDR <0.05), demonstrating that the deep quantitative proteomics method we optimized is accurate and not cell type specific (Figure 26).

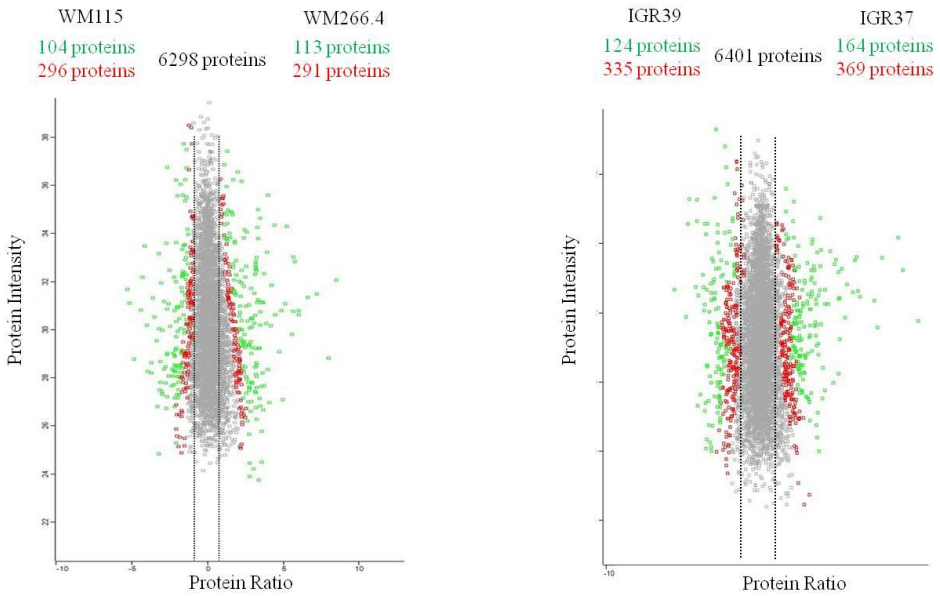

Figure 26: Deep quantitative proteomics can be used to compare different samples.

Proteins distribution according to their intensity and Log_2 ratios is similar between WM115/WM266.4 and IGR39/IGR37 cells. The number of quantified and significant regulated proteins is similar between the two samples. Significantly regulated proteins are highlighted in red (p value <0.05) and in green (FDR<0.05).

3.2 Primary and metastatic isogenic melanoma cells show differences in their proteome

Clustering regulated proteins in pathways according to EnrichR (Gene Ontology: Biological Process), we observed that both WM266.4 and IGR37 metastatic cells up-regulate proteins involved in glucose and fatty acids metabolism, indicating that these cells need height ATP production. Moreover, our analysis shows the up-regulation of proteins belonging to the vesicles trafficking pathway, which includes both extracellular vesicles secretion and intracellular vesicles trafficking. On the opposite, WM115 and IGR39 primary melanoma cells are enriched in proteins regulating adhesion and intracellular signaling pathways (Figure 27).

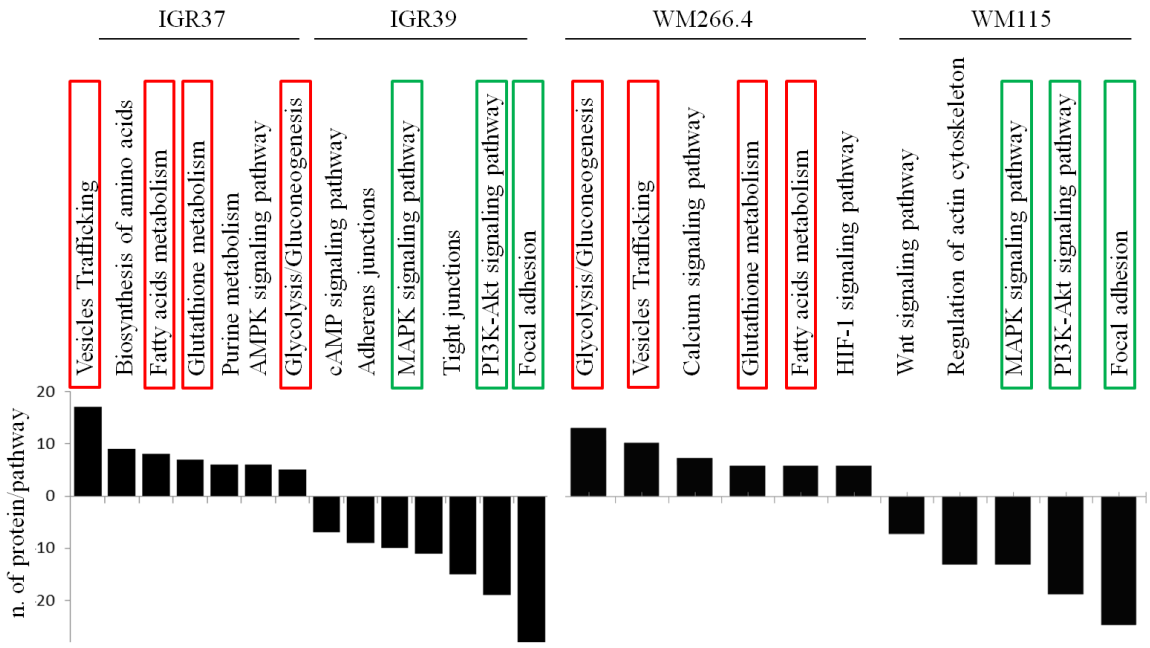

Figure 27: Primary tumor and metastatic melanoma cells from different origin up-regulate similar pathways.

Schematic representation of the up-regulated pathways in primary tumor and metastatic melanoma cells. The bars represent the numbers of proteins in each pathway. Pathways shared between WM266.4 and IGR37 are highlighted in red, while pathways shared among WM115 and IGR39 cells are highlighted in green.

3.3 EVs proteome reflect the cells proteome but the secretion of the proteins in EVs is specifically regulated

By comparing the results obtained by deep quantitative proteomics analysis on cells proteome and EVs proteome, we found that 65% and 83% of identified proteins in EVs proteome was in common with the identified proteins in WM cells and IGR cells proteome respectively (Figure 28, A). Moreover, proteins such as WNT5A are enriched in EVs respect to the cells proteome but maintain their ratio between primary tumor and metastatic samples (Figure 28, B). This result indicates that the EVs proteome can reflect the cells proteome and can thus be used to identify cancer type-specific biomarker, as recently hypothesized by Hurwitz and colleagues {Hurwitz S.N., et al., 2016}. However, we found proteins specifically enriched in EVs that were not identified by proteomics analysis on the total cell lysate because their expression level inside the cells was too low, as in the case of EVs specific proteins (Figure 28, B). For this reason, the correlation between the normalized ratios of significantly regulated

proteins in EVs proteome and cells proteome is very low (Figure 28, C), suggesting that the secretion of proteins in EVs is highly regulated.

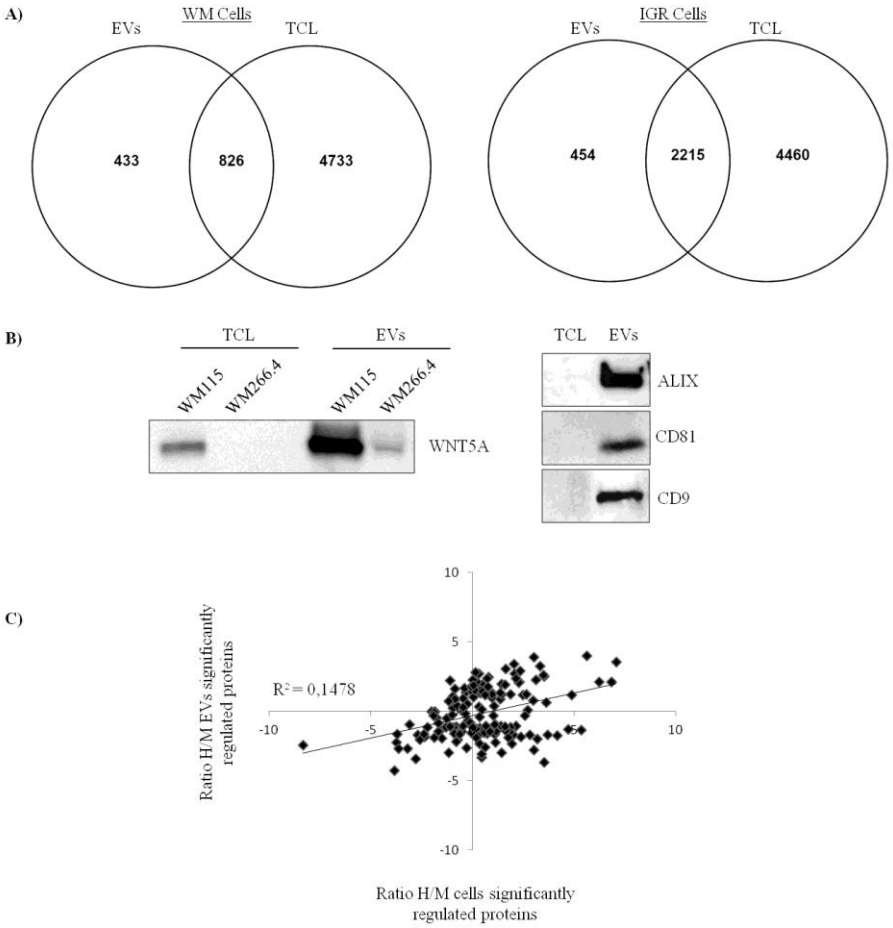

Figure 28: The secretion of proteins in EVs is regulated.

A) Venn diagrams show that the majority of the identified proteins in EVs are in common with the cells proteome (Venn diagrams were done with Venny2.1.0 {Oliveros J.C., 2007-2015}).

B) Left: WB analysis demonstrates that WNT5A is enriched in EVs and maintain higher levels in WM115 respect to WM266.4 both in cellular and in vesicular proteome; Right: EVs enriched proteins ALIX, CD81 and CD9 are too low abundant in the TCL to be detected by WB analysis (Loading: 30µg of each lysate).

C) The low R^2 value demonstrates a low Pearson correlation between significantly regulated proteins in EVs and cells proteome.

3.4 RAB27A is up-regulated in metastasis vs primary tumor

In order to understand if and how the proteome of cancer cells can sustain metastatic progression, we performed deep quantitative proteomics analysis on isogenic primary tumor and metastatic melanoma cell lines. We identify specifically enriched proteins and we clustered them in pathways (Figure 27). Of note, in metastatic cells we observed an up-regulation of the vesicles trafficking pathway, that included a significant increase of the Ras-Related protein Rab-27A (RAB27A), a member of the

RAB GTPase family, and of its known effectors (Table 7). These proteins are involved in melanosome transport and secretion in normal melanocytes and are required for both granules maturation and granules docking at the immunological synapses {Soldati T. and Schliwa M., 2006}.

Protein Name	Gene Name	WM266.4/WM115 Log_2 Ratio	IGR39/IGR37 Log_2 Ratio
Ras-related protein RAB27A	*RAB27A*	2.093624	4.466504
Melanophilin	*MLPH*	2.201719	2.201719
Unconventional myosin-Va	*MYO5A*	1.141185	2.954031
Syntaxin-binding protein 1	*STXBP1*	1.338558	2.914434
Synaptotagmin-like protein 4	*SYTL4*	0.978171	0.190721

Table 7: List of RAB27A and its known effectors significantly enriched in metastatic melanoma cells proteome.

We validated by WB RAB27A increased expression in metastatic *vs* primary tumor cells in both WM266.4 and IGR37 cells. Furthermore, we confirmed RAB27A expression also in 6 non-isogenic primary tumor and metastatic melanoma cell lines, suggesting that this protein might be important for metastasis progression (Figure 29, A-B). Moreover, we observed a close to 10-fold increase of RAB27A expression in IGR37 with respect to WM266.4 cells (Figure 29, C), suggesting an increased melanosomes secretion in these cells, as demonstrated by the high pigmentation of IGR37 cells (Figure 29, D).

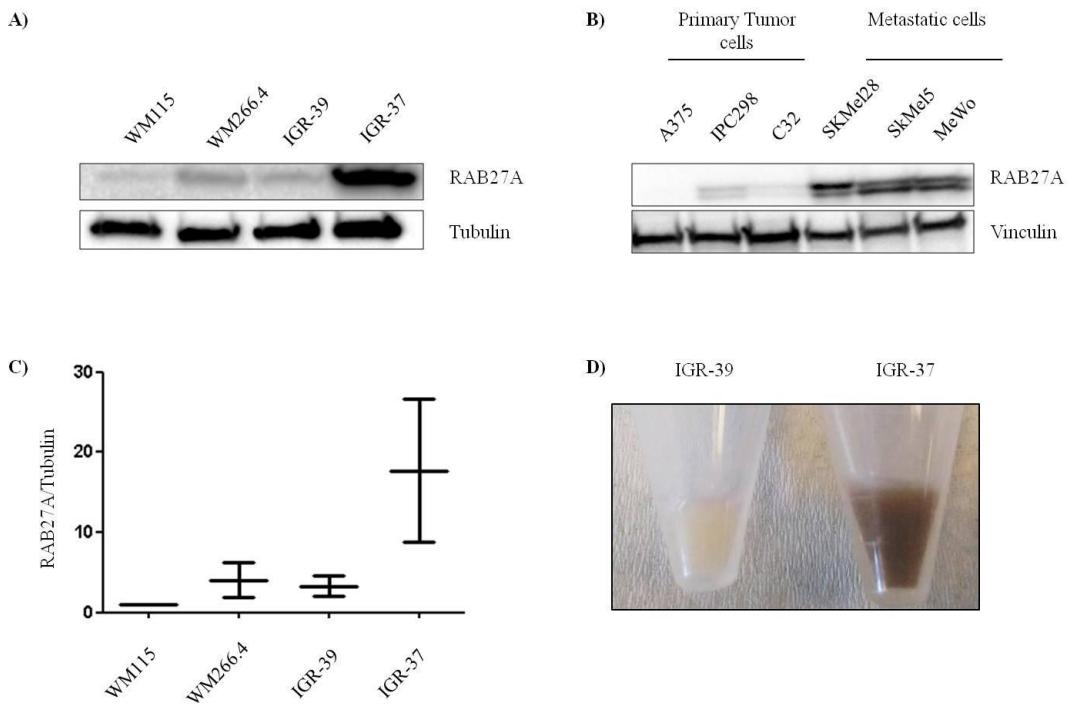

Figure 29: RAB27A is overexpressed in metastatic melanoma cells.

A) WB analysis of isogenic melanoma cell lines WM115/WM266.4 and IGR39/IGR37 reveals high RAB27A protein levels in metastasis versus primary tumor cells.

B) RAB27A overexpression in metastatic melanoma cells is confirmed also in non-isogenic melanoma cell lines.

C) Densitometric analysis of RAB27A protein levels in isogenic melanoma cell lines.

D) IGR37 cells are highly pigmented, consistently with the high levels of RAB27A expression.

4. *RAB27A* Knock Down affects metastatic melanoma cells clonogenic ability and motility and impairs EVs release

In our quantitative proteomics analysis, we observed an overexpression of RAB27A in metastasis derived melanoma cell lines compared to their isogenic primary tumor-derived cells. A correlation between high RAB27A mRNA levels and exosomal protein recovery has been previously reported in melanoma cells {Peinado H., et al., 2012} but, in contrast to what was previously described, we could not detect an increased exosomes production in metastatic cells, despite their high levels of RAB27A expression (Figure 16). For this reason, we hypothesized that in metastatic cells the secretion of a different population of EVs (such as melanosomes) could be predominant and we performed *RAB27A* KD to investigate if this phenomenon is controlled by RAB27A and its effectors.

To test the role of RAB27A in EVs secretion, we used lentiviral infection to stably KD *RAB27A* in metastasis derived WM266.4 and IGR37 cells.

4.1 RAB27A KD affects IGR37 cells pigmentation and conformation

In KD cells, we observed that the pigmentation of IGR37 cells was clearly impaired, indicating that this protein is involved in melanosomes trafficking (Figure 30, A). Moreover, IGR37 cells, instead of the usual spindle-like shape conformation preferentially clustered in a round-shape conformation (Figure 30, B), while no difference in cell shape was observed in WM266.4 cells upon *RAB27A* KD (Figure 30, C).

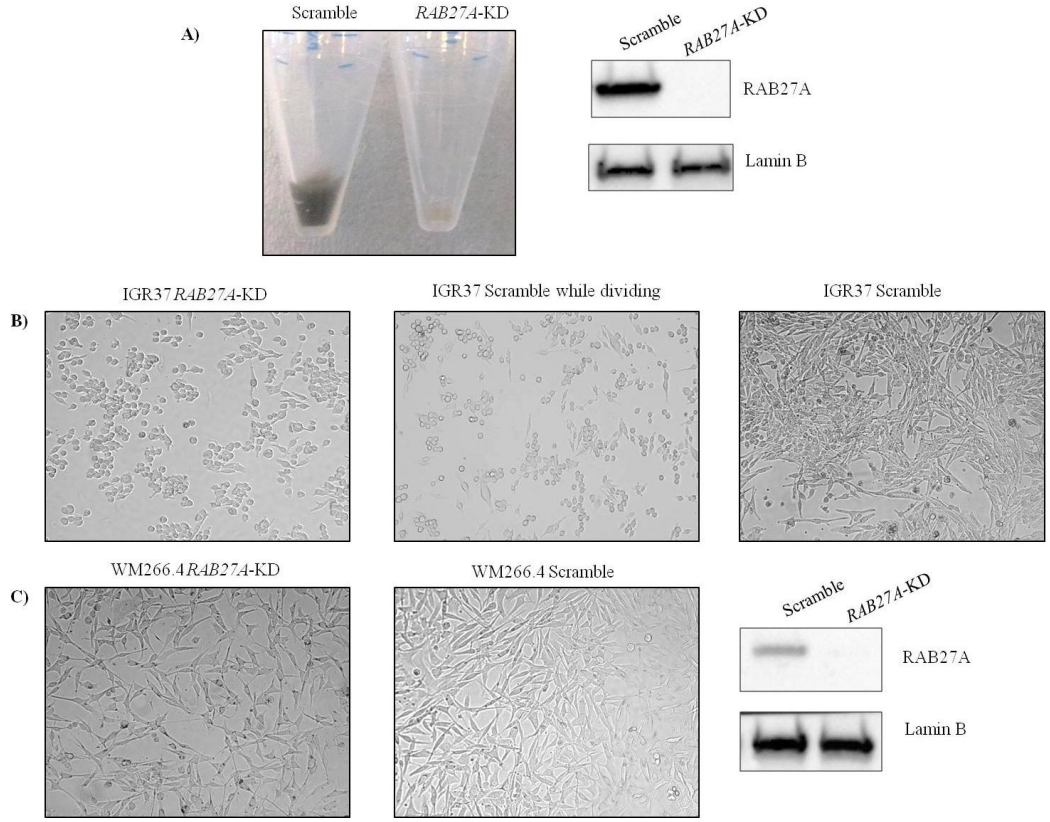

Figure 30: *RAB27A* KD affects IGR37 cells pigmentation and conformation

A) IGR37 KD cells lose their pigmentation (left); WB analysis shows the efficiency of KD (right) in IGR37.

B) IGR37 *RAB27A*-KD cells cluster together and show round-shape conformation (left picture) that is typical of dividing cells (middle picture).

C) No differences in shape are observed in WM266.4 KD cells in respect to the scramble (left); WB analysis shows the reduced level of RAB27A upon KD (right) in WM266.4.

4.2 RAB27A-KD metastatic melanoma cells have increased clonogenic ability

4.2.1 RAB27A KD increases the number of colonies formed by metastatic melanoma cells

IGR37 cells assume rounded shape as soon as they detach from the plate to divide (Figure 30, B). Thus, we hypothesize that RAB27A could have an impact not only on vesicles secretion but also on cells proliferation. We set up a colony formation assay to test the ability of isogenic melanoma cell lines to undergo unlimited division, forming colonies from individual cells.

We demonstrated that, after 10 days, primary tumor cells form more colonies than metastatic cells (Figure 31, A). Furthermore, knocking down *RAB27A* increases the number of colonies formed by metastatic melanoma cells, even if it does not restore completely the condition of primary tumor cells (Figure 31, B). We can therefore conclude that RAB27A expression reduces the clonogenic ability of metastatic melanoma cells. In order to better elucidate this phenomenon, we are investigating a correlation with EVs secretion.

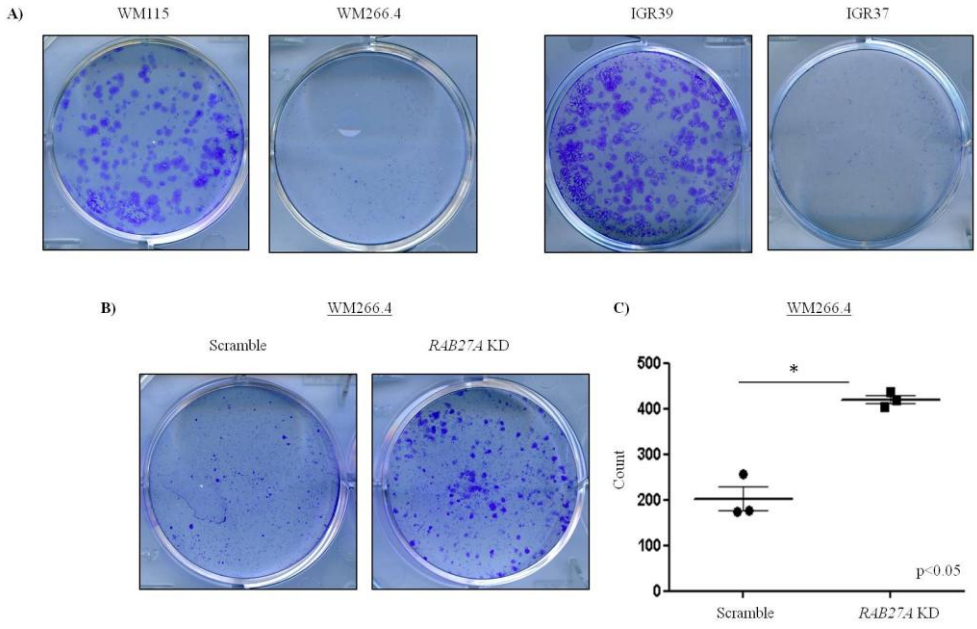

Figure 31: *RAB27A* KD affects the clonogenic ability of metastatic melanoma cells.

A) In both isogenic melanoma cell pairs, primary tumor cells formed more colonies than metastatic cells.

B) After *RAB27A* KD, the number of colonies formed by metastatic cells is increased.

C) Statistical analysis of the number of colonies demonstrates that *RAB27A* KD significantly increases metastatic cells clonogenic ability

4.2.2 EVs secreted by wild type metastatic melanoma cells impair the clonogenic ability of RAB27A-KD cells

Given the established role of RAB27A in EVs secretion {Ostrowski M., et al., 2010} and since we observed high colony formation in the presence of low levels of RAB27A expression, we tested if EVs or other secreted soluble factors could influence metastatic melanoma cells clonogenic ability. To perform this analysis, we set the protocol described in Materials and Methods (Figure 6).

We observed that EVs enriched from WT metastatic melanoma cells are able to significantly reduce the number of colonies at the same levels of WT cells. This phenomenon does not occur in the presence of EVs-depleted secreted factors. Moreover, *RAB27A*-KD cells derived soluble factors do not promote colonies formation in WM266.4-WT cells (Figure 32). This result suggests the presence of a RAB27A-independent vesicles population that could affect the clonogenic ability of metastatic melanoma cells.

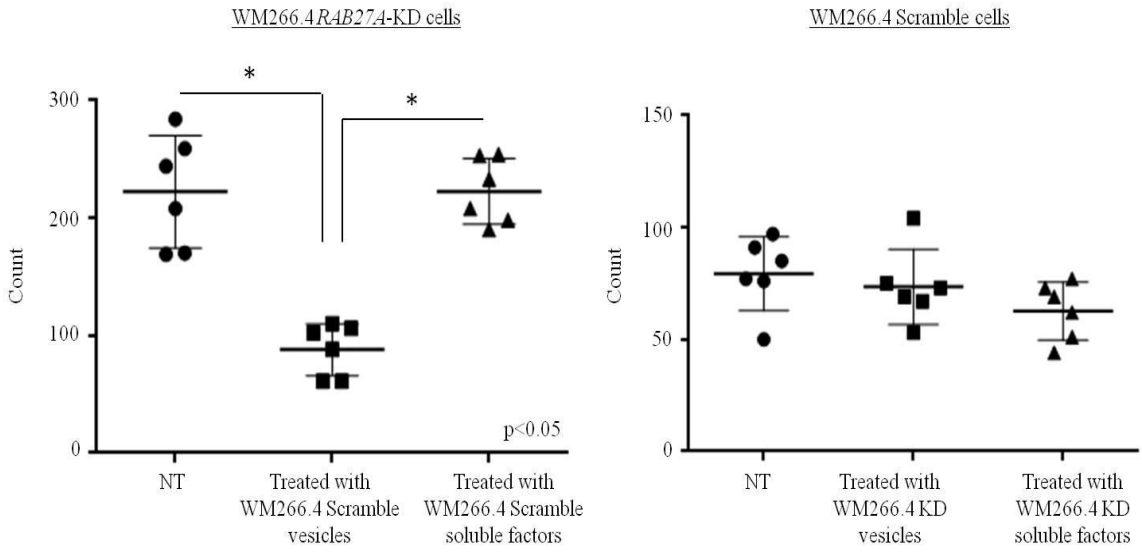

Figure 32: EVs secreted by WT cells impair *RAB27A*-KD cells clonogenic ability.

The number of colonies formed by *RAB27A*-KD cells is significantly impaired when these cells are treated for 6 hours with EVs coming from WM266.4-WT (Scramble) cells but not with the corresponding soluble factors (left). Neither EVs nor soluble factors secreted by *RAB27A*-KD cells are able to modulate WT cells clonogenic ability (right), but the number of colonies formed by these cells is too low to perform a reliable statistical analysis.

NT: Non-Treated control.

However, treating WT cells with EVs secreted by *RAB27A*-KD cells resulted in no increase in colonies possibly because the number of colonies generated by WT cells is too low to see an effect. To overcome this problem we will perform the same assay increasing both the number of starting cells and the duration of the experiment.

4.3 RAB27A KD reduces both EVs number and EVs size

Our preliminary analyses demonstrate that *RAB27A* KD impacts cells behavior and that this fact might be related to EVs secretion. To better dissect the mechanism that regulate this phenomenon, we looked for qualitative and quantitative differences in EVs secretion after *RAB27A* KD. We performed AFM analysis on EVs secreted by the same number of *RAB27A*-WT and *RAB27A*-KD WM266.4 and IGR37 cells.

In both cases, we not only counted less vesicles after *RAB27A* KD, as reported in literature, but we also observed a significant reduction of the EVs area in *RAB27A*-KD. These results suggest that suggesting that RAB27A could participate in the regulation of a specific vesicles subpopulation, affecting in particular the biggest one (Figure 33).

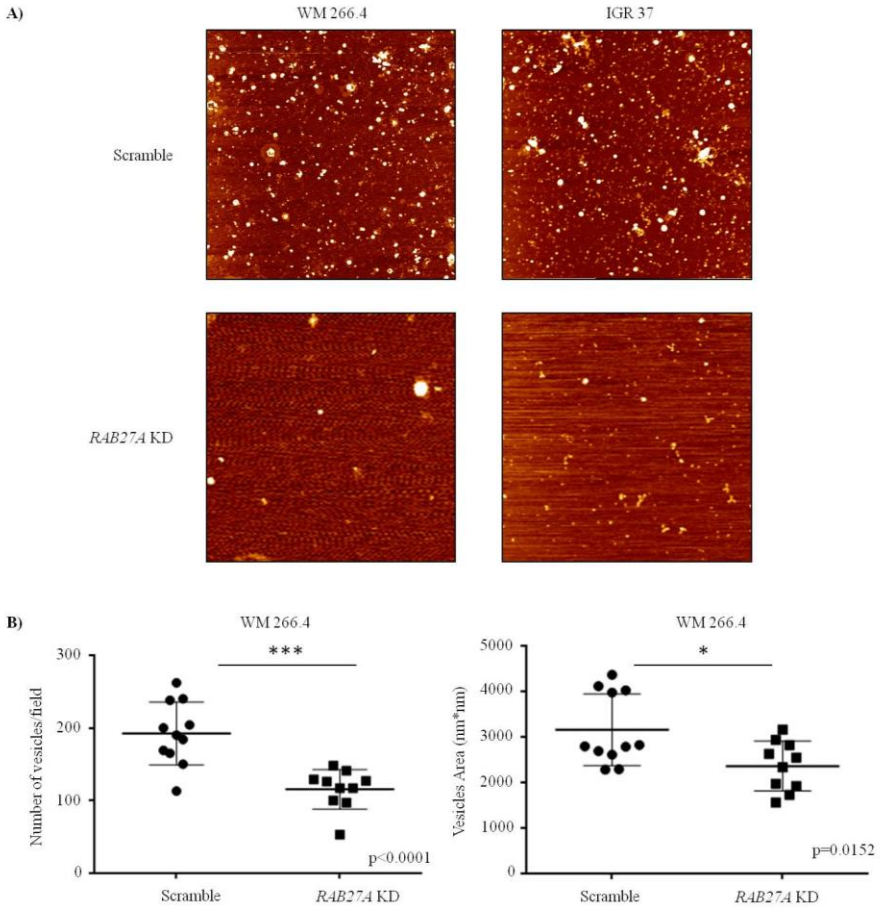

Figure 33: *RAB27A* KD reduces both EVs number and EVs size

A) AFM images show that EVs coming from both *RAB27A*-KD WM266.4 and *RAB27A*-KD IGR37 cells are less and smaller when compared to the WT counterpart.

B) Statistical analysis shows that both the reduction of EVs number and size are significant. Only the images taken from the same EVs dilution were considered as biological replicates for statistical analysis.

4.4 Proteomics analysis of RAB27A-KD cells secreted vesicles

Given the differences in EVs number and size observed by AFM analysis, we performed SILAC-based deep quantitative proteomics analysis as previously reported (section 1.4) to identify proteins that can be considered markers of RAB27A-dependent EVs subpopulation.

EVs were enriched from the supernatant of the same number of either *RAB27A*-WT and *RAB27A*-KD metastatic melanoma cells, and four biological replicates were considered for the analysis because of the low amount of recovered vesicles.

4.4.1 RAB27A KD affects the levels of specific EVs enriched proteins

We focused our attention on those proteins whose enrichment was different between primary tumor and metastatic cells derived EVs, starting from the known EVs

enriched proteins. We observed that CD9 and CD81 levels are decreased after *RAB27A* KD, and we confirmed this result by WB analysis, in which samples were normalized on protein content and no more on donor cells number (Figure 34, A and B). To further corroborate our findings, we observed CD81 in IF performed on metastatic melanoma cells. When observed at the confocal microscopy, cells treated with siRNA targeting RAB27A show impaired CD81 expression at the plasma membrane (Figure 34, C).

Finally, the same WB analysis showed that ALIX and CD63 seem to be increased in EVs after *RAB27A* KD (Figure 34, B), suggesting that CD81, ALIX and CD63 could be used as markers of RAB27A-dependent and RAB27A-independent EVs subpopulations, respectively.

A)

Protein Name	Gene Name	Rab27aWT/Rab27a KD Log_2 Ratio
CD9 antigen	CD9	-1,39747
CD81 antigen	CD81	-0,91049

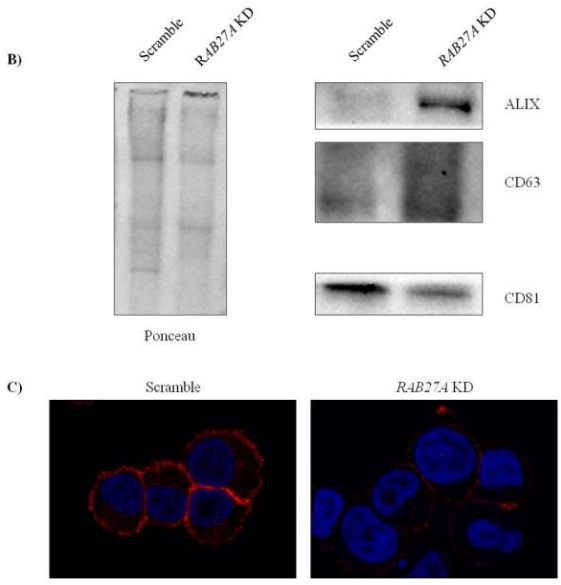

Figure 34: Not all the EVs enriched proteins decrease after *RAB27A* KD

A) CD9 and CD81 Log_2 Ratio shows that these proteins are decreased in EVs after *RAB27A* KD.

B) WB analysis confirmed the decrease of CD81 and shows the increase of ALIX and CD63 proteins in WM266.4 *RAB27A*-KD cells secreted EVs. Ponceau is shown to demonstrate the loading of the same amount of total EVs proteins (Loading: 15µg).

C) Immunofluorescence analysis on IGR37-WT (Scramble) and IGR37 *RAB27A*-KD cells shows decreased levels of CD81 expression at the plasma membrane.

To test this hypothesis, we will sort CD9 and CD81 positive EVs and we will perform proteomics analysis to compare their proteome to the *RAB27A*-WT cells secreted EVs. This experiment will allow us to better define this specific vesicles population and to understand if these vesicles contain proteins that can be followed as markers of melanoma metastatic progression.

4.4.2 RAB27A KD impairs the secretion of proteins related to ECM organization

Proteins related to ECM organization, in particular Fibronectin, were found significantly enriched in metastatic cells derived EVs (Table 5). We observed that, after *RAB27A* KD, the level of these proteins in EVs is decreased (Table 8), possibly demonstrating a role of RAB27A in regulating the selective delivery of ECM proteins to EVs.

Protein name	Gene name	*RAB27A*-KD/*RAB27A*-WT Log_2 Ratio
Tenascin	***TNC***	**-2,31691**
Fibronectin	***FN1***	**-0,89898**
Collagen alpha-2(IV) chain	***COL4A2***	**-1,22394**
Inter-alpha-trypsin inhibitor heavy chain H5	***ITIH5***	**-0,88674**
Collagen alpha-1(I) chain	***COL1A1***	**-0,61099**
Collagen triple helix repeat-containing protein 1	*CTHRC1*	-1,87065
Collagen alpha-1(XXII) chain	*COL22A1*	-1,26925
Procollagen-lysine,2-oxoglutarate 5-dioxygenase 3	*PLOD3*	-0,62027
Thrombospondin-4	*THBS4*	-0,73975
Collagen alpha-1(XII) chain	*COL12A1*	-0,34195
Matrilin-2	*MATN2*	-3,41468
Lactadherin	*MFGE8*	-1,40422
Thrombospondin-1	*THBS1*	-1,16988
Dystroglycan	*DAG1*	-1,02717

Table 8: Proteins related to ECM organization decrease in EVs after *RAB27A* KD

The Log_2 Ratio of identified and quantified proteins related to ECM organization is reported. Proteins highlighted in red were found enriched in metastatic cells derived EVs. Among those, the ones in bold have a significant enrichment (p value <0.05) in metastasis derived EVs.

4.4.3 WNT5A secretion in EVs is increased after RAB27A KD, while APOE does not change

Through the combined analysis of the the proteomics results on EVs and secretome in WM115/WM266.4 and IGR39/IGR37 cells, we found WNT5A and APOE as abundant

components of primary tumor and metastatic microenvironment respectively. Moreover, we demonstrated that WNT5A is mainly enriched in primary tumor cells secreted EVs respect to their soluble factors. The opposite behavior was found for APOE is enriched in metastatic melanoma cells soluble factors, even if a little amount of this protein seems to be EVs-associated (Figures 21 and 22).

After *RAB27A* KD, we observed an increase in EVs-associated WNT5A, that is typical of primary tumor EVs, while its levels in the Soluble Factors sample were unchanged. On the contrary, *RAB27A* KD does not affect the secretion of APOE both in vesicles and as soluble factor (Figure 35, A). This result suggests the possibility to use WNT5A as marker of the RAB27A-independent EVs subpopulation. Interestingly, we observed the same increase in WNT5A levels also in the proteome of *RAB27A*-KD metastatic cells (Figure 35, B). To understand if RAB27A could interact with WNT5A to promote its turnover at the cellular level or if it does modulate WNT5A expression we will perform further experiments, starting with an immunoprecipitation of intracellular RAB27A to test its possible interaction to WNT5A or to proteins that could regulate cellular WNT5A expression.

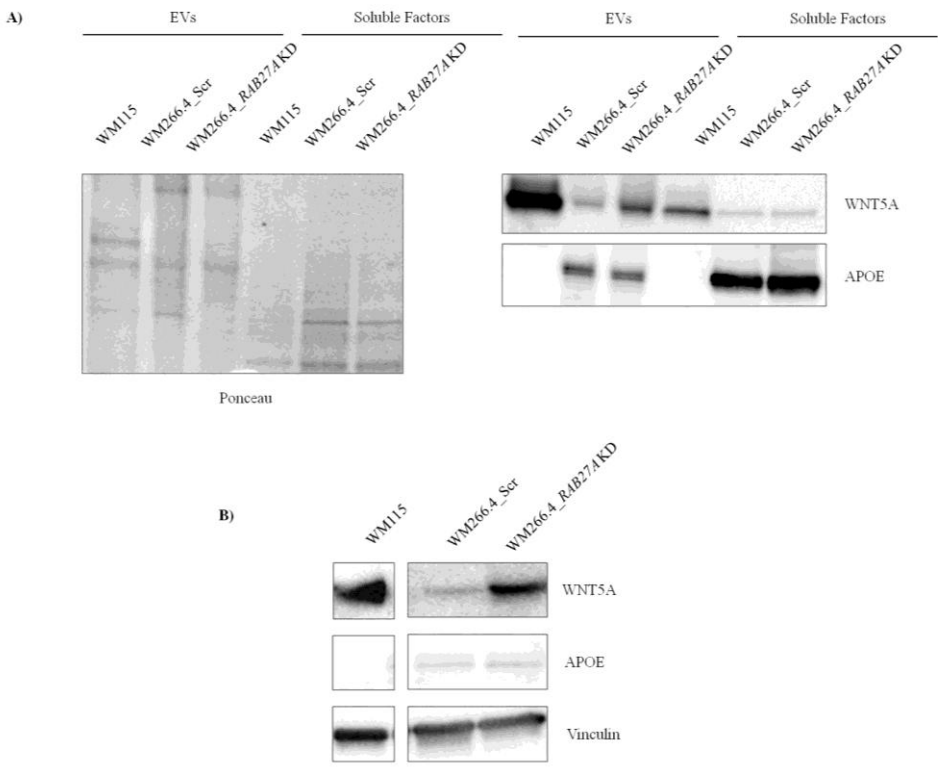

Figure 35: WNT5A secretion in EVs is increased after *RAB27A* KD.

A) WB analysis on the same amount of EVs lysates and soluble factor containing sample demonstrates the increase of WNT5A levels only in EVs after *RAB27A* KD, while both EVs-associated and soluble APOE remain unchanged. Ponceau staining is shown to demonstrate the loading of the same amount of sample in each lane (Loading: 15µg).

B) WNT5A levels are increased in the total cell lysate after *RAB27A* KD, while APOE remains unchanged.

4.5 RAB27A KD increases the motility of metastatic melanoma cells

WNT5A was reported to promote directional cells movement both in physiological and pathological conditions in mouse and human cells {He F., et al., 2008; Bakker E.R., et al., 2013; Arabzadeh S., et al., 2016}. We observed that *RAB27A* KD increases the levels of cellular and EVs-associated WNT5A, thus we used Wound Healing (WH) assay to assess the effect of *RAB27A* KD on cells motility. Notably, we observed that *RAB27A*-KD cells close the wound earlier than WT cells (Figure 36, A). This result confirmed our hypothesis that the increase of WNT5A as consequence of *RAB27A* KD lead to higher cells motility. To test if EVs-associated WNT5A can act as an autocrine signal to affect melanoma cells motility, our future plan is to perform the same WH assay after the stimulation of metastatic cells with EVs and other secreted soluble factors released by either WT or *RAB27A*-KD cells.

Moreover, we used WH assay to analyze differences in cells motility between isogenic primary tumor and metastatic melanoma cells. For both the isogenic melanoma cells pairs, primary cells have higher motility if compared to metastatic cells (Figure 36, B), in accordance with the invasive phenotype that we hypothesized by combining secretome analysis and gelatin degradation assay.

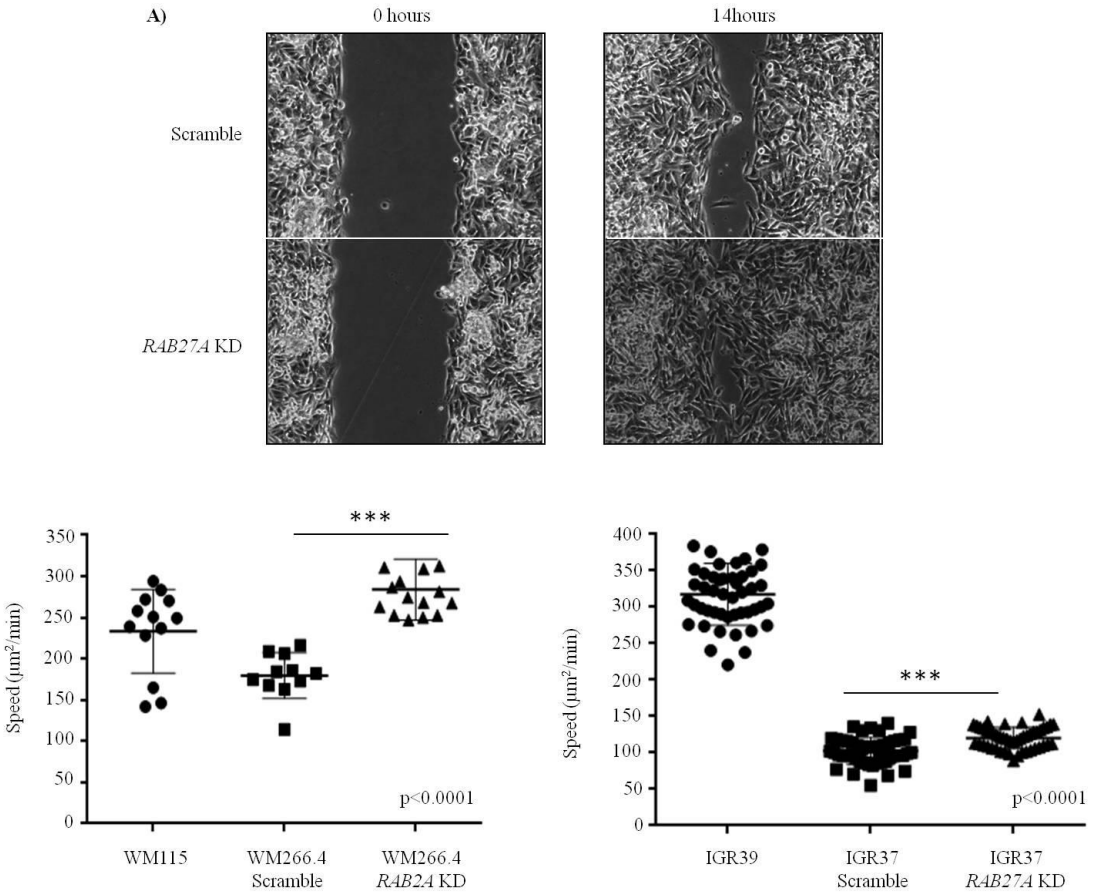

Figure 36: *RAB27A* KD increases the motility of metastatic melanoma cells

A) Images of the wound at the beginning (0 hours) and at the moment of wound closure for WM266.4-WT (Scramble) or KD samples. *RAB27A*-KD cells close the wound faster than WT cells.

B) Quantification and statistical analysis of the wound closure speed for each cell line. In both cases, primary tumor cells are faster than metastatic cells and *RAB27A* KD significantly increases metastatic cells wound closure speed. The speed is expressed in μm^2/min as the software calculated the area covered by cells in every time frame.

During metastasis formation, the secondary organs are selectively modified by the primary tumor through the Pre Metastatic Niche (PMN) establishment, an abnormal, tumor growth-favoring microenvironment devoid of cancer cells. The survival and proliferation of metastases is a consequence of PMN evolution, as the combined result of bone marrow derived cells recruitment, extracellular matrix remodeling and inflammation {Peinado H., et al., 2017}. Nonetheless it was demonstrated that a pre-conditioned microenvironment is necessary to allow the outgrowth of cancer cells in the secondary organ {Kaplan R.N., et al., 2005}, the understanding of which characteristics distinguish the PMNs established in each organ is still matter of debate. Moreover, cancer cells that reach the PMNs before surgical removal of the primary tumor continue to secrete PMNs-promoting factors, that support the formation of further metastases. For this reason, targeting PMNs is highly desirable in cancer therapy to reduce or to prevent metastatic disease {Sceneay J., et al., 2013}.

Tumor derived secreted factors are key players in PMN establishment and facilitate organotropic metastasis {Hoshino A., et al., 2015}. Those factors include molecules directly secreted from the cell in the extracellular space (secreted factors) and Extracellular Vesicles (EVs), a heterogeneous population of vesicles constituted by a lipid bilayer and containing all of the known families of biomolecules (nucleic acids, lipids, proteins, metabolites) {Mittelbrunn M. and Sánchez-Madrid F., 2013}. Altough the gold standard procedure to enrich and characterize EVs subfamilies is still missing, the community refers to “exosomes” as the small-size vesicles (30-100 nm) originating in the endosomal compartment, and to “microvesicles” as the vesicles that originate by the budding from the plasma membrane and have a size comprised between 100 and 1000 nm. Tumor cells-derived EVs have been shown to contribute to PMN formation by the transfer of their cargo to stromal cells which populate PMNs

{Ratajczak J., et al., 2006}, that are reprogrammed towards a pro-metastatic and a pro-inflammatory phenotype in a cancer type and pre-metastatic organ depending manner. Notably, EVs are stable, abundant and easy accessible in body fluids, becoming the most promising biomarkers for assessing the risk of tumor progression and metastasis. For this reason, a full characterization of secreted vesicles subpopulations and of their associated cargo is necessary to understand how EVs affect PMN formation.

In this context, the aim of this project was to characterize the different secretion between isogenic primary tumor and metastatic melanoma cells. Indeed, we used a comparative proteomics analysis on cancer cells and on their secreted factors (both EVs and soluble secreted factors) to investigate how differences in primary tumor versus metastatic microenvironment affect the behavior of cancer cells.

We focused our analysis on melanoma since it is among the most aggressive human cancers and its survival rate dramatically decreases once the tumor has metastasized {Miller A.J. and Mihm M.C. Jr, 2006}. Compared to normal melanocytes, melanoma cells produce a large quantity of exosomes, that can be detected in the plasma of melanoma patients {Peinado H., et al., 2012}. So far, a comparative proteomic characterization of the exosomes secreted by isogenic melanoma cell lines to address different contribution to the PMN establishment in metastatic versus primary tumor melanoma cells has never been performed.

To dissect the differences in the proteome of cells and of their secreted vesicles, we choose the isogenic cell lines WM115 (primary tumor)/WM266.4 (skin metastasis), and IGR39 (primary tumor)/IGR37 (lymph node metastasis). These cells share the same karyotype, thus allowing us to focus on differences in the proteomic content of cells and of their secreted vesicles. Despite originating from different organs, both metastatic cells have a spindle-like shape and grow faster than primaru tumor cells (Figure 10). The use of isogenic cells to compare the proteome of EVs secreted from primary tumor and metastatic cells has been already reported in literature. However,

the cancer cells used as “parental line” and injected in mice to induce metastasis from which the “metastatic line” was established were not necessarily isolated from the primary tumor, thus impairing the discovery of biomarkers for early-stage tumors {Maus R.L.G., et al., 2017}. For this reason, we started our study with commercially-available cell lines that were isolated from the primary tumor and the metastasis of the same patient. This approach will also allow us to identify candidates that could be successively validated in EVs secreted by non-isogenic primary tumor and metastatic melanoma cells.

Moreover, we chose cell lines with different *BRAF* mutation. Indeed, WM115 and WM266.4 cells have V600D *BRAF* mutation, while IGR39 and IGR37 cells have V600E *BRAF* mutation, most common in melanoma (source: Cancel Cell Line Encyclopedia). *BRAF* somatic missense mutations are characteristic of approximately half of all malignant melanoma {Davies H., et al., 2002}. The inhibition of mutated *BRAF* results in rapid regression of metastatic melanoma, even if the reactivation of MAPK pathways or alternative *BRAF* splicing are often able to induce resistance after the immediate antitumor effect {Monsma D.J., et al., 2015}, in a process that could depend on the increasing of cellular WNT5A {Anastas J.N., et al., 2014}. Given that the studies on the role of EVs in *BRAF*-inhibitors resistance are referred only to $BRAF^{V600E}$ mutations, we selected cells with different mutations of *BRAF*. This approach would help us in the future to understand if *BRAF* inhibitors alter the global EVs proteomic content in a *BRAF* mutation-dependent manner, in order to better understand which molecules contribute to the resistance after *BRAF* inhibitors treatment.

In this study, we demonstrated for the first time that the EVs enriched by differential centrifugation from the conditioned media of isogenic primary tumor and metastatic cells are qualitatively and quantitatively different. Indeed, we observed an increased release of EVs from the primary tumor in comparison with metastatic cells. Moreover, the area of EVs released by primary tumor cells was bigger when compared to the

area of EVs released by metastatic cells (Figure 15). This phenomenon can influence the EVs cargo because the differences in size can be reflected in differences of molecules concentration inside the EVs. Of note, the size of EVs could also provide information about the metabolic state of the cells. Indeed, a large quantity of lipids is necessary to produce the external lipids bilayer of these big vesicles, but lipids synthesis is an energy-dependent process that require a highly active metabolic state to provide to the cells the energy needed to exploit all the physiological functions.

To understand if the cargo of EVs reflects the qualitative and quantitative differences that we observed by AFM, we performed a SILAC-based deep quantitative proteomics analysis on EVs enriched from the same number of isogenic melanoma cells. We found an increased amount of proteins coming from the primary tumor *vs* the metastatic cells (Figure 16), consistent with the observation that EVs secreted from primary tumor are bigger in number and size than the ones released by metastatic cells.

Furthermore, to have a complete overview of the extracellular factors differentially secreted by primary tumor and metastatic cells, we used SILAC-based deep quantitative proteomics to analyze the cells secretome, that is the sample obtained after the concentration of the whole cell culture supernatant, containing both EVs and soluble secreted factors. Since the secretome contains EVs, the results obtained with this analysis validated what we observed by deep quantitative proteomics on EVs, indicating candidates that can be considered markers secreted by primary tumor or metastatic melanoma cells. For what concern EVs, about 350 proteins were identified and quantified in common between the two isogenic melanoma cells pairs, and we noticed that the majority of the proteins significantly enriched in EVs released by metastatic cells ($p<0.05$) have a function in ECM organization (Table 5). This result is in accordance with the fact that BMDCs adhesion to PMN sites is promoted by the local increase of ECM deposition induced by EVs. Moreover, Fibronectin (FN) was found as the major component of WM266.4 EVs, and its specific EVs enrichment was sustained by the observation that this protein is not significantly enriched in

metastatic cells proteome and secretome (Figure 19). To better characterize the role of EVs associated FN, we optimized a discontinuous iodixanol gradient for EVs fractionation. We demonstrated that, in primary tumor cells-derived EVs, FN is enriched in the same fraction of known EVs protein, suggesting the association of this protein to the vesicles membrane, while in the metastatic cells-derived EVs FN is enriched at higher densities, suggesting that it may be mainly fibrillar (Figure 20). This phenomenon could be due to a higher FN secretion in metastatic cells EVs respect to primary tumor EVs and might have a biological function during metastatic progression. Indeed, a similar behavior of FN, both membrane-associated and fibrillar, was reported by Sung and colleagues in fibrosarcoma-derived exosomes, in which the EVs-associated FN regulated the directional cell movement through tissues in an integrins/FN interaction-dependent process {Sung B.H., et al., 2015}, and this mechanism could be the same used by primary tumor cells to start metastatization. Then, the enrichment of fibrillar FN on the surface of metastatic cells-derived EVs might facilitate the interaction of these vesicles with BMDCs in PMN, as it was reported for exosomes isolated from the serum of multiple myeloma patients {Purushothaman A., et al., 2016}.

Moreover, we demonstrated that APOE secretion is predominant in metastatic melanoma cells. In accordance with its function of secreted lipid transporter {Mahley R.W. and Rall S.C.Jr, 2000}, we detected the majority of APOE in the EVs-depleted soluble factors sample (Figure 22). However, APOE specific enrichment at vesicular level (Figure 22) may reveal a so far not described function of this protein in metastatic melanoma EVs. Indeed, Bissig and colleagues demonstrated that, in normal melanocytes, the association of APOE to the membrane of vesicles regulates the clearance of PMEL amyloid fibrils {Bissig C., et al., 2016}. Furthermore, it was recently hypothesized that pigment cells eliminate immature amyloid fibrils through exosomes secretion {van Niel G., et al., 2015}. Since our preliminary analysis demonstrated the presence of protein aggregates outside metastatic melanoma cells

and since we observed that that EVs enriched from metastatic melanoma cells are surrounded by fibrillar structures (Figure 23), we hypothesize that the specific enrichment of APOE on EVs might mediate fibril deposition from metastatic cells.

Finally, the quantitative proteomics analysis revealed that WNT5A is significantly enriched in primary tumor released EVs (FDR <0.05). This protein is known to be secreted as soluble factor, but very little is kown about WNT5A presence and function in EVs. We validated WNT5A as EVs' cargo after EVs fractionation on iodixanol gradient, demonstrating that WNT5A is mainly enriched in EVs pellet rather than in the EVs-depleted-soluble factors both in primary tumor and metastatic melanoma cell lines (Figure 21). It has been reported that, in malignant melanoma cell lines, WNT5A up-regulation induces the release of exosomes containing pro-angiogenic and immunosuppressive factors, correlating with the formation of distant metastasis {Ekström E.J. et al., 2014}. Of note, no *WNT5A* gene amplification or rearrangement were found in *WNT5A* overexpressing cells {Weeraratna A.T., et al., 2002}, and for this reason it is reasonable to think that the levels of this protein inside the cell are modulated by other mechanisms, such as its uptake from EVs, and that this phenomenon might have a biological function. Indeed, it was reported that *WNT5A* overexpression in melanoma cells leads to an increased motility and invasion {Weeraratna A.T., et al., 2002}. Since primary tumor cells have higher levels of WNT5A expression compared to theit isogenic metastatic counterpart (Figure 21, B), we used Wound Healing (WH) assay to analyze differences in cells motility between isogenic primary tumor and metastatic melanoma cells. For both our isogenic couples, we observed that primary tumor cells motility was significantly higher than metastatic cells motility (Figure 36), in accordance with the idea that WNT5A promotes directional cells movement {He F., et al., 2008; Bakker E.R.M., et al., 2013; Arabzadeh S., et al., 2016}.

To evaluate the specificity of the EVs proteome and to dissect how the cells proteome can sustain metastatic progression, we optimized the deep quantitative proteomics

protocol published by Kulak et al. to dissect the proteome of isogenic primary tumor and metastatic melanoma cell lines. Coupling the canonical SILAC-based approach with Strong Cationic Exchange peptide fractionation, we obtained a robust quantitative result. Indeed, a considerable number of peptides was detected only in one of the five fractions in which the digested sample was split (Figure 24), increasing the number of identified proteins and improving protein quantitation accuracy. Moreover, the quantitative method is accurate and not cell type specific, as we identified and quantified more than 6000 proteins for both isogenic melanoma cells pairs and around 200 proteins were significantly regulated (FDR <0.05) (Figure 26). Taken together, these findings lead to the conclusion that the deep quantitative proteomics protocol we developed is a useful tool to dissect the proteome of cell lines couples, opening the possibility to have an untargeted approach to identify changes in the entire proteome.

By comparing the results obtained by deep quantitative proteomics analysis on cells proteome and on EVs proteome for both isogenic melanoma cell pairs, we demonstrated that a fraction of proteins was shared between the two samples, in accordance with the hypothesis that EVs can be used to identify cancer-specific biomarkers {Hurwitz S.N., et al., 2016}. Moreover, since those proteins have the same behavior in primary tumor *vs* metastatic sample both in EVs and in the total cells proteome, it is reasonable to think that specific molecules can be used as markers of metastatic progression in melanoma. However, the correlation between the normalized ratios of significantly regulated proteins in EVs proteome and cells proteome is very low, indicating that isogenic primary tumor and metastatic melanoma cells highly regulate both their cellular proteome and their EVs proteome (Figure 28).

Looking at the pathways enhanced in metastatic cells, we found a significant up-regulation of proteins belonging to the vesicles trafficking pathway, that include both extracellular secretion and intracellular trafficking. Among those, we observed a

significant increase of the RAB GTPase RAB27A and of its known effectors in WM266.4 and IGR37 metastatic cells (Table 7) and we validated its enhanced expression also in other 6 non-isogenic metastatic melanoma cell lines compared to primary tumor cell lines, suggesting that this protein can be important for metastasis progression (Figure 29).

This observation is in contrast with our AFM and proteomics analyses, that demonstrate a higher EVs secretion by primary tumor cells, despite their low level of RAB27A expression. Indeed, RAB27A was reported to promote exosomes secretion in HeLa cells by mediating multivesicular endosomes docking at the plasma membrane {Ostrowski M., et al., 2010}. Moreover, in a panel of Sk-Mel melanoma cells series, Peinado and colleagues demonstrated that high levels of RAB27A mRNA positively correlate with metastatic potential and high recovery of exosomal proteins. On the opposite, they also showed that *RAB27A* KD reduce exosomal proteins recovery {Peinado H., et al., 2012}. Since RAB27A is involved in melanosome transport and secretion in normal melanocytes {Soldati T. and Schliwa M. 2006} and since we observed a high pigmentation in IGR37 cells (Figure 29), we hypothesized that, in metastatic cells, the secretion of a different population of EVs, such as melanosomes, could be predominant.

To investigate if this phenomenon is controlled by RAB27A and its effectors, we performed *RAB27A* KD in metastatic cell lines. First of all, we observed an impairment of IGR37 cells pigmentation, in accordance with the involvement of this protein in melanosomes trafficking. Moreover, IGR37 *RAB27A*-KD cells clustered in a round-shape conformation, that is the shape usually assumed by these cells as soon as they detach from the plate to duplicate (Figure 30). For this reason, we hypothesize that RAB27A expression could have an impact on cells growth, as its involvement to promote or to impair cells proliferation has been reported for glioma and gastric cancer cells, respectively {Wu X., et al., 2013 and Li Y., et al., 2017}. Having observed that metastatic cells grow faster than primary tumor cells (Figure 10), we set a colony

formation assay to test the ability of isogenic melanoma cell lines to undergo unlimited division, forming colonies from individual cells. We demonstrated that primary tumor cells have higher clonogenic ability than metastatic cells and that knocking down *RAB27A* increases the number of colonies formed by metastatic melanoma cells (Figure 31), suggesting that RAB27A has a negative effect on colony formation. Notably, our preliminary results demonstrated that EVs enriched from WT metastatic melanoma cells are able to significantly reduce the number of colonies formed by *RAB27A*-KD cells, suggesting that a RAB27A-independent vesicles population could improve or maintain the clonogenic ability of these cells. As further confirmation of this hypothesis, we observed that *RAB27A*-KD EVs-depleted soluble factors do not promote colonies formation in WM266.4-WT cells (Figure 32).

So far, the idea that EVs act in a paracrine manner to maintain a stem cell-like phenotype was established with the observation that EVs released from embryonic stem cells sustained the maintenance of hematopoietic cell stemness and multipotency by delivering specific proteins and mRNA {Ratajczak J., et al., 2006}. Moreover, recent evidences explain the interplay between stem progenitors and their secreted vesicles in tumor progression {Nawaz M., et al., 2016}. The mechanisms by which cancer stem cell-derived EVs initiate and promote tumor progression are still uncertain, but with our study we have the first evidence that a specific subpopulation of EVs (that is, RAB27A-independent) has an important role in maintaining clonogenic ability, that is one particular characteristic of cancer stem cells.

AFM analysis on EVs secreted by the same number of *RAB27A*-WT and *RAB27A*-KD melanoma cells supported the hypothesis of the presence of RAB27A-dependent and –independent subpopulations. Indeed, we not only counted less vesicles after *RAB27A* KD, as reported in literature, but we also observed for the first time a significant reduction of the EVs area in *RAB27A*-KD sample, indicating that RAB27A is involved in particular in the secretion of bigger vesicles (Figure 33).

To identify proteins that could be considered markers of RAB27A-dependent EVs sub population, we performed SILAC-based deep quantitative proteomics analysis on EVs enriched from the supernatant of the same number of either *RAB27A*-WT and *RAB27A*-KD metastatic melanoma cells. Since it was shown that the distribution of the known EVs enriched proteins is not homogeneous among EVs sub populations {Kowal J., et al., 2016}, we started our analysis focusing on tetraspanins, observing that only CD9 and CD81 levels are decreased after *RAB27A* KD, while CD63 seems to be increased together with ALIX that is used to identify EVs even if it does not belong to tetraspanins family (Figure 33). This result is in accordance with the previous hypothesis that CD63-bearing EVs represent a sub population {Kowal J., et al., 2016} and suggests that CD9/CD81 and CD63/ALIX could be used as markers of RAB27A-dependent and RAB27A-independent EVs subpopulations, respectively. Furthermore, EVs secreted by *RAB27A*-KD cells showed an increase in EVs-associated WNT5A, that is typical of primary tumor EVs, while the levels of its soluble form remain unchanged (Figure 35), suggesting the possibility to use WNT5A as auxiliary marker of the RAB27A-independent EVs subpopulation. To investigate if these EVs subpopulations have different secretion routes that can be affected by *RAB27A* KD, we followed the intracellular distribution of tetraspanins and preliminary results on IGR37-WT and IGR37 *RAB27A*-KD cells showed that *RAB27A* KD impairs CD81 expression at the plasma membrane (Figure 28).

Proteomics analysis demonstrated also that *RAB27A* KD impairs the expression of ECM proteins in metastatic cells secreted EVs (Table 8), suggesting a role of RAB27A in regulating the selective secretion of ECM-delivering EVs.

Finally, WH assay showed that the motility of *RAB27A*-KD cells was higher than the one of WT cells (Figure 36). Since *RAB27A*-KD cells secrete EVs with higher WNT5A levels compared to WT cells, this finding supports our hypothesis that vesicular WNT5A can be horizontally transferred to increase cells motility trough the increase

of its cellular levels. Indeed, we observed that *RAB27A* KD increases the levels of cellular WNT5A (Figure 35).

The role of RAB27A –independent EVs subpopulation in maintaining cells clonogenic ability and in promoting cells motility through WNT5A delivery needs further experiments to be assessed, but our preliminary results demonstrate that RAB27A –independent EVs could possibly sustain cancer progression by paracrine stimulation of cancer cells and mediate tumor-PMN communication by long-range activity.

Future Plans

1. Evaluation of ECM proteins association to EVs

Considering that mass spectrometry analysis on isogenic cells' secretome demonstrated the specific FN enrichment in WM266.4 EVs, that were isolated from skin, we want to further investigate if this mechanism is restricted to specific cell lines depending on their metastatic origin, reflecting the way that metastatic cells use to induce a tumor sustaining phenotype on secondary organs resident cells. To this aim, we will use MS analysis to quantify ECM proteins association to EVs in isogenic WM115/WM266.4 and IGR39/IGR37 cells, performing immunoaffinity EVs enrichment targeting tetraspanins as well-known EVs membrane proteins.

Moreover, to demonstrate that RAB27A is involved in the secretion of ECM-enriched EVs, we will overexpress RAB27A in primary tumor cells and we will use MS analysis to evaluate the increase of ECM proteins in their EVs.

Finally, to assess the different functions of EVs-associated FN in isogenic primary tumor and metastatic cell-derived EVs, we will perform directional motility assay in the presence of primary tumor derived EVs, bearing membrane-associated FN. We will then evaluate the different ability of primary tumor-derived or metastasis-derived EVs to recruit BMDC to demonstrate the role of fibrillar fibronectin in mediating this event.

2. Characterization of the biological function of EVs-associated APOE

We will overexpress *APOE* in WM115 and IGR39 cells to understand if its sorting to EVs could be affected by its higher expression at the cellular level. Furthermore, we will investigate if higher levels of APOE in metastatic melanoma cells correlate with higher PMEL fibril deposition, and if this process is mediated by vesicles secretion. To this aim, co-localization assays with PMEL in fibrils are needed to demonstrate that these structures can be considered as amyloid plaques precursors. Moreover, we will co-stain APOE and known EVs enriched proteins to demonstrate that fibril deposition is an EVs-mediated process that could protect metastatic cells, preventing them to be reached from external agents such as drugs.

3. Characterization of the biological function of the EVs-associated WNT5A

We will stably express GFP-WNT5A in primary tumor cells to track the protein inside the cells by live imaging and to follow its internalization into recipient cells after co-culture assays or after EVs addition in recipient cells medium. To test if WNT5A is exposed on vesicles surface or it is just delivered inside the vesicles from donor to recipient cells, we will remove EVs surface proteins with proteinase K and we will look at the presence or absence of GFP signal in vesicles as readout for WNT5A removal. We hypothesize that the presence of WNT5A on vesicles surface would indicate the possibility that primary melanoma cells use EVs to activate the non-canonical WNT signaling pathway in neighboring cells to promote survival and metastatization through PI3K/AKT signaling activation {Katoh M., 2017}. On the opposite, WNT5A delivery inside EVs could dock the protein to reach targets that are distant from cancer cells, such as the PMN in the secondary organ.

To demonstrate the involvement of EVs-associated WNT5A in increasing cells motility, we will perform WH assay stimulating recipient cells with EVs carrying low levels of WNT5A. For this reason, we will establish *WNT5A* KD primary tumor cells, that will be used as donors for WNT5A-depleted vesicles with whom WT primary tumor cells will be stimulated before performing WH.

To understand if cellular WNT5A increase is due to vesicles uptake, we will measure the levels of this protein in metastatic cells, that have low WNT5A expression, after a stimulation with both primary tumor and *RAB27A*-KD cells derived EVs. Moreover, to exclude the hypothesis that RAB27A directly inhibit WNT5A expression, we will immunoprecipitate RAB27A both in primary tumor and metastatic melanoma cells to test its binding to WNT5A or to proteins that could regulate its cellular expression.

We will also perform WH assay after the stimulation of metastatic cells with EVs and secreted soluble factors released by either WT or *RAB27A*-KD cells to test the possibility that RAB27A -dependent and -independent EVs subpopulations can act as a paracrine signal to affect melanoma cells motility, for example through WNT5A delivery.

4. Investigation of the role of RAB27A-dependent EVs sub population

We expect that *RAB27A* overexpression in primary tumor cells would impair their clonogenic ability promoting the secretion of EVs whose cargo would be similar to the one of metastatic cells derived EVs. The analysis of the EVs cargo will take into consideration not only the proteome but also the presence of mRNAs and miRNAs, to understand if these vesicles could modify the phenotype of neighboring cells by modulating their gene expression.

Moreover, to understand if RAB27A-dependent vesicles contain proteins that can be followed as markers of metastatic progression in melanoma, we will sort CD9 and CD81 positive EVs and we will perform proteomics analysis to compare their proteome to the *RAB27A*-WT secreted EVs.

To better characterize the role of EVs cargo proteins in inducing changes in recipient cells we will establish non-contact co-culture transwell system to mimic a long-range communication due to the continuous production of EVs and secreted proteins. SILAC will be used to define how secreted factors impact on recipient cells: heavy and medium-labeled recipient cells will be respectively exposed to melanoma donor cells and, after 8-16-24 hours of co-culture, cells will be lysed and analyzed by deep

quantitative proteomics. Proteins with a significant ratio will give us readout of the molecular pathways affected by the exposure to primary tumor or metastatic donor cells secreted factors and indicate how and if recipient cells are educated towards a pro-tumoral phenotype.

Aebi M.; N-linked protein glycosylation in the ER.; Biochim Biophys Acta. 2013; 1833(11):2430-7; doi: 10.1016/j.bbamcr.2013.04.001; PMID: 23583305

Al-Nedawi K, Meehan B, Rak J.; Microvesicles: messengers and mediators of tumor progression.; Cell Cycle. 2009; 8(13):2014-8; PMID:19535896

Anastas JN, Kulikauskas RM, Tamir T, Rizos H, Long GV, von Euw EM, Yang PT, Chen HW, Haydu L, Toroni RA, Lucero OM, Chien AJ, Moon RT.; WNT5A enhances resistance of melanoma cells to targeted BRAF inhibitors.; J Clin Invest. 2014; 124(7):2877-90.; doi: 10.1172/JCI70156.; PMID: 24865425

Arabzadeh S, Hossein G, Salehi-Dulabi Z, Zarnani AH.; WNT5A-ROR2 is induced by inflammatory mediators and is involved in the migration of human ovarian cancer cell line SKOV-3.; Cell Mol Biol Lett. 2016; 28;21:9; doi: 10.1186/s11658-016-0003-3; PMID: 28536612

Artym VV, Yamada KM, Mueller SC.; ECM degradation assays for analyzing local cell invasion.; Methods Mol Biol. 2009; 522:211-9; doi: 10.1007/978-1-59745-413-1_15; PMID: 19247615

Bachmann IM, Straume O, Puntervoll HE, Kalvenes MB, Akslen LA.; Importance of P-cadherin, beta-catenin, and Wnt5a/frizzled for progression of melanocytic tumors and prognosis in cutaneous melanoma.; Clin Cancer Res. 2005; 11(24 Pt 1):8606-14; PMID: 16361544

Bakker ER, Das AM, Helvensteijn W, Franken PF, Swagemakers S, van der Valk MA, ten Hagen TL, Kuipers EJ, van Veelen W, Smits R.; Wnt5a promotes human colon cancer cell migration and invasion but does not augment intestinal tumorigenesis in Apc1638N mice.; Carcinogenesis. 2013; 34(11):2629-38; doi: 10.1093/carcin/bgt215; PMID: 23764752

Bellingham SA, Coleman BM, Hill AF.; Small RNA deep sequencing reveals a distinct miRNA signature released in exosomes from prion-infected neuronal cells.; Nucleic Acids Res. 2012; 40(21):10937-49.; doi: 10.1093/nar/gks832.; PMID: 22965126

Beloribi S, Ristorcelli E, Breuzard G, Silvy F, Bertrand-Michel J, Beraud E, Verine A, Lombardo D.; Exosomal lipids impact notch signaling and induce death of human pancreatic tumoral SOJ-6 cells.; PLoS One. 2012; 7(10):e47480.; doi: 10.1371/journal.pone.0047480; PMID: 23094054

Bissig C, Rochin L, van Niel G.; PMEL Amyloid Fibril Formation: The Bright Steps of Pigmentation.; Int J Mol Sci. 2016; 17(9). pii: E1438; doi: 10.3390/ijms17091438; PMID: 27589732

Bobrie A, Krumeich S, Reyal F, Recchi C, Moita LF, Seabra MC, Ostrowski M, Théry C.; Rab27a supports exosome-dependent and -independent mechanisms that modify the tumor microenvironment and can promote tumor progression.; Cancer Res. 2012; 72(19):4920-3;. doi: 10.1158/0008-5472.CAN-12-0925; PMID: 22865453

Bobrie A, Théry C; Unraveling the physiological functions of exosome secretion by tumors.; Oncoimmunology. 2013; 2(1):e22565; PMID: 23483742

Chargaff E, West R. The biological significance of the thromboplastic protein of blood.; J Biol Chem. 1946; 166(1):189-97; PMID: 20273687.

Chen KG, Valencia JC, Lai B, Zhang G, Paterson JK, Rouzaud F, Berens W, Wincovitch SM, Garfield SH, Leapman RD, Hearing VJ, Gottesman MM.; Melanosomal sequestration of cytotoxic drugs contributes to the intractability of malignant melanomas.; Proc Natl Acad Sci U S A. 2006; (26):9903-7; PMID: 16777967

Choi DS, Kim DK, Kim YK, Gho YS.; Proteomics, transcriptomics and lipidomics of exosomes and ectosomes.; Proteomics. 2013; 13(10-11):1554-71.; doi: 10.1002/pmic.201200329.; PMID: 23401200

Clark WH Jr, Elder DE, Guerry D 4th, Epstein MN, Greene MH, Van Horn M.; A study of tumor progression: the precursor lesions of superficial spreading and nodular melanoma.; Hum Pathol. 1984; 15(12):1147-65; PMID: 6500548

Cocucci E, Meldolesi J.; Ectosomes and exosomes: shedding the confusion between extracellular vesicles.; Trends Cell Biol. 2015; 25(6):364-72; doi: 10.1016/j.tcb.2015.01.004; PMID: 25683921

Colombo M, Raposo G, Thery C.; Biogenesis, secretion, and intercellular interactions of exosomes and other extracellular vesicles.; Annu Rev Cell Dev Biol. 2014; 30:255-89. doi: 10.1146/annurev-cellbio-101512-122326; PMID: 25288114

Conde-Vancells J, Rodriguez-Suarez E, Embade N, Gil D, Matthiesen R, Valle M, Elortza F, Lu SC, Mato JM, Falcon-Perez JM.; Characterization and comprehensive proteome profiling of exosomes secreted by hepatocytes.; J Proteome Res. 2008; 7(12):5157-66.; PMID: 19367702

Costa-Silva B, Aiello NM, Ocean AJ, Singh S, Zhang H, Thakur BK, Becker A, Hoshino A, Mark MT, Molina H, Xiang J, Zhang T, Theilen TM, García-Santos G, Williams C, Ararso Y, Huang Y, Rodrigues G, Shen TL, Labori KJ, Lothe IM, Kure EH, Hernandez J, Doussot A, Ebbesen SH, Grandgenett PM, Hollingsworth MA, Jain M, Mallya K, Batra SK, Jarnagin WR, Schwartz RE, Matei I, Peinado H, Stanger BZ, Bromberg J, Lyden D.; Pancreatic cancer exosomes initiate pre-metastatic niche formation in the liver.; Nat Cell Biol. 2015 ; 17(6):816-26; doi: 10.1038/ncb3169 PMID:25985394

Cox TR, Rumney RMH, Schoof EM, Perryman L, Høye AM, Agrawal A, Bird D, Latif NA, Forrest H, Evans HR, Huggins ID, Lang G, Linding R, Gartland A, Erler JT.; The hypoxic cancer secretome induces pre-metastatic bone lesions through lysyl oxidase.; Nature. 2015; 522(7554):106-110; doi: 10.1038/nature14492; PMID: 26017313

Cox J, Mann M.; 1D and 2D annotation enrichment: a statistical method integrating quantitative proteomics with complementary high-throughput data.; BMC Bioinformatics. 2012; 13 Suppl 16:S12; doi: 10.1186/1471-2105-13-S16-S12; PMID: 23176165

Cox J, Mann M.; MaxQuant enables high peptide identification rates, individualized p.p.b.-range mass accuracies and proteome-wide protein quantification.; Nat Biotechnol. 2008; 26(12):1367-72;. doi: 10.1038/nbt.1511; PMID: 19029910

Damaghi M, Tafreshi NK, Lloyd MC, Sprung R, Estrella V, Wojtkowiak JW, Morse DL, Koomen JM, Bui MM, Gatenby RA, Gillies RJ.; Chronic acidosis in the tumour microenvironment selects for overexpression of LAMP2 in the plasma membrane.; Nat Commun. 2015; 6:8752; doi: 10.1038/ncomms9752; PMID: 26658462

Davies H, Bignell GR, Cox C, Stephens P, Edkins S, Clegg S, Teague J, Woffendin H, Garnett MJ, Bottomley W, Davis N, Dicks E, Ewing R, Floyd Y, Gray K, Hall S, Hawes R, Hughes J, Kosmidou V, Menzies A, Mould C, Parker A, Stevens C, Watt S, Hooper S, Wilson R, Jayatilake H, Gusterson BA, Cooper C, Shipley J, Hargrave D, Pritchard-Jones K, Maitland N, Chenevix-Trench G, Riggins GJ, Bigner DD, Palmieri G, Cossu A, Flanagan A, Nicholson A, Ho JW, Leung SY, Yuen ST, Weber BL, Seigler HF, Darrow TL, Paterson H, Marais R, Marshall CJ, Wooster R, Stratton MR, Futreal PA.; Mutations of the BRAF gene in human cancer.; Nature. 2002; 417(6892):949-54; PMID: 12068308

Deatherage BL, Cookson BT.; Membrane vesicle release in bacteria, eukaryotes, and archaea: a conserved yet underappreciated aspect of microbial life.; Infect Immun. 2012;80(6):1948-57.; doi: 10.1128/IAI.06014-11; PMID: 22409932

Deng J, Liu Y, Lee H, Herrmann A, Zhang W, Zhang C, Shen S, Priceman SJ, Kujawski M, Pal SK, Raubitschek A, Hoon DS, Forman S, Figlin RA, Liu J, Jove R, Yu H.; S1PR1-STAT3

signaling is crucial for myeloid cell colonization at future metastatic sites.; Cancer Cell. 2012; 21(5):642-54; doi: 10.1016/j.ccr.2012.03.039; PMID: 22624714

Deregibus MC, Cantaluppi V, Calogero R, Lo Iacono M, Tetta C, Biancone L, Bruno S, Bussolati B, Camussi G.; Endothelial progenitor cell derived microvesicles activate an angiogenic program in endothelial cells by a horizontal transfer of mRNA.; Blood. 2007; 110(7):2440-8.; doi: 10.1182/blood-2007-03-078709; PMID: 17536014

Dror S, Sander L, Schwartz H, Sheinboim D, Barzilai A, Dishon Y, Apcher S, Golan T, Greenberger S, Barshack I, Malcov H, Zilberberg A, Levin L, Nessling M, Friedmann Y, Igras V, Barzilay O, Vaknine H, Brenner R, Zinger A, Schroeder A, Gonen P, Khaled M, Erez N, Hoheisel JD, Levy C.; Melanoma miRNA trafficking controls tumour primary niche formation.; Nat Cell Biol. 2016 ; 18(9):1006-17; doi: 10.1038/ncb3399; PMID: 27548915

D'Souza-Schorey C, Clancy JW.; Tumor-derived microvesicles: shedding light on novel microenvironment modulators and prospective cancer biomarkers.; Genes Dev. 2012; 26(12):1287-99; doi: 10.1101/gad.192351.112; PMID: 22713869

Ekström EJ, Bergenfelz C, von Bülow V, Serifler F, Carlemalm E, Jönsson G, Andersson T, Leandersson K.; WNT5A induces release of exosomes containing pro-angiogenic and immunosuppressive factors from malignant melanoma cells.; Mol Cancer. 2014; 13:88; doi: 10.1186/1476-4598-13-88; PMID: 24766647

Ekström EJ, Bergenfelz C, von Bülow V, Serifler F, Carlemalm E, Jönsson G, Andersson T, Leandersson K.; WNT5A induces release of exosomes containing pro-angiogenic and immunosuppressive factors from malignant melanoma cells.; Mol Cancer. 2014 ; 13:88; doi: 10.1186/1476-4598-13-88; PMID: 24766647

Erler JT, Bennewith KL, Cox TR, Lang G, Bird D, Koong A, Le QT, Giaccia AJ.; Hypoxia-induced lysyl oxidase is a critical mediator of bone marrow cell recruitment to form the premetastatic niche.; Cancer Cell. 2009; 15(1):35-4; doi: 10.1016/j.ccr.2008.11.012; PMID: 19111879

Fidler IJ, Nicolson GL; Organ selectivity for implantation survival and growth of B16 melanoma variant tumor lines.; J. Natl Cancer Inst. 1976; 57 (5):1199–1202 PMID:1003551

Fong MY, Zhou W, Liu L, Alontaga AY, Chandra M, Ashby J, Chow A, O'Connor ST, Li S, Chin AR, Somlo G, Palomares M, Li Z, Tremblay JR, Tsuyada A, Sun G, Reid MA, Wu X, Swiderski P, Ren X, Shi Y, Kong M, Zhong W, Chen Y, Wang SE.; Breast-cancer-secreted miR-122 reprograms glucose metabolism in premetastatic niche to promote metastasis.; Nat Cell Biol. 2015; 17(2):183-94; doi:10.1038/ncb3094; PMID: 25621950

Francia G, Cruz-Munoz W, Man S, Xu P, Kerbel RS.; Mouse models of advanced spontaneous metastasis for experimental therapeutics.; Nat. Rev. Cancer. 2011; 11(2):135-41; doi: 10.1038/nrc3001; PMID: 21258397

Franken NA, Rodermond HM, Stap J, Haveman J, van Bree C.; Clonogenic assay of cells in vitro.; Nat Protoc. 2006; 1(5):2315-9; PMID: 17406473

García-Silva S, Peinado H.; Melanosomes foster a tumour niche by activating CAFs.; Nat Cell Biol. 2016;18(9):911-3; 10.1038/ncb3404.; PMID: 27571736

Gardiner C, Di Vizio D, Sahoo S, Thery C, Witwer KW, Wauben M,Hill AF.; Techniques used for the isolation and characterization of extracellular vesicles: results of a worldwide survey.; J Extracell Vesicles. 2016; 5:32945.; doi: 10.3402/jev.v5.32945.; PMID: 27802845

Gasser O, Hess C, Miot S, Deon C, Sanchez JC, Schifferli JA.; Characterisation and properties of ectosomes released by human polymorphonuclear neutrophils.; Exp Cell Res. 2003; 285(2):243-57.; PMID: 12706119

Gay LJ, Felding-Habermann B.; Contribution of platelets to tumour metastasis.; Nat. Rev. Cancer 2011; 11 (2):123–134; doi: 10.1038/nrc3004; PMID: 21258396

Gold B, Cankovic M, Furtado LV, Meier F, Gocke CD.; Do Circulating Tumor Cells, Exosomes, and Circulating Tumor Nucleic Acids Have Clinical Utility?: A Report of the Association for Molecular Pathology.; J Mol Diagn. 2015; S1525-1578(15)00047-1;
doi: 10.1016/j.jmoldx.2015.02.001; PMID: 25908232

Gould SJ, Raposo G.; As we wait: coping with an imperfect nomenclature for extracellular vesicles.; J Extracell Vesicles. 2013; 2. doi: 10.3402/jev.v2i0.20389; PMID: 24009890

Hanson AJ, Craft S, Banks WA.; The APOE genotype: modification of therapeutic responses in Alzheimer's disease.; Curr Pharm Des. 2015; 21(1):114-20; PMID: 25330331

He F, Xiong W, Yu X, Espinoza-Lewis R, Liu C, Gu S, Nishita M, Suzuki K, Yamada G, Minami Y, Chen Y.; Wnt5a regulates directional cell migration and cell proliferation via Ror2-mediated noncanonical pathway in mammalian palate development.; Development. 2008; 135(23):3871-9; doi: 10.1242/dev.025767; PMID: 18948417

Hiratsuka S, Goel S, Kamoun WS, Maru Y, Fukumura D, Duda DG, Jain RK. Endothelial focal adhesion kinase mediates cancer cell homing to discrete regions of the lungs via E-selectin up-regulation.; Proc Natl Acad Sci U S A. 2011; 108(9):3725-30; doi: 10.1073/pnas.1100446108; PMID: 21321210

Hodi FS.; Well-defined melanoma antigens as progression markers for melanoma: insights into differential expression and host response based on stage.; Clin Cancer Res. 2006; 12 (3 Pt 1):673-8; PMID: 16467076

Hornick NI, Huan J, Doron B, Goloviznina NA, Lapidus J, Chang BH, Kurre P.; Serum Exosome MicroRNA as a Minimally-Invasive Early Biomarker of AML.; Sci Rep. 2015; 5:11295.; doi: 10.1038/srep11295; PMID: 26067326

Hoshino A, Costa-Silva B, Shen TL, Rodrigues G, Hashimoto A, Tesic Mark M, Molina H, Kohsaka S, Di Giannatale A, Ceder S, Singh S, Williams C, Soplop N, Uryu K, Pharmer L, King T, Bojmar L, Davies AE, Ararso Y, Zhang T, Zhang H, Hernandez J, Weiss JM, Dumont-Cole VD, Kramer K, Wexler LH, Narendran A, Schwartz GK, Healey JH, Sandstrom P, Labori KJ, Kure EH, Grandgenett PM, Hollingsworth MA, de Sousa M, Kaur S, Jain M, Mallya K, Batra SK, Jarnagin WR, Brady MS, Fodstad O, Muller V, Pantel K, Minn AJ, Bissell MJ, Garcia BA, Kang Y, Rajasekhar VK, Ghajar CM, Matei I, Peinado H, Bromberg J, Lyden D.; Tumour exosome integrins determine organotropic metastasis.; Nature. 2015; 19;527(7578):329-35; doi: 10.1038/nature15756; PMID: 26524530

Hu L, Wickline SA, Hood JL.; Magnetic resonance imaging of melanoma exosomes in lymph nodes.; Magn Reson Med. 2014; doi: 10.1002/mrm.25376; PMID: 25052384

Huang X, Yuan T, Tschannen M, Sun Z, Jacob H, Du M, Liang M, Dittmar RL, Liu Y, Liang M, Kohli M, Thibodeau SN, Boardman L, Wang L.; Characterization of human plasma-derived exosomal RNAs by deep sequencing.; BMC Genomics. 2013; 14:319.; doi: 10.1186/1471-2164-14-319; PMID: 23663360

Hurwitz SN, Rider MA, Bundy JL, Liu X, Singh RK, Meckes DG Jr.; Proteomic profiling of NCI-60 extracellular vesicles uncovers common protein cargo and cancer type-specific biomarkers.; Oncotarget. 2016; 7(52):86999-87015; doi: 10.18632/oncotarget.13569; PMID: 27894104

Jung T, Castellana D, Klingbeil P, Cuesta Hernández I, Vitacolonna M, Orlicky DJ, Roffler SR, Brodt P, Zöller M.; CD44v6 dependence of premetastatic niche preparation by exosomes.; Neoplasia. 2009 ; 11(10):1093-105; PMID: 19794968

Kalra H, Drummen GP, Mathivanan S. ; Focus on Extracellular Vesicles: Introducing the Next Small Big Thing.; Int J Mol Sci. 2016; 17(2):170; doi: 10.3390/ijms17020170; PMID: 26861301

Kalra H, Simpson RJ, Ji H, Aikawa E, Altevogt P, Askenase P, Bond VC, Borràs FE, Breakefield X, Budnik V, Buzas E, Camussi G, Clayton A, Cocucci E, Falcon-Perez JM, Gabrielsson S, Gho YS, Gupta D, Harsha HC, Hendrix A, Hill AF, Inal JM, Jenster G,

Krämer-Albers EM, Lim SK, Llorente A, Lötvall J, Marcilla A, Mincheva-Nilsson L, Nazarenko I, Nieuwland R, Nolte-'t Hoen EN, Pandey A, Patel T, Piper MG, Pluchino S, Prasad TS, Rajendran L, Raposo G, Record M, Reid GE, Sánchez-Madrid F, Schiffelers RM, Siljander P, Stensballe A, Stoorvogel W, Taylor D, Thery C, Valadi H, van Balkom BW, Vázquez J, Vidal M, Wauben MH, Yáñez-Mó M, Zoeller M, Mathivanan S.; Vesiclepedia: a compendium for extracellular vesicles with continuous community annotation.; PLoS Biol. 2012; 10(12):e1001450.; doi: 10.1371/journal.pbio.1001450; PMID: 23271954

Kaplan RN, Riba RD, Zacharoulis S, Bramley AH, Vincent L, Costa C, MacDonald DD, Jin DK, Shido K, Kerns SA, Zhu Z, Hicklin D, Wu Y, Port JL, Altorki N, Port ER, Ruggero D, Shmelkov SV, Jensen KK, Rafii S, Lyden D.; VEGFR1-positive haematopoietic bone marrow progenitors initiate the pre-metastatic niche.; Nature. 2005; 438(7069):820-7; PMID: 16341007

Katoh M.; Canonical and non-canonical WNT signaling in cancer stem cells and their niches: Cellular heterogeneity, omics reprogramming, targeted therapy and tumor plasticity (Review).; Int J Oncol. 2017; 51(5):1357-1369; doi: 10.3892/ijo.2017.4129; PMID: 29048660

Kim CW, Lee HM, Lee TH, Kang C, Kleinman HK, Gho YS.; Extracellular membrane vesicles from tumor cells promote angiogenesis via sphingomyelin.; Cancer Res. 2002; 62(21):6312-7.; PMID: 12414662.

Kim DK, Lee J, Simpson RJ, Lötvall J, Gho YS.; EVpedia: A community web resource for prokaryotic and eukaryotic extracellular vesicles research.; Semin Cell Dev Biol. 2015; doi: 10.1016/j.semcdb.2015.02.005; PMID: 25704310

Kowal J, Arras G, Colombo M, Jouve M, Morath JP, Primdal-Bengtson B, Dingli F, Loew D, Tkach M, Théry C., Proteomic comparison defines novel markers to characterize heterogeneous populations of extracellular vesicle subtypes.; Proc Natl Acad Sci U S A. 2016; 113(8):E968-77; doi: 10.1073/pnas.1521230113; PMID: 26858453

Kreimer S, Belov AM, Ghiran I, Murthy SK, Frank DA, Ivanov AR.; Mass-spectrometry-based molecular characterization of extracellular vesicles: lipidomics and proteomics.; J Proteome Res. 2015; 14(6):2367-84; doi: 10.1021/pr501279t; PMID: 25927954.

Kudo A.; Periostin in fibrillogenesis for tissue regeneration: periostin actions inside and outside the cell.; Cell. Mol. Life Sci. 2011; 68 (19):3201–3207; doi: 10.1007/s00018-011-0784-5.; PMID: 21833583

Kulak NA, Pichler G, Paron I, Nagaraj N, Mann M.; Minimal, encapsulated proteomic-sample processing applied to copy-number estimation in eukaryotic cells.; Nat Methods. 2014; 11(3):319-24; doi: 10.1038/nmeth.2834; PMID: 24487582

Kuleshov MV, Jones MR, Rouillard AD, Fernandez NF, Duan Q, Wang Z, Koplev S, Jenkins SL, Jagodnik KM, Lachmann A, McDermott MG, Monteiro CD, Gundersen GW, Ma'ayan A.; Enrichr: a comprehensive gene set enrichment analysis web server 2016 update.; Nucleic Acids Res. 2016; 44(W1):W90-7; doi: 10.1093/nar/gkw377; PMID: 27141961

Kumar B, Garcia M, Weng L, Jung X, Murakami JL, Hu X, McDonald T, Lin A, Kumar AR, DiGiusto DL, Stein AS, Pullarkat VA, Hui SK, Carlesso N, Kuo YH, Bhatia R, Marcucci G, Chen CC.; Acute myeloid leukemia transforms the bone marrow niche into a leukemia-permissive microenvironment through exosome secretion.; Leukemia. 2017; doi: 10.1038/leu.2017.259; PMID: 28816238

Lasser C, Eldh M, Lotvall J.; Isolation and characterization of RNA-containing exosomes.; J Vis Exp. 2012; (59):e3037.; doi: 10.3791/3037; PMID: 22257828

Li Y, Chen S, Shan Z, Bi L, Yu S, Li Y, Xu S.; miR-182-5p improves the viability, mitosis, migration, and invasion ability of human gastric cancer cells by down-regulating RAB27A.; Biosci Rep. 2017; 37(3). pii: BSR20170136; doi: 10.1042/BSR20170136; PMID: 28546229

Liberti MV, Locasale JW.; The Warburg Effect: How Does it Benefit Cancer Cells?; Trends Biochem Sci. 2016; 41(3):211-8; doi: 10.1016/j.tibs.2015.12.001; PMID: 26778478

Logozzi M, De Milito A, Lugini L, Borghi M, Calabrò L, Spada M, Perdicchio M, Marino ML, Federici C, Iessi E, Brambilla D, Venturi G, Lozupone F, Santinami M, Huber V, Maio M, Rivoltini L, Fais S.; High levels of exosomes expressing CD63 and caveolin-1 in plasma of melanoma patients; PLoS One. 2009; 4(4):e5219; doi: 10.1371/journal.pone.0005219; PMID: 19381331

Lötvall J, Hill AF, Hochberg F, Buzás EI, Di Vizio D, Gardiner C, Gho YS, Kurochkin IV, Mathivanan S, Quesenberry P, Sahoo S, Tahara H, Wauben MH, Witwer KW, Théry C.; Minimal experimental requirements for definition of extracellular vesicles and their functions: a position statement from the International Society for Extracellular Vesicles.; J Extracell Vesicles. 2014; 3:26913; doi: 10.3402/jev.v3.26913; PMID: 25536934

Lötvall J, Hill AF, Hochberg F, Buzás EI, Di Vizio D, Gardiner C, Gho YS, Kurochkin IV, Mathivanan S, Quesenberry P, Sahoo S, Tahara H, Wauben MH, Witwer KW, Théry C.; Minimal experimental requirements for definition of extracellular vesicles and their functions: a position statement from the International Society for Extracellular Vesicles.; J Extracell Vesicles. 2014; 3:26913; doi: 10.3402/jev.v3.26913; PMID: 25536934

Lukanidin E, Sleeman JP, Building the niche: the role of the S100 proteins in metastatic growth. Semin. Cancer Biol. 2012; 22 (3), 216–225; doi: 10.1016/j.semcancer.2012.02.006; PMID: 22381352

Luke JJ, Flaherty KT, Ribas A, Long GV.; Targeted agents and immunotherapies: optimizing outcomes in melanoma.; Nat Rev Clin Oncol. 2017; 14(8):463-482.; doi: 10.1038/nrclinonc.2017.43; PMID: 28374786

Lunavat TR, Cheng L, Einarsdottir BO, Olofsson Bagge R, Veppil Muralidharan S, Sharples RA, Lässer C, Gho YS, Hill AF, Nilsson JA, Lötvall J.; BRAFV600 inhibition alters the microRNA cargo in the vesicular secretome of malignant melanoma cells.; Proc Natl Acad Sci U S A. 2017; 114(29):E5930-E5939.; doi: 10.1073/pnas.1705206114.; PMID: 28684402

Maddodi N, Setaluri V.; Prognostic significance of melanoma differentiation and trans-differentiation.; Cancers (Basel). 2010; 2(2):989-99; doi: 10.3390/cancers2020989; PMID: 22545195

Mahley RW, Rall SC Jr.; Apolipoprotein E: far more than a lipid transport protein.; Annu Rev Genomics Hum Genet. 2000; 1:507-37; PMID: 11701639

Malinverno C, Corallino S, Giavazzi F, Bergert M, Li Q, Leoni M, Disanza A, Frittoli E, Oldani A, Martini E, Lendenmann T, Deflorian G, Beznoussenko GV, Poulikakos D, Haur OK, Uroz M, Trepat X, Parazzoli D, Maiuri P, Yu W, Ferrari A, Cerbino R, Scita G.; Endocytic reawakening of motility in jammed epithelia.; Nat Mater. 2017; 16(5):587-596; doi: 10.1038/nmat4848; PMID: 28135264

Martin KH, Hayes KE, Walk EL, Ammer AG, Markwell SM, Weed SA.; Quantitative measurement of invadopodia-mediated extracellular matrix proteolysis in single and multicellular contexts.; J Vis Exp. 2012; (66):e4119; doi: 10.3791/4119; PMID: 22952016

Mathivanan S, Fahner CJ, Reid GE, Simpson RJ.; ExoCarta 2012: database of exosomal proteins, RNA and lipids.; Nucleic Acids Res. 2012; 40(Database issue):D1241-4. doi: 10.1093/nar/gkr828; PMID: 21989406

Mathivanan S, Ji H, Simpson RJ.; Exosomes: extracellular organelles important in intercellular communication.; J Proteomics. 2010; 73(10):1907-20; doi: 10.1016/j.jprot.2010.06.006.; PMID: 20601276

Maus RLG, Jakub JW, Nevala WK, Christensen TA, Noble-Orcutt K, Sachs Z, Hieken TJ, Markovic SN.; Human Melanoma-Derived Extracellular Vesicles Regulate Dendritic Cell Maturation.; Front Immunol. 2017; 29;8:358; doi: 10.3389/fimmu.2017.00358; PMID: 28424693

Miller AJ, Mihm MC Jr.; Melanoma.; N Engl J Med. 2006; 355(1):51-65; PMID: 16822996

Minciacchi VR, Freeman MR, Di Vizio D.; Extracellular vesicles in cancer: exosomes, microvesicles and the emerging role of large oncosomes.; Semin Cell Dev Biol. 2015; 40:41-51.; doi: 10.1016/j.semcdb.2015.02.010; PMID: 25721812

Mittelbrunn M, Sánchez-Madrid F.; Intercellular communication: diverse structures for exchange of genetic information.; Nat Rev Mol Cell Biol. 2012; 13(5):328-35; doi: 10.1038/nrm3335; PMID: 22510790

Monsma DJ, Cherba DM, Eugster EE, Dylewski DL, Davidson PT, Peterson CA, Borgman AS, Winn ME, Dykema KJ, Webb CP, MacKeigan JP, Duesbery NS, Nickoloff BJ, Monks NR.; Melanoma patient derived xenografts acquire distinct Vemurafenib resistance mechanisms.; Am J Cancer Res. 2015; 5(4):1507-18, PMID: 26101714

Muralidharan-Chari V, Clancy JW, Sedgwick A, D'Souza-Schorey C.; Microvesicles: mediators of extracellular communication during cancer progression.; J Cell Sci. 2010; 123(Pt 10):1603-11; doi: 10.1242/jcs.064386; PMID: 20445011

Nawaz M, Fatima F, Vallabhaneni KC, Penfornis P, Valadi H, Ekström K, Kholia S, Whitt JD, Fernandes JD, Pochampally R, Squire JA, Camussi G.; Extracellular Vesicles: Evolving Factors in Stem Cell Biology.; Stem Cells Int. 2016; 2016:1073140; doi: 10.1155/2016/1073140; PMID: 26649044

Oliveros, J.C. (2007-2015) Venny. An interactive tool for comparing lists with Venn's diagrams. http://bioinfogp.cnb.csic.es/tools/venny/index.html

Osteikoetxea X, Balogh A, Szabo-Taylor K, Nemeth A, Szabo TG, Paloczi K, Sodar B, Kittel A, Gyorgy B, Pallinger E, Matko J, Buzas E.; Improved characterization of EV preparations based on protein to lipid ratio and lipid properties.; PLoS One. 2015; 10(3):e0121184; doi: 10.1371/journal.pone.0121184; PMID: 25798862

Ostrowski M, Carmo NB, Krumeich S, Fanget I, Raposo G, Savina A, Moita CF, Schauer K, Hume AN, Freitas RP, Goud B, Benaroch P, Hacohen N, Fukuda M, Desnos C, Seabra MC, Darchen F, Amigorena S, Moita LF, Thery C., Rab27a and Rab27b control different steps of the exosome secretion pathway., Nat Cell Biol., 2010 Jan;12(1):19-30; sup pp 1-13; doi: 10.1038/ncb2000; PMID: 19966785

Paget S.; The distribution of secondary growths in cancer of the breast.; Lancet. 1889; 133(3421); 571-573

Pan BT, Johnstone RM.; Fate of the transferrin receptor during maturation of sheep reticulocytes in vitro: selective externalization of the receptor.; Cell. 1983; 33(3):967-78.; PubMed PMID: 6307529.

Park JE, Tan HS, Datta A, Lai RC, Zhang H, Meng W, Lim SK, Sze SK.; Hypoxic tumor cell modulates its microenvironment to enhance angiogenic and metastatic potential by secretion of proteins and exosomes.; Mol Cell Proteomics. 2010; 9(6):1085-99.; doi: 10.1074/mcp.M900381-MCP200; PMID: 20124223

Peinado H, Alečković M, Lavotshkin S, Matei I, Costa-Silva B, Moreno-Bueno G, Hergueta-Redondo M, Williams C, García-Santos G, Ghajar C, Nitadori-Hoshino A, Hoffman C, Badal K, Garcia BA, Callahan MK, Yuan J, Martins VR, Skog J, Kaplan RN, Brady MS, Wolchok JD, Chapman PB, Kang Y, Bromberg J, Lyden D.; Melanoma exosomes educate bone marrow progenitor cells toward a pro-metastatic phenotype through MET.; Nat Med. 2012; 18(6):883-91; doi: 10.1038/nm.2753; PMID: 22635005

Peinado H, Lavotshkin S, Lyden D.; The secreted factors responsible for pre-metastatic niche formation: old sayings and new thoughts.; Semin Cancer Biol. 2011; 21(2):139-46; doi: 10.1016/j.semcancer.2011.01.002; PMID: 21251983

Peinado H, Zhang H, Matei IR, Costa-Silva B, Hoshino A, Rodrigues G, Psaila B, Kaplan RN, Bromberg JF, Kang Y, Bissell MJ, Cox TR, Giaccia AJ, Erler JT, Hiratsuka S, Ghajar CM, Lyden D.; Pre-metastatic niches: organ-specific homes for metastases.; Nat Rev Cancer. 2017; 17(5):302-317; doi: 10.1038/nrc.2017.6; PMID:28303905

Prasad CP, Mohapatra P, Andersson T.; Therapy for BRAFi-Resistant Melanomas: Is WNT5A the Answer?; Cancers (Basel). 2015; 7(3):1900-24.; doi: 10.3390/cancers7030868.; PMID: 26393652

Psaila B, Lyden D.; The metastatic niche: adapting the foreign soil.; Nat Rev Cancer. 2009; 9(4):285-93; doi: 10.1038/nrc2621; PMID:19308068

Purushothaman A, Bandari SK, Liu J, Mobley JA, Brown EE, Sanderson RD.; Fibronectin on the Surface of Myeloma Cell-derived Exosomes Mediates Exosome-Cell Interactions.; J Biol Chem. 2016; 291(4):1652-63; doi: 10.1074/jbc.M115.686295; PMID: 26601950

Raposo G, Stoorvogel W.; Extracellular vesicles: exosomes, microvesicles, and friends.; J Cell Biol. 2013; 200(4):373-83.; doi: 10.1083/jcb.201211138; PMID: 23420871

Raposo G, Marks MS.; Melanosomes--dark organelles enlighten endosomal membrane transport.; Nat Rev Mol Cell Biol. 2007; 8(10):786-97; PMID: 17878918

Rappsilber J, Ishihama Y, Mann M.; Stop and go extraction tips for matrix-assisted laser desorption/ionization, nanoelectrospray, and LC/MS sample pretreatment in proteomics.; Anal Chem. 2003; 75(3):663-70; PMID: 12585499

Ratajczak J, Wysoczynski M, Hayek F, Janowska-Wieczorek A, Ratajczak MZ.; Membrane-derived microvesicles: important and underappreciated mediators of cell-to-cell communication.; Leukemia. 2006 ; 20(9):1487-95; PMID: 16791265

Regente M, Pinedo M, Elizalde M, de la Canal L.; Apoplastic exosome-like vesicles: a new way of protein secretion in plants?; Plant Signal Behav. 2012; 7(5):544-6.; doi: 10.4161/psb.19675; PMID: 22516827

Riss TL, Moravec RA, Niles AL, Duellman S, Benink HA, Worzella TJ, Minor L.; Cell Viability Assays.; Advancing Translational Sciences 2013; PMID: 23805433

Scadden DT.; Nice neighborhood: emerging concepts of the stem cell niche.; Cell. 2014; 157(1):41-50; doi: 10.1016/j.cell.2014.02.013; PMID: 24679525

Sceneay J, Smyth MJ, Möller A.; The pre-metastatic niche: finding common ground.; Cancer Metastasis Rev. 2013; 32(3-4):449-64; doi: 10.1007/s10555-013-9420-1; PMID: 23636348

Schindelin J, Arganda-Carreras I, Frise E, Kaynig V, Longair M, Pietzsch T, Preibisch S, Rueden C, Saalfeld S, Schmid B, Tinevez JY, White DJ, Hartenstein V, Eliceiri K, Tomancak P, Cardona A.; Fiji: an open-source platform for biological-image analysis.; Nat Methods. 2012 ; 9(7):676-82; doi: 10.1038/nmeth.2019; PMID: 22743772

Sharma S, Gillespie BM, Palanisamy V, Gimzewski JK.; Quantitative nanostructural and single-molecule force spectroscopy biomolecular analysis of human-saliva-derived exosomes.; Langmuir. 2011; 27(23):14394-400; doi: 10.1021/la2038763; PMID: 22017459

Simpson RJ. ; Extracellular Microvesicles: The Need for Internationally Recognised Nomenclature and Stringent Purification Criteria.; J Proteomics Bioinform. 2012.; doi: 10.4172/jpb.10000e10

Skog J, Wurdinger T, van Rijn S, Meijer DH, Gainche L, Sena-Esteves M, Curry WT Jr, Carter BS, Krichevsky AM, Breakefield XO.; Glioblastoma microvesicles transport RNA and proteins that promote tumour growth and provide diagnostic biomarkers.; Nat Cell Biol. 2008; 10(12):1470-6.; doi: 10.1038/ncb1800; PMID: 19011622

Sleeman,JP; The lymph node pre-metastatic niche.; J. Mol. Med. (Berl) 2015; 93 (11):1173–1184 PMID: 26489604

Smalley KS, Lioni M, Dalla Palma M, Xiao M, Desai B, Egyhazi S, Hansson J, Wu H, King AJ, Van Belle P, Elder DE, Flaherty KT, Herlyn M, Nathanson KL.; Increased cyclin D1 expression can mediate BRAF inhibitor resistance in BRAF V600E-mutated melanomas.; Mol Cancer Ther. 2008; 7(9):2876-83; doi: 10.1158/1535-7163.MCT-08-0431; PMID: 18790768

Soldati T, Schliwa M.; Powering membrane traffic in endocytosis and recycling.; Nat Rev Mol Cell Biol. 2006; 7(12):897-908; PMID: 17139330

Sung BH, Ketova T, Hoshino D, Zijlstra A, Weaver AM.; Directional cell movement through tissues is controlled by exosome secretion.; Nat Commun. 2015; 6:7164; doi: 10.1038/ncomms8164; PMID: 25968605

Taylor DD, Gercel-Taylor C.; MicroRNA signatures of tumor-derived exosomes as diagnostic biomarkers of ovarian cancer.; Gynecol Oncol. 2008; 110(1):13-21.; doi: 10.1016/j.ygyno.2008.04.033; PMID: 18589210

Taylor DD, Shah S.; Methods of isolating extracellular vesicles impact down-stream analyses of their cargoes.; Methods. 2015; 87:3-10.; doi: 10.1016/j.ymeth.2015.02.019; PMID: 25766927

Tetta C, Ghigo E, Silengo L, Deregibus MC, Camussi G.; Extracellular vesicles as an emerging mechanism of cell-to-cell communication.; Endocrine. 2013; 44(1):11-9; doi: 10.1007/s12020-012-9839-0; PMID: 23203002

Théry C, Amigorena S, Raposo G, Clayton A.; Isolation and characterization of exosomes from cell culture supernatants and biological fluids.; Curr Protoc Cell Biol. 2006; Chapter 3:Unit 3.22; doi: 10.1002/0471143030.cb0322s30; PMID: 18228490

Tkach M, Théry C.; Communication by Extracellular Vesicles: Where We Are and Where We Need to Go.; Cell. 2016; 164(6):1226-1232.; doi: 10.1016/j.cell.2016.01.043; PMID: 26967288

Valadi H, Ekstrom K, Bossios A, Sjostrand M, Lee JJ, Lotvall JO.; Exosome-mediated transfer of mRNAs and microRNAs is a novel mechanism of genetic exchange between cells.; Nat Cell Biol. 2007; 9(6):654-9; doi: 10.1038/ncb1596; PMID: 17486113

Van Deun J, Mestdagh P, Agostinis P, Akay Ö, Anand S, Anckaert J, Martinez ZA, Baetens T, Beghein E, Bertier L, Berx G, Boere J, Boukouris S, Bremer M, Buschmann D, Byrd JB, Casert C, Cheng L, Cmoch A, Daveloose D, De Smedt E, Demirsoy S, Depoorter V, Dhondt B, Driedonks TA, Dudek A, Elsharawy A, Floris I, Foers AD, Gärtner K, Garg AD, Geeurickx E, Gettemans J, Ghazavi F, Giebel B, Kormelink TG, Hancock G, Helsmoortel H, Hill AF, Hyenne V, Kalra H, Kim D, Kowal J, Kraemer S, Leidinger P, Leonelli C, Liang Y, Lippens L, Liu S, Lo Cicero A, Martin S, Mathivanan S, Mathiyalagan P, Matusek T, Milani G, Monguió-

Tortajada M, Mus LM, Muth DC, Németh A, Nolte-'t Hoen EN, O'Driscoll L, Palmulli R, Pfaffl MW, Primdal-Bengtson B, Romano E, Rousseau Q, Sahoo S, Sampaio N, Samuel M, Scicluna B, Soen B, Steels A, Swinnen JV, Takatalo M, Thaminy S, Théry C, Tulkens J, Van Audenhove I, van der Grein S, Van Goethem A, van Herwijnen MJ, Van Niel G, Van Roy N, Van Vliet AR, Vandamme N, Vanhauwaert S, Vergauwen G, Verweij F, Wallaert A, Wauben M, Witwer KW, Zonneveld MI, De Wever O, Vandesompele J, Hendrix A.; EV-TRACK: transparent reporting and centralizing knowledge in extracellular vesicle research.; Nat Methods. 2017; 14(3):228-232. doi: 10.1038/nmeth.4185; PMID: 28245209

van Niel G, Bergam P, Di Cicco A, Hurbain I, Lo Cicero A, Dingli F, Palmulli R, Fort C, Potier MC, Schurgers LJ, Loew D, Levy D, Raposo G.; Apolipoprotein E Regulates Amyloid Formation within Endosomes of Pigment Cells.; Cell Rep. 2015; 13(1):43-51; doi: 10.1016/j.celrep.2015.08.057; PMID: 26387950

Vella LJ, Behren A, Coleman B, Greening DW, Hill AF, Cebon J.; Intercellular Resistance to BRAF Inhibition Can Be Mediated by Extracellular Vesicle-Associated PDGFRβ.; Neoplasia. 2017; 19(11):932-940.; doi: 10.1016/j.neo.2017.07.002.; PMID: 28963969

Venning FA, Wullkopf L, Erler JT.; Targeting ECM Disrupts Cancer Progression.; Front Oncol. 2015; 5:224; doi: 10.3389/fonc.2015.00224; PMID: 26539408

Weber GF.; Time and Circumstances: Cancer Cell Metabolism at Various Stages of Disease Progression.; Front Oncol. 2016; 6:257; doi: 10.3389/fonc.2016.00257; PMID: 28018856

Weeraratna AT, Jiang Y, Hostetter G, Rosenblatt K, Duray P, Bittner M, Trent JM.; Wnt5a signaling directly affects cell motility and invasion of metastatic melanoma.; Cancer Cell. 2002; 1(3):279-88; PMID: 12086864

Wu X, Hu A, Zhang M, Chen Z.; Effects of Rab27a on proliferation, invasion, and anti-apoptosis in human glioma cell.; Tumour Biol. 2013; 34(4):2195-203; doi: 10.1007/s13277-013-0756-5; PMID: 23553027

Yamaguchi Y, Hearing VJ.; Melanocytes and their diseases.; Cold Spring Harb Perspect Med. 2014; 4(5). pii: a017046; doi: 10.1101/cshperspect.a017046; PMID: 24789876

Zerial M, McBride H.; Rab proteins as membrane organizers.; Nat Rev Mol Cell Biol. 2001; 2(2):107-17; PMID: 11252952

Zhang HG, Grizzle WE.; Exosomes: a novel pathway of local and distant intercellular communication that facilitates the growth and metastasis of neoplastic lesions.; Am J Pathol. 2014 ;184(1):28-41; doi: 10.1016/j.ajpath.2013.09.027; PMID: 24269592

Zhou W, Fong MY, Min Y, Somlo G, Liu L, Palomares MR, Yu Y, Chow A, O'Connor ST, Chin AR, Yen Y, Wang Y, Marcusson EG, Chu P, Wu J, Wu X, Li AX, Li Z, Gao H, Ren X, Boldin MP, Lin PC, Wang SE.; Cancer-secreted miR-105 destroys vascular endothelial barriers to promote metastasis.; Cancer Cell. 2014; 25(4):501-15. doi:10.1016/j.ccr.2014.03.007; PMID: 24735924

Zhu L, Wang K, Cui J, Liu H, Bu X, Ma H, Wang W, Gong H, Lausted C, Hood L, Yang G, Hu Z.; Label-free quantitative detection of tumor-derived exosomes through surface plasmon resonance imaging.; Anal Chem. 2014; 86(17):8857-64; doi: 10.1021/ac5023056; PMID: 25090139